

# UNIVERSIDAD DE CANTABRIA

PROGRAMA INTERUNIVERSITARIO DE DOCTORADO EN  
TECNOLOGÍAS DE LA INFORMACIÓN Y COMUNICACIONES EN  
REDES MÓVILES POR LAS UNIVERSIDADES DE A CORUÑA,  
OVIEDO, CANTABRIA, PAÍS VASCO Y ZARAGOZA



## TESIS DOCTORAL

ANÁLISIS Y EVALUACIÓN EXPERIMENTAL DE FLEXIBLE  
DUPLEXING PARA REDES MIMO MULTI-CAPA

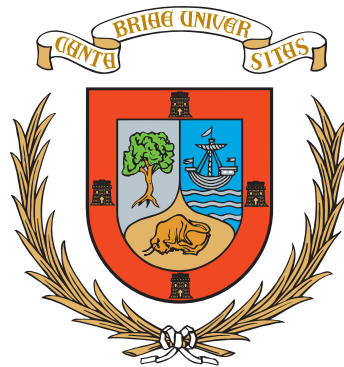
AUTOR: JACOBO FANJUL FERNÁNDEZ  
TUTOR/DIRECTOR: IGNACIO SANTAMARÍA CABALLERO

ESCUELA DE DOCTORADO DE LA UNIVERSIDAD DE CANTABRIA  
SANTANDER 2019



UNIVERSITY OF CANTABRIA

DEPARTMENT OF COMMUNICATIONS ENGINEERING



PHD DISSERTATION

ANALYSIS AND EXPERIMENTAL EVALUATION OF  
FLEXIBLE DUPLEXING FOR MULTI-TIER MIMO  
NETWORKS

AUTHOR: JACOBO FANJUL FERNÁNDEZ  
SUPERVISOR: IGNACIO SANTAMARÍA CABALLERO

SANTANDER 2019



**Análisis y Evaluación Experimental**  
**de *Flexible Duplexing***  
**para Redes MIMO Multi-capa**

Tesis que se presenta para optar al título de  
Doctor por la Universidad de Cantabria

**Autor:** Jacobo Fanjul Fernández  
**Director:** Ignacio Santamaría Caballero

Programa Interuniversitario de Doctorado en Tecnologías de  
la Información y Comunicaciones en Redes Móviles

Grupo de Tratamiento Avanzado de Señal

Departamento de Ingeniería de Comunicaciones

Escuela de Doctorado

Universidad de Cantabria

2019



Un objectif sans plan s'appelle un vœu.

—*Antoine de Saint-Exupéry*

## **Affiliations**

Advanced Signal Processing Group  
Department of Communications Engineering  
University of Cantabria, Spain

This work was supported by the Ministerio de Economía y Competitividad of Spain under FPI grant BES-2014-069786.

# Agradecimientos

No tengo muy claro si esta Tesis se me ha hecho eterna o si se me ha pasado volando. Pero si hay algo de lo que estoy seguro al 100%, es de lo infinitamente AGRADECIDO que me siento. Tanto es así que me tomaré la licencia de reservar unas cuantas líneas, antes de meternos de lleno con el *interference alignment* y el *flexible duplexing*, para daros las GRACIAS a todos los que, en mayor o menor medida, habéis hecho este viaje posible.

En primer lugar, GRACIAS a mi director, Nacho, por guiarme a lo largo de todo el trabajo de investigación desde que me acogiste en el Grupo hace ya más de cinco años. GRACIAS, porque en realidad yo sólo fui un día a tu despacho a consultar una duda para un examen en 4º de Teleco, pero aquí estamos, acabando una Tesis Doctoral. GRACIAS, Steven, por las charlas sobre tecnología, o sobre el formato perfecto de un documento, o sobre noticias cómicas absurdas de cualquier temática. No podría haber tenido mejor vecino en el despacho de al lado. GRACIAS, Jesús (Pérez), por los valores y convicciones tan fuertes que tienes sobre todo en el ámbito docente. GRACIAS a Luis Vielva y Javier Vía, porque es un placer (aunque a la vez intimida un poco) charlar sobre matemáticas y comunicaciones con personas de una capacidad de cómputo y una forma de pensar tan asombrosa como la vuestra. Y especialmente, GRACIAS, Jesús (Ibáñez), por confiar en mí para impartir las clases de prácticas de tus asignaturas. También por los principios que demuestras como profesor. Pero sobre todo, GRACIAS por estar ahí siempre que necesitaba ayuda en el laboratorio. Cualquier problema que tenía, ya lo habías tenido antes, ya habías localizado la causa, y ya tenías dos o tres sugerencias para tratar de solucionarlo. No podría describir hasta qué punto he aprendido en ese sentido.

GRACIAS también a todos los compañeros que he ido teniendo a lo largo de estos años, aunque unos ya se hayan ido y otros, prácticamente, acaben de llegar. GRACIAS, Óscar, por ser mi primer guía, junto con Nacho, en mi investigación. GRACIAS por transmitirme tu perfeccionismo a la hora de trabajar, y por tu ayuda al principio de este viaje. No he conseguido convencer a nadie más para que vea conmigo la Formula E y reírnos de los comentarios sobre el no-ruido de los coches. GRACIAS, Christian, por ayudarme también en mis primeros pasos, primeras *submissions* y demás, cuando aún estaba tratando de poner todo en orden. Además, no sé si habría sido capaz de completar con éxito esta Tesis sin que me explicaras que las ecuaciones de Cauchy-Riemann. Muchas GRACIAS también, Carlos, porque tu presencia en el despacho ha sido un buen soplo de aire fresco, y has sido un gran compañero. GRACIAS por escucharme cuando me desesperaba con papeleos y trámites interminables. GRACIAS también a Ramírez, Víctor y Luengo, por pasaros de visita de vez en cuando y echarme algún que otro cable que haya podido necesitar. GRACIAS, Vaibhav, por

confiar en mí para ayudarte ahora que empiezas tu propio trabajo. Muchísimas GRACIAS, Renzo, por elegirme para guiarte en tu trabajo fin de grado. Has hecho un gran trabajo en el laboratorio, y me has dado pie a aprender mientras te iba enseñando. Por otra parte, GRACIAS a Carlos Beltrán por darme la oportunidad de trabajar contigo. El mero hecho de hablar de continuación homotópica y variedades polinómicas contigo ha sido probablemente la actividad intelectual más exigente a la que haya podido enfrentarme. Y por supuesto, mil GRACIAS al Grupo GTEC de la Universidad da Coruña, y en especial a José Antonio, por vuestra inestimable e imprescindible contribución a que las campañas de medidas fueran realizadas con éxito.

I would like to THANK Professor Jafar for hosting me in his Group at University of California, Irvine. Also, THANKS, Charlotte (and Mr. Bear) for making my stay comfortable and warm. But most importantly, THANK YOU for hosting Ben as well, because by letting him into your house, you let a friend into my life. THANK YOU, Ben, for your open-minded perspective, your will to learn about other cultures, and the passion for Baseball that you transmitted to me.

THANKS to Professor Nosratinia as well, for hosting me at University of Texas at Dallas, and for his guidance when selecting a research line or a problem to be addressed. THANKS, Monica, for being an amazing host and, especially, for being such a humble and honest human being. Also, THANKS to the UTD Swim Club for taking me in for the first part of 2017-18 season and providing an enjoyable experience.

A lo largo del desarrollo de la tesis, he podido comprobar que el entorno personal es tan importante como el académico cuando se trata de mantener una mentalidad estable y una actitud positiva. Por ello quiero AGRADECER a todo mi entorno el apoyo durante estos años. Ha habido personas que estuvieron al principio de este viaje y no han llegado conmigo hasta este punto. Eso sí, se llevan mi más profundo AGRADECIMIENTO por haberme apoyado entonces, y por contribuir a mi salud mental cuando aún eran parte de mi vida. También ha habido gente que se había ido y posteriormente ha vuelto, por lo que también les doy las GRACIAS.

Álvaro, Marta, Adán, me acostumbré a trabajar con vosotros durante cinco años y estos últimos cuatro ha sido durísimo hacerlo solo. Pero aunque ya no nos veamos tanto, seguís significando mucho para mí y seguís dándome “oxígeno” cada vez que hablo con vosotros. GRACIAS a la gente que me ha rodeado desde el mundo del deporte, sobre todo de la natación. El agua es una medicina excelente, pero las personas que he conocido en las piscinas y que siguen acompañándome son incluso mejores. GRACIAS a la gente que he ido conociendo en el ámbito de la música. Desde Trueba, y pasando por otras formaciones como Almatrampa o Trinidad, he ido disfrutando de la música y mi mente lo ha agradecido (aunque el tiempo que le dedicaba haya ido cuesta abajo). Lo mejor es que además de la propia música, he podido disfrutar de los Amigos que he conocido gracias a ella. Muy especialmente, GRACIAS al Señor Adrián Simón Palacios (a.k.a. Petu). Por una parte, sencillamente, por ser uno de mis mejores Amigos. Pero además, porque me has demostrado un nivel de superación y de lucha increíble. Si pudiera contagiarme de la décima parte de tu fortaleza, me quedaría más que satisfecho.

Muchísimas GRACIAS a Mariano y a Cristian (a.k.a. Derrick) por los fines de semana infinitos de basket. Basket por la mañana, comer, basket por la tarde, cenar, NBA en la consola, y partidos de la NBA hasta la madrugada. Mucha NBA, sí, pero no hay equipo de baloncesto profesional en el mundo que iguale nuestro Big Three. Muchísimas GRACIAS a mi Familia, porque me habéis hecho fuerte de mil maneras y os habéis dejado la espalda por mí.

Luis, empecé llamándote “El jefe de Adán” y después vino lo de “El ex-compañero de piso de Óscar”. Rápidamente pasaste a ser una especie de *coach* que me daba y sigue dando los mejores consejos para recorrer el duro camino que ha sido esta Tesis... y desde hace ya bastante tiempo puedo llamarte “Uno de mis mejores Amigos”. GRACIAS de verdad.

Infinitas GRACIAS, Juan Carlos. Llevamos ya más años lejos que cerca, y hemos pasado de la infancia a la edad adulta siguiendo caminos distintos. A pesar de esto, seguimos conociéndonos igual de bien, seguimos convergiendo hacia los mismos gustos, y seguimos contando chistes igual de lamentables (es decir, brillantes), lo cual es algo que deberíamos hacernos mirar. No existe forma humana de estar lo suficientemente AGRADECIDO por poder disfrutar de una conexión así. GRACIAS.

Una vez me dijo alguien que el amor tiene su raíz más profunda en la admiración. Dee, eres la persona más fuerte que conozco, te he visto superarte, luchar hasta el agotamiento, cumplir retos que parecían imposibles por todo lo que conllevaban... y eso me ha ido empujando a mí mismo para alcanzar mis propios retos. GRACIAS por ser mi inspiración en ese sentido, GRACIAS por ser mi compañera de aventuras, pedradas imposibles y desafíos. GRACIAS por ser como eres conmigo, y por estar ahí empujando conmigo en cada “brazada”.

Por último, GRACIAS a las dos personas que me ayudaron a descubrir mi vocación hace ya unos cuantos años. Por una parte a Humberto, porque sin tener la más mínima obligación, me dedicabas horas y horas por las tardes en el instituto, horas y horas de cacharreo, estaño por aquí y transistor por allá. Eres uno de esos que yo llamo Profesores de Verdad, de los que sienten que Enseñar consiste en dejar huella. Finalmente, a Salvador. Las agujas de tu reloj ya no se mueven, pero yo me lo sigo llevando de viaje por todo el mundo y miro la hora en él todos los días.

Jacobo Fanjul Fernández

Santander, Febrero de 2019



# Abstract

The last two decades have witnessed a revolution in the way that mobile networks are conceived. The 4th and 5th generations of mobile communications have progressively lead to a world where data traffic demands have long overpassed voice traffic. As subsequent generations went through consistent development, the infrastructure topology has evolved in order to support the increasing diversity of devices and information nature. The network structure has followed a progression from homogeneous cellular systems onto a variety of cell sizes (macro, micro, pico and femtocells) and data characteristics (e.g. voice, multimedia, live streaming, etc). This entire assortment is encompassed under the denomination of heterogeneous networks (HetNets).

Since the nodes in a wireless network share the propagation medium, interference management becomes one of the most paramount tasks. In this sense, conventional orthogonal access techniques, such as time-division duplex (TDD) or frequency-division duplex (FDD), are no longer sufficient if we wish to exploit the potential of the arising HetNets. Consequently, one of the candidate access techniques that are considered in the context of 5G is flexible duplexing. Unlike conventional TDD/FDD, flexible duplexing is an access scheme that allows the coexistence of uplink (UL) and downlink (DL) cells within the same time/frequency resource block. The main intuition behind this approach is that different UL/DL combinations lead to different interference levels at the input of the corresponding receivers, hence providing different performance. By selecting the optimal UL/DL configuration, together with a robust linear processing technique, we are able to take a better advantage of the network capacity.

In this thesis, we study the potential benefits of flexible duplexing regarding three main figures of merit, namely: degrees of freedom (DoF), throughput, and power efficiency. Additionally, we compare the impact of flexible duplexing when different linear processing techniques are applied.

First, we analyze the DoF improvements that flexible duplexing can provide in multiple-input multiple-output (MIMO) multi-cell networks with several users per cell. In other words, we study the additional number of interference-free data streams that can be transmitted in the network when different UL/DL combinations are enabled. For this purpose, flexible duplexing is applied together with the interference alignment (IA) strategy, which is known to be optimal in terms of capacity at high signal-to-noise ratio (SNR) regimes. This part of the analysis relies on the general X network model, which is later on particularized into different well-known topologies, including flexible duplexing networks. An IA algorithm is presented in order to calculate IA precoders and decoders for X networks. The proposed scheme, based on homotopy continuation, is validated over a number of wireless scenarios,

showing to outperform other IA methods in the literature. After a brief review of the prior work on 2-cell networks, we propose necessary conditions for the feasibility of IA in multi-cell flexible duplexing networks. Additionally, by means of the homotopy continuation-based algorithm, we provide numerical evidence of the DoF benefits of flexible duplexing in the multi-cell systems under evaluation.

Moving on to a simplified network model, we analyze the data rate performance of flexible duplexing when compared to conventional TDD access. For this study, we consider MIMO multi-cell networks with a single user per cell. Moreover, each user transmits/receives a single data stream. In this context, our goal is to maximize the data rate for given traffic asymmetry parameters. The problem is subsequently decoupled into an interference alignment problem for each UL/DL configuration, followed by a discrete search to determine the best UL/DL combination. Since calculating IA precoders and decoders for every UL/DL can be computationally demanding, we provide a statistical characterization of the average rate achievable by IA for a given channel realization. In addition, we propose a suboptimal approach, which we denote as hierarchical switching (HS), that allows to reduce the number of UL/DL combinations to be evaluated. The simulation results show that significant benefits can be attained by means of flexible duplexing in terms of rate. The impact of the linear precoding technique on the benefits of flexible duplexing is also considered. To this end, we compare IA to the multi-cell minimum-mean square error (M-MMSE) receiver, proving that flexible duplexing is even more important when the communication strategy presents a lack of robustness against interference.

Afterwards, flexible duplexing is further evaluated in terms of power efficiency. Analogously to the rate study, we intend to minimize the total transmitted power in the network by enabling the coexistence of UL and DL cells. In this case, we present a general optimization problem that addresses precoder and decoder design, as well as UL/DL selection. The general problem is again decoupled into a power minimization problem for a fixed UL/DL and given QoS (quality-of-service) requirements, followed by a discrete search. For the former, we present an algorithm that alternatively optimizes the beamformers and filters for a given flexible duplexing setting. The latter follows the same lines as the aforementioned HS approach, relying on the tier hierarchy of the different cells to determine the UL/DL switching sequence. Our simulation results illustrate the power efficiency benefits provided by flexible duplexing together with the proposed power minimization scheme.

Finally, we present an experimental evaluation of flexible duplexing in order to complete the theoretical results provided in the rest of the thesis. More specifically, we carry out a measurement campaign over a small-scale 3-cell network with 1 macro-cell and 2 small cells. The performance of the user equipments is tested for different inter-cell interference regimes generated from the base station. Additionally, three different precoding/decoding strategies are compared, namely, IA, M-MMSE with dominant eigenmode transmission (DET), and M-MMSE only. It is worth highlighting that this experiment is the first real-time implementation of IA with full channel knowledge at the transmitter end. On top, the empirical results corroborate that significant benefits can be achieved in the HetNets context by enabling flexible duplexing.

# Resumen extendido

A lo largo de las últimas dos décadas, hemos sido testigos de una revolución en el ámbito de las comunicaciones celulares. La 4<sup>a</sup> y 5<sup>a</sup> generación de redes móviles han seguido una progresión en la que el tráfico de datos ha superado sobradamente las demandas de tráfico de voz, especialmente en los últimos diez años. Debido al continuo desarrollo y la evolución seguida por las infraestructuras de comunicaciones, se ha dado lugar a una creciente diversidad en lo referente a tamaño de las redes y celdas que las componen, así como en cuanto a la naturaleza de la propia información transmitida. En dicho contexto, esta tesis centra su foco de atención en el tratamiento de interferencias y el diseño de transceptores en redes heterogéneas (HetNets) inalámbricas. El concepto de HetNet engloba un amplio abanico de topologías de red y estrategias de comunicación. En este trabajo abordamos el estudio de algunas de las mencionadas técnicas, con el fin de poner de relieve el potencial de las próximas generaciones de comunicaciones móviles.

Haciendo especial hincapié en técnicas de procesamiento lineal para sistemas de múltiple entrada y múltiple salida (MIMO), nuestro estudio se centra en esquemas de duplexado flexible. Concretamente, el duplexado flexible consiste en habilitar la coexistencia de celdas en subida (UL) y celdas en bajada (DL) en el mismo bloque de recursos temporales y frecuenciales. Las diferentes combinaciones UL/DL contribuyen, potencialmente, a reducir el nivel de interferencia a la entrada de los distintos nodos en la red, obteniendo de esta manera un rendimiento superior a las técnicas de acceso ortogonal más convencionales, como son las basadas en división temporal, frecuencial, o por código (TDMA, FDMA o CDMA, respectivamente). Para caracterizar específicamente dicha mejora en el rendimiento, a lo largo de nuestros análisis hemos considerado tres figuras de mérito principales: los grados de libertad (DoF), la tasa de transmisión, y la eficiencia energética.

## Grados de libertad (DoF)

El estudio del duplexado flexible comienza con la caracterización de los grados de libertad. Dicha medida se identifica con el número de hilos de información independientes y libres de interferencia que pueden ser transmitidos a través de la red. Es sabido que, en regímenes de alta relación señal-a-ruido (SNR), la técnica de alineado de interferencias (IA) es óptima en términos de capacidad. En este sentido, el análisis se ha basado en un modelo de red general conocido en el ámbito de IA como *X network*. A pesar de que se trata de un modelo complejo, dicha red es posteriormente particularizada para dar soporte a las topologías en las que se centra la tesis. En este contexto, se ha desarrollado un algoritmo, basado en continuación homotópica, que

permite obtener soluciones de alineado para  $X$  networks con un número arbitrario de transmisores, receptores, antenas por nodo, e hilos de información. El hecho de que dicha técnica haya sido validada en diversas configuraciones de red permitirá posteriormente aplicarla para la evaluación del duplexado flexible.

Tras hacer una breve revisión del trabajo previamente disponible para redes de 2 celdas, en este trabajo se presentan condiciones necesarias para la aplicabilidad del alineado de interferencia en redes de múltiples celdas, con múltiples usuarios por celda que, adicionalmente, pueden demandar un número arbitrario de hilos de información. De dichas condiciones hemos podido extraer valiosas conclusiones en lo referente a la asimetría de este tipo de redes. Como se ha mencionado con anterioridad, las HetNets se caracterizan por una amplia diversidad en cuanto a topología de red y naturaleza de la información. Cabe destacar que, a juzgar por las condiciones necesarias para la aplicación de IA, los beneficios debidos al duplexado flexible en términos de DoF son especialmente significativos para redes con una asimetría pronunciada. Por el contrario, cuando la red es completamente simétrica (asemejándose a una red homogénea tradicional), las condiciones dejan de depender de la combinación UL/DL seleccionada, por lo que el duplexado flexible no aporta incremento alguno en los DoF. En resumidas cuentas, la heterogeneidad de la red juega un papel fundamental en el potencial del acceso por duplexado flexible. Dichas conclusiones analíticas han sido a su vez validadas numéricamente mediante la aplicación del algoritmo de continuación homotópica previamente presentado.

### **Tasa de transmisión**

Cuando se trata de estudios asintóticos, los DoF son una excelente métrica para caracterizar el comportamiento de los sistemas de comunicaciones bajo estudio. Sin embargo, en escenarios más prácticos, con unos valores de SNR de nivel medio, existen otras figuras de mérito más interesantes para cuantificar el rendimiento. Debido a ello, nos hemos centrado también en la tasa de transmisión a la hora de analizar los beneficios debidos a la implementación de duplexado flexible. Más específicamente, hemos abordado la optimización de la red para maximizar la tasa binaria, tanto en lo referente a los precodificadores y decodificadores, como en términos de selección de UL/DL. Dicho problema de optimización ha sido desacoplado en dos facetas. En primer lugar, la optimización de precodificadores y decodificadores para una configuración UL/DL fija. Dicha tarea se identifica directamente con la maximización de la relación señal-a-interferencia-más-ruido (SINR), la cual, a partir de un valor suficientemente elevado de SNR, se traduce en un problema de alineado de interferencia. Por otra parte, se plantea la necesidad de seleccionar la combinación UL/DL con mejor tasa de transmisión, lo que supone un problema combinatorial cuya solución óptima pasa por evaluar todos los posibles casos. Llevar a cabo la evaluación exhaustiva de todas y cada una de las posibles configuraciones UL/DL en la red tiene un elevado coste computacional. Además del incremento exponencial de dicha carga de cómputo con el número de celdas en la red, cabe destacar que cada evaluación supondría, en un principio, resolver un problema de alineado de interferencia. Con

el objetivo de aliviar la complejidad computacional, se ha recurrido a dos medidas fundamentales.

Por un lado, se propone una sencilla estrategia de búsqueda que permite reducir considerablemente el número de combinaciones UL/DL a evaluar en el proceso de selección. Pese a que se trata de un criterio subóptimo, los resultados de las simulaciones realizadas prueban que dicha aproximación produce resultados extremadamente cercanos a la solución óptima (búsqueda exhaustiva). En otras palabras, la pérdida de rendimiento por dicho criterio es despreciable, con la indudable ventaja de reducir significativamente la carga computacional del proceso.

Adicionalmente, se presenta una caracterización estadística de la tasa de transmisión media que puede alcanzarse mediante alineado de interferencia, dado que se eligiera una solución aleatoria de entre todas las posibles soluciones de alineado disponibles para una realización de canal concreta. En resumidas cuentas, dicha caracterización estadística permite aproximar la tasa binaria alcanzada para una combinación UL/DL dada, sin la necesidad de obtener explícitamente las matrices de precodificación y decodificación correspondientes.

Con esta considerable reducción en la complejidad del estudio, se aborda la comparación del impacto que el duplexado flexible tiene sobre distintas técnicas de procesamiento de interferencia. Más concretamente, se compara IA con una adaptación de la conocida técnica de mínimo error cuadrático medio (MMSE) al entorno de las redes celulares. Dicha estrategia recibe en la literatura la denotación de MMSE multi-celda (M-MMSE). Al ser M-MMSE la técnica más penalizada por la presencia de interferencias, es en este caso donde el duplexado flexible proporciona unos beneficios más notorios. No obstante, y como era de esperar, el rendimiento bruto obtenido por el conjunto IA + duplexado flexible demuestra ser notablemente superior al de M-MMSE.

### **Eficiencia energética**

Sobre los mismos escenarios que en el caso del análisis de tasa binaria, se aborda el estudio del duplexado flexible en lo referente a la potencia transmitida. En este contexto, buscamos optimizar, de nuevo, los precodificadores y decodificadores, así como la combinación UL/DL, con el fin de minimizar la potencia total que se requiere para satisfacer unas restricciones mínimas de calidad de servicio (QoS). Una vez más, las asimetrías de tráfico características en este tipo de redes son también tenidas en cuenta en la formulación del problema. Al igual que se hiciera previamente con la tasa de transmisión, el problema de minimización de potencia es desacoplado en dos tareas. Se presenta un algoritmo que, para una configuración UL/DL fija, permite optimizar las matrices de precodificación y decodificación. Dicho algoritmo puede ser aplicado para explorar distintas combinaciones UL/DL. Además, se sigue un criterio subóptimo de selección similar al adoptado previamente para la tasa binaria, reduciendo así de nuevo el coste computacional del problema. Los resultados obtenidos muestran dos principales fuentes de beneficio en términos de potencia transmitida. Por un lado, el algoritmo propuesto presenta un rendimiento superior a otros esquemas de minimización de potencia conocidos. Finalmente, la mejor combinación de

duplexado flexible muestra una eficiencia significativamente superior al acceso TDD convencional.

### **Evaluación experimental**

Por último, el estudio de los beneficios que potencialmente puede proveer la estrategia de duplexado flexible se cierra con la evaluación de dicha técnica mediante la transmisión de señales reales por el aire. Para dicho fin, se ha desarrollado una plataforma a pequeña escala en el laboratorio, formando una red de 3 celdas, incluyendo 1 macro-celda y 2 celdas de menor radio de cobertura. En dicho montaje experimental, se transmiten señales multiplexadas en subportadoras ortogonales (OFDM) replicando el formato habitual en los estándares de redes de área local. Análogamente al caso teórico, se compara el impacto del duplexado flexible sobre distintas técnicas de tratamiento de interferencia, a saber: IA, M-MMSE con transmisión por modo dominante (DET), y M-MMSE en recepción sin precodificación en el lado del transmisor. Cabe destacar que, pese a la existencia de trabajos experimentales previos en los que se aplica alineado ciego de interferencia (BIA) en tiempo real, este trabajo supone la primera implementación empírica de alineado de interferencia con precodificación y decodificación en tiempo real. En lo referente a la comparación entre los distintos esquemas de comunicación, IA muestra el mejor rendimiento en la mayoría de los regímenes de SNR y SINR considerados. Finalmente, los resultados obtenidos corroboran las conclusiones teóricas sobre los beneficios de implementar duplexado flexible en las redes bajo estudio.

# Notation and Acronyms

## Used Notation

$a$	Scalar (lowercase)
$\mathbf{a}$	Column vector (lowercase boldface)
$\mathbf{A}$	Matrix (uppercase boldface)
$\mathbf{A}^{-1}$	Inverse of square matrix $\mathbf{A}$
$\mathbf{A}^+$	Moore-Penrose pseudoinverse of matrix $\mathbf{A}$
$\mathbf{A}^T$	Transpose of matrix $\mathbf{A}$
$\mathbf{A}^H$	Conjugate transpose (Hermitian) of matrix $\mathbf{A}$
$\mathbf{A}^*$	Complex conjugate of matrix $\mathbf{A}$
$\text{Tr}(\mathbf{A})$	Trace of matrix $\mathbf{A}$
$\text{rank}(\mathbf{A})$	Rank of matrix $\mathbf{A}$
$\Re(a), \Im(a)$	Real and imaginary part of $a$
$ a $	Absolute value of $a$
$\ \mathbf{a}\ $	$\ell^2$ -norm of vector $\mathbf{a}$
$ \mathbf{A} $	Determinant of square matrix $\mathbf{A}$
$\ \mathbf{A}\ _F$	Frobenius norm of matrix $\mathbf{A}$
$\text{diag}(a_1, \dots, a_N)$	Diagonal matrix with elements $a_1, \dots, a_N$ along the main diagonal
$\text{vec}(\mathbf{A})$	Column-wise vectorization of a matrix $\mathbf{A}$
$[\mathbf{A}_1 \dots \mathbf{A}_N]$	Horizontal concatenation of matrices $\mathbf{A}_1, \dots, \mathbf{A}_N$
$\text{cat}_s(\mathbf{A}_s)$	Horizontal concatenation of the indexed matrices $\mathbf{A}_s$ where the members $s$ of the set $S$ are taken in reflected lexicographic order
$D\mathbf{G}(\mathbf{A})$	Jacobian of a matrix function $\mathbf{G}(\mathbf{A})$ at $\mathbf{A}$
$\Delta\mathbf{A}$	Increment in variable $\mathbf{A}$
$\mathbf{A}_{k,i:j}$	Horizontal concatenation of elements in row $k$ , columns $i$ to $j$ of matrix $\mathbf{A}$
$\mathbf{A}_{k:\ell,i}$	Vertical concatenation of elements in rows $k$ to $\ell$ , column $i$ of matrix $\mathbf{A}$
$\mathbf{A}_{k:\ell,i:j}$	Submatrix comprised of elements in rows $k$ to $\ell$ , columns $i$ to $j$ of matrix $\mathbf{A}$
$\text{ev}_{\max}(\mathbf{A})$	Maximum eigenvalue of square matrix $\mathbf{A}$
$\mathbf{A} \succeq \mathbf{B}$	Matrix $\mathbf{A} - \mathbf{B}$ is positive semidefinite
$\mathbf{A} \otimes \mathbf{B}$	Kronecker product of matrices $\mathbf{A}$ and $\mathbf{B}$

$\mathbf{A}^*$	Optimal solution of an optimization problem in the matrix variable $\mathbf{A}$
$\mathbf{I}_N$	$N \times N$ identity matrix (subscript is omitted when the dimension is self-evident)
$\mathbf{0}_{M,N}$	$M \times N$ zero matrix (subscript is omitted when the dimensions are self-evident)
$\mathbb{R}^{M \times N}$	Space of $M \times N$ real matrices
$\mathbb{N}^{M \times N}$	Ring of $M \times N$ integer matrices
$\mathbb{C}^{M \times N}$	Space of $M \times N$ complex matrices
$\stackrel{\text{def}}{=}$	Defined as
$\sim$	Distributed as
$\mathcal{CN}(\boldsymbol{\mu}, \boldsymbol{\Sigma})$	Multivariate circularly-symmetric complex Gaussian distribution with mean $\boldsymbol{\mu}$ and covariance matrix $\boldsymbol{\Sigma}$
$\text{Beta}(a, b)$	Beta distribution with shape parameters $a$ and $b$
$\Gamma(N)$	Gamma function of scalar $N$
$E[X]$	Mathematical expectation of random variable $X$
$\sigma_x$	Standard deviation of random variable $X$

## General symbol use and conventions

$G$	Number of cells in a cellular network
$K$	Number of users in a given interference channel
$M_k$	Number of transmit antennas of user $k$
$N_k$	Number of receive antennas of user $k$
$P_k$	Transmit power at transmitter $k$
$K_g$	Number of users in cell $g$
$G_d$	Number of downlink cells in a cellular network
$G_u$	Number of uplink cells in a cellular network
$G_m$	Number of macrocells in a multi-tier network
$G_s$	Number of small cells in a multi-tier network
$N_{BS}$	Number of antennas in a base station
$N_{AP}$	Number of antennas in an access point
$N_{UE}$	Number of antennas in a user equipment
$P_{BS}$	Transmit power at the base stations
$P_{AP}$	Transmit power at the access points
$P_{UE}$	Transmit power at the user equipments
$D_{kl}$	Number of streams from transmitter $\ell$ to receiver $k$
$D_k^{Rx}$	Total number of streams received at receiver $k$ such that $D_k^{Rx} = \sum_{\ell} D_{kl}$
$\mathbf{H}_{kl}$	Channel matrix between transmitter $\ell$ and receiver $k$ within a given network
$d_{kl}$	Distance from transmitter $\ell$ to receiver $k$
$\mathbf{U}_k$	Decoding matrix of transmitter $k$ ( $\mathbf{U}_i \in \mathbb{C}^{N_k \times D_k^{Rx}}$ )
$\mathbf{V}_{kl}$	Precoding matrix of transmitter $\ell$ for receiver $k$ ( $\mathbf{V}_{kl} \in \mathbb{C}^{M_{\ell} \times D_{kl}}$ )
$\mathbf{r}_k$	Received signal at receiver $k$
$t$	Homotopy continuation parameter
$a_g$	Uplink/downlink asymmetry parameter for cell $g$
$i_g$	Uplink/downlink indication variable for cell $g$
$\mathcal{P}_i$	Optimization problem

## Acronyms

3GPP	3rd generation partnership project
AP	Access point
AWGN	Additive white Gaussian noise
BC	Broadcast channel
BIA	Blind interference alignment
BS	Base station
CCDF	Complementary cumulative distribution function
CDMA	Code-division multiple access
CSI	Channel state information
DET	Dominant eigenmode transmission
DL	Downlink
DoF	Degrees of freedom
EVM	Error vector magnitude
FDD	Frequency-division duplex
FDMA	Frequency-division multiple access
FFT	Fast Fourier transform
FPGA	Field-programmable gate array
GDoF	Generalized degrees of freedom
GSVD	Generalized singular value decomposition
HC	Homotopy continuation
HetNets	Heterogeneous networks
HS	Hierarchical switching
IA	Interference alignment
IBC	Interference broadcast channel
IC	Interference channel
IL	Interference leakage
IMAC	Interference multiple-access channel
IoT	Internet of things
IRC	Interference rejection combining
ISM	Industrial, scientific and medical
LAN	Local area network
LT	Long-training
LTE	Long-term evolution
MIMO	Multiple-input multiple-output
MinIL	Minimum interference leakage
MISO	Multiple-input single-output
MMSE	Minimum-mean square error
M-MMSE	multi-cell minimum-mean square error
mmWave	Millimeter Wave
MUI	Multiuser interference
OFDM	Orthogonal frequency-division multiplexing
OTA	Over-the-air

PDF	Probability density function
PPP	Poisson point process
PPS	Pulse-per-second
QoS	Quality-of-service
QPSK	Quadrature phase-shift keying
R-TDD	Reverse time-division duplex
SDR	Software-defined radio
SF	Signal field
SIMO	Single-input multiple-output
SINR	Signal-to-interference-plus-noise ratio
SISO	Single-input single-output
SNR	Signal-to-noise ratio
SSH	Secure shell
ST	Short-training
SVD	Singular-value decomposition
TDD	Time-division duplex
TDMA	Time-division multiple access
TIN	Treating interference as noise
UE	User equipment
UHD	USRP hardware driver
UL	Uplink
USRP	Universal software radio peripheral
WARP	Wireless open access research platform
WSN	Wireless sensor network



# Contents

<b>Agradecimientos</b>	<b>ix</b>
<b>Abstract</b>	<b>xiii</b>
<b>Resumen extendido</b>	<b>xv</b>
<b>Notation and Acronyms</b>	<b>xix</b>
<b>Contents</b>	<b>xxvii</b>
<b>I Introduction and background</b>	<b>1</b>
<b>1 Introduction</b>	<b>3</b>
1.1 Scope . . . . .	4
1.2 Outline and contributions . . . . .	5
<b>2 Interference in multi-tier networks</b>	<b>11</b>
2.1 Fundamentals of interference management . . . . .	11
2.1.1 Interference channel . . . . .	12
2.1.2 Interference regimes . . . . .	13
2.1.3 Degrees of freedom . . . . .	14
2.1.4 Interference alignment in the interference channel . . . . .	16
2.2 Heterogeneous networks . . . . .	18
2.3 Flexible duplexing for multi-tier networks . . . . .	20
2.3.1 Degrees of freedom benefits . . . . .	21
2.3.2 Throughput benefits . . . . .	21
2.3.3 Power efficiency benefits . . . . .	22
<b>II DoF benefits of flexible duplexing in multi-cell networks</b>	<b>23</b>
<b>3 Network model and interference alignment</b>	<b>25</b>
3.1 System model and interference alignment . . . . .	25
3.1.1 X Network . . . . .	26
3.1.2 Interference alignment in X networks: Conditions and feasibility . . . . .	27
3.1.3 Particular network topologies . . . . .	28
3.2 Homotopy continuation . . . . .	33
3.2.1 The pentagon example . . . . .	33
3.2.2 Path tracking procedures . . . . .	35

3.3	HC-based algorithm for interference alignment . . . . .	37
3.3.1	Start system . . . . .	39
3.3.2	Implementation details . . . . .	40
3.3.3	Convergence analysis . . . . .	43
3.3.4	Simulation results . . . . .	44
<b>4</b>	<b>DoF analysis of flexible duplexing</b>	<b>51</b>
4.1	IA for flexible duplexing schemes . . . . .	51
4.2	IA feasibility for 2-cell networks . . . . .	53
4.3	Extension to multi-cell networks . . . . .	55
4.3.1	Necessary condition for the feasibility of IA . . . . .	56
4.3.2	Numerical evaluation and results . . . . .	57
<b>III</b>	<b>Optimization of flexible duplexing configurations</b>	<b>63</b>
<b>5</b>	<b>Sum-rate analysis of flexible duplexing</b>	<b>65</b>
5.1	Problem statement . . . . .	66
5.1.1	UL/DL selection by exhaustive search . . . . .	67
5.2	Statistical analysis of IA . . . . .	69
5.2.1	Average achievable rates . . . . .	73
5.2.2	Interference leakage characterization . . . . .	74
5.2.3	Average achievable rates for IA with flexible duplexing . . . . .	75
5.3	Determining the best UL/DL configuration . . . . .	77
5.4	Simulation results . . . . .	78
5.4.1	Hierarchical approaches for PPP distributed deployments . . . . .	79
5.4.2	IA vs M-MMSE . . . . .	80
<b>6</b>	<b>Power efficiency analysis of flexible duplexing</b>	<b>83</b>
6.1	System model . . . . .	83
6.1.1	Prior work for MISO downlink channels . . . . .	84
6.2	Power minimization in flexible duplexing networks . . . . .	86
6.2.1	MinPower-MaxSINR algorithm . . . . .	87
6.2.2	Determining the best UL/DL configuration . . . . .	88
6.2.3	Feasibility and complexity . . . . .	89
6.3	Simulation results . . . . .	90
<b>IV</b>	<b>Experimental analysis of flexible duplexing</b>	<b>93</b>
<b>7</b>	<b>Flexible duplexing experiments: context, setup and results</b>	<b>95</b>
7.1	An overview on interference alignment testbeds . . . . .	95
7.1.1	Highlights of testbed implementations . . . . .	97
7.1.2	Future directions . . . . .	101
7.2	Experimental evaluation of flexible duplexing . . . . .	103
7.2.1	Multiuser MIMO testbed . . . . .	104
7.2.2	Experimental setup . . . . .	105
7.2.3	Measurement methodology . . . . .	108
7.2.4	Experimental results . . . . .	109

---

<b>V Conclusion</b>	<b>115</b>
<b>8 Conclusions and further lines</b>	<b>117</b>
8.1 Conclusions . . . . .	117
8.2 Further lines . . . . .	119
<b>Appendices</b>	<b>121</b>
<b>A Proofs of the results in Part II</b>	<b>123</b>
A.1 Proof of Theorem 3.1 . . . . .	123
<b>Publications</b>	<b>125</b>
Publications derived from the dissertation . . . . .	125
Related work by the author . . . . .	127
<b>List of Figures</b>	<b>130</b>
<b>List of Tables</b>	<b>131</b>
<b>List of Algorithms</b>	<b>133</b>
<b>Bibliography</b>	<b>135</b>



Part **I**

**Introduction and background**



# Chapter 1

## Introduction

Over the last decade, spectrum availability has been one of the most relevant concerns for standardization bodies and manufacturers in the wireless communication landscape. As the commercial deployment of 5th generation of cellular networks approaches, the number of connected devices has increased exponentially, and the current predictions suggest that this progression will keep the same trend. Therefore, the next generation launch is expected to be the most paramount milestone since mobile data traffic surpassed mobile voice traffic in December 2009 [1]. To illustrate with some statistics, Ericsson have recently established that the number of mobile suscriptions was around 7.9 billion in early 2018, keeping the consistent growth of 4% from previous years [2]. This growth is even more remarkable when focusing on mobile broadband suscriptions, which have increased at 20% every year, achieving 5.5 billion in the first quarter of 2018. The two main sources of growth are expected to be the Internet of Things (IoT) and the previously mentioned 5G.

Cellular IoT is expanding rapidly, and by 2023, the number of connected devices is estimated around 3.5 billion due to the first large-scale deployment. In other words, the annual growth is rated at 30%, from which 2.2 billion will be located in North East Asia. Another point to take into account is that larger-scale deployments lead to high-volume chipsets, which are expected to reduce the production prices. The decrease in terms of costs will imply a further acceleration of the growth in cellular IoT connected devices.

On the other hand, and despite Long-Term Evolution (LTE) becoming the dominant mobile access technology by the end of 2017, the same year also witnessed the first 5G-related standardization with 3GPP Release-15 for Non-Standalone 5G New Radio (NR). With the Standalone version being initially scheduled on June 2018, the first 5G commercial launches are expected for mid-2019 in Japan, South Korea and Singapore. Additionally, global 5G network deployments are expected for 2020 with the second phase in Release-16. Notice that, following the same lines as in previous standards, new technologies have a low penetration of compliant devices at the very first launches. Nevertheless, the milestone of 1 billion 5G devices is listed to be achieved by 2023.

Regarding global data traffic, Cisco have measured an average of around 130 exobytes per month during 2018, which translates into a 30% growth with respect to 2017 (54% in terms of traffic from/to mobile devices [2]). This trend is predicted to

keep an exponential behaviour to reach up to 350 exobytes per month by 2022 [3]. Further, keeping track of this massive amount of users and their generated traffic presents economic and environmental concerns in terms of energy consumption [4] by the base stations. Also, the design of the devices is strongly dependent on the battery life requirements of communication standards and user satisfaction [5]. For this reason, power efficiency plays a relevant role in the spectrum usage profiles under consideration.

In this context, the spectrum scarcity question should be reconsidered to determine if the causes have been correctly identified. Recall that 5G has brought the shift to the millimeter wave (mmWave) bands, which do not overlap with previous mobile standards and allow for larger bandwidths. However, the conventional approaches to deal with interference in previous generations consisted of orthogonalizing the access, e.g., time-division multiple access (TDMA), frequency-division multiple access (FDMA) or code-division multiple access (CDMA), combined with frequency reuse. In other words, the main idea consisted of avoiding the interference, and treating the residual inter-cell interference due to frequency reuse as noise. In order to make an optimal use of the spectrum in the next generation of wireless networks, more efficient approaches to handle the interference are required. Significant benefits can be achieved in terms of both performance and energy consumption if we remember that interference is, by definition, *information*.

## 1.1 Scope

This thesis focuses on interference management and transceiver design for wireless heterogeneous networks (HetNets). This context encompasses a wide variety of network topologies and transmission techniques that can be analyzed regarding different figures of merit. Our goal in this work is studying some of the aforementioned topologies regarding several metrics, in order to provide a complete insight into the potential improvements that the next generation of mobile communications can achieve.

With a special emphasis on linear processing techniques for multiple-input multiple-output (MIMO) systems, our study puts the spotlight on techniques and schemes for flexible duplexing. More specifically, flexible duplexing consists of allowing the coexistence of uplink (UL) and downlink (DL) cells within the same time, frequency, and spatial domain. Different UL/DL combinations lead to different interference levels at the input of the receivers, hence providing different performance for each case. In these scenarios, a certain level of cooperation between the different devices in the network is required. On the one hand, channel state information (CSI) is assumed to be globally available in order to implement the aforementioned processing techniques. On the other hand, some performance metrics need to be globally known when selecting the optimal flexible duplexing configuration.

The first figure of merit that we study is the number of degrees of freedom (DoF) in the system, or equivalently, the number of independent, interference-free data streams that can be transmitted in the network. Even though DoF are an asymptotic

measure of system performance, this analysis allows us to envision the potential of flexible duplexing.

As previously remarked, DoF are a theoretical tool, and hence our journey towards realistic scenarios requires a more practical figure of merit to quantify the improvements that flexible duplexing is capable of providing. For this reason, we analyze the UL/DL selection in terms of sum-rate. Despite the fact that the number of streams that a system can handle is crucial, developers and manufacturers in the industry focus their research efforts on enhancing throughput. That being said, we take into consideration the service providers trends by considering typical traffic asymmetries in our models and algorithm design.

When accounting for the main concerns in real 5G implementations, one of the most important items in the list is power efficiency. In this thesis, we also address the study of flexible duplexing in terms of power. Together with the sum-rate analysis, investigating the impact of flexible UL/DL configurations on the required transmit power levels brings us a step closer to real-world implementation.

Finally, the aforementioned journey towards a real deployment brings this thesis from the theoretical models onto the laboratory. Specifically, we conduct an experimental evaluation of flexible duplexing with over-the-air (OTA) transmissions. With the hardware implementation of the previously studied models, we close the circle of our analysis, showing that remarkable benefits can be achieved when flexible UL/DL scheduling is enabled.

## 1.2 Outline and contributions

This dissertation is structured in five parts, namely: an introduction, three central parts with a detailed description of the technical content and contributions, and a final part summarizing the main conclusions and a brief reflection on the research lines to be considered as further work. In this section, we summarize the contents provided in each part:

- Part I places this thesis in the context of next-generation wireless communications. Chapter 1 presents the main spotlights of this work, and Chapter 2 introduces the background and the state-of-the-art.

Additionally, Chapter 2 includes a brief review on the interference management basics. The fundamental interference regimes are explained, and concepts such as the DoF are defined. Furthermore, we provide a description of the heterogeneous networks of interest, and the main characteristics of such topologies are depicted from a general perspective. Further details on how to deal with interfering signals in these scenarios are the focus on Part II, where a DoF analysis is made.

We provide some insights into practical aspects of heterogeneous networks and how the most general model is usually particularized for more realistic models. Additionally, some figures of merit such as sum-rate and transmit power, which

are preferred in practice, are mentioned and related to the networks under study. Both rate and power optimization, relying on an appropriate selection of the UL/DL combinations for a given system, are the topic to be addressed throughout Part III.

- As mentioned above, Part II provides an analysis on the DoF benefits associated to flexible duplexing in multi-cell HetNets. More specifically, different UL/DL settings can handle a larger number of interference-free data streams for a given network topology, and therefore significant benefits can be achieved with respect to conventional time-division duplex (TDD).

Chapter 3 describes the X network, a general system model that encompasses multi-cell networks among other particular topologies. Also, the main ideas associated to the interference alignment (IA) technique in this scenario are explained. An homotopy continuation-based algorithm to design the IA precoders and decoders is proposed and described in detail, and simulation results for general X networks validate the performance of the presented method. This chapter has produced the following publications:

- [6] J. Fanjul, Ó. González, I. Santamaria and C. Beltrán, “Homotopy continuation for spatial interference alignment in arbitrary MIMO X networks,” *IEEE Transactions on Signal Processing*, vol. 65, no. 7, pp. 1752-1764, Apr. 2017.
- [7] Ó. González, J. Fanjul and I. Santamaria, “Homotopy Continuation for Vector Space Interference Alignment in MIMO X Networks,” in *Proceedings of the International Conference on Acoustics, Speech and Signal Processing (ICASSP)*, Florence, Italy, May. 2014, pp. 6232-6236.

Chapter 4 presents a DoF study of flexible duplexing for HetNets with multiple users per cell. First, a test for the feasibility of interference alignment (IA) for a 2-cell setup is reviewed. The test is afterwards generalized to multi-cell networks with a single reversed cell. Finally, the homotopy continuation IA algorithm is applied as a numerical approach to evaluate the DoF benefits of flexible duplexing in the HetNets of interest. This chapter has produced the following publication:

- [8] J. Fanjul and I. Santamaria, “On the spatial degrees of freedom benefits of reverse TDD in multicell MIMO networks,” in *Proceedings of the European Signal Processing Conference (EUSIPCO)*, Budapest, Hungary, Aug. 2016, pp. 1363-1367.
- Since DoF is a theoretical measure that can be viewed as a proxy for the network capacity, Part III takes a step closer to realistic scenarios by studying flexible duplexing in terms of sum-rate and power efficiency. In this part, we assume that small-cell deployments handle the intra-cell interference internally. As a

consequence, each cell includes a single active user per channel use, hence simplifying our theoretical model to the management of inter-cell interference.

Chapter 5 focuses on the sum-rate aspect of the flexible duplexing approach. A statistical analysis for the average sum-rate achievable by IA is included. The approximation is further enhanced to support IA with imperfect channel knowledge, thus characterizing the impact of interference leakage on the achievable rates. The statistical approximation is applied to the rate analysis of flexible duplexing taking into account the typical traffic asymmetries in cellular networks, i.e., with a higher emphasis for downlink throughput. The problem of selecting the optimal UL/DL combination is addressed, and suboptimal approaches are considered in order to obtain a selection criterion with a reduced computational cost. This chapter has produced the following publications:

- [9] I. Santamaria and J. Fanjul, “Statistical analysis of single-beam interference alignment schemes,” in *Proceedings of the International Workshop on Signal Processing Advances in Wireless Communications (SPAWC)*, Edinburgh, UK, Jul. 2016.
- [10] J. Fanjul and I. Santamaria, “Flexible duplexing for maximum downlink rate in multi-tier MIMO networks,” in *Proceedings of the Telecommunications Forum (TELFOR)*, Belgrade, Serbia, Nov. 2018.

Chapter 6 replicates the study for the same scenarios as in Chapter 5, but in terms of total transmit power. The problem to be addressed in this sense is finding a configuration that minimizes the total transmit power in the network. Again, we have taken into account typical asymmetries when prioritizing downlink power vs. uplink. An algorithm is proposed to minimize total transmit power for a given UL/DL combination. By means of the developed algorithm, the different UL/DL settings in the network are explored, and a selection of the optimal solution is made. As in the case of the sum-rate analysis, we propose a suboptimal approach to reduce the computational cost of UL/DL selection. This chapter has produced the following publication:

- [11] J. Fanjul and I. Santamaria, “Power minimization in multi-tier networks with flexible duplexing,” in *Proceedings of the International Conference on Acoustics, Speech and Signal Processing (ICASSP)*, Brighton, UK, May. 2019.
- Part IV represents a step towards practical implementation, since we evaluate the potential benefits of flexible UL/DL scheduling in an experimental testbed with OTA transmissions. Despite interference alignment being impaired by several mismatches in practice, we rely on previous advances in the matter to build a small-scale representation of a 3-cell network. In this scenario, we evaluate the benefits of flexible duplexing for different communication schemes including IA-based techniques.

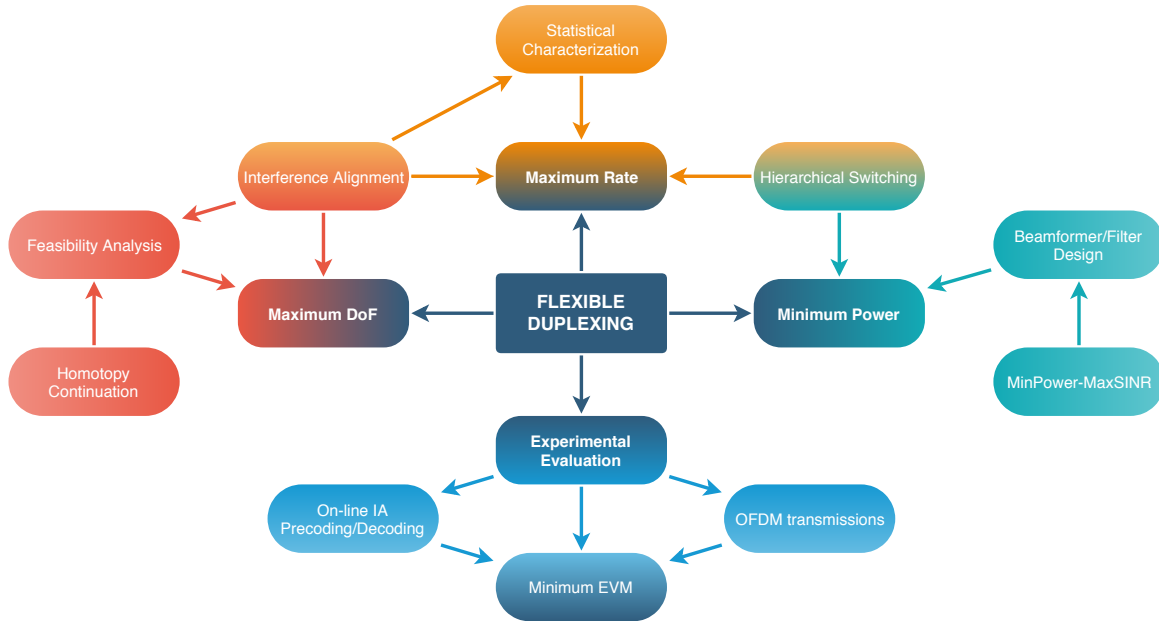


**Figure 1.1:** Relationship between flexible duplexing and the different concepts analyzed in this thesis.

Chapter 7 reviews previous advances on practical implementations of IA, including some aspects about equipment and cost. We reflect on the main challenges when applying IA in realistic systems, as well as the future directions to be explored. The content of Chapter 7 then focuses on a detailed description of the hardware and software tools that we have used throughout our experiments. The characteristics of the network and the frame format are included, together with the methodology that we have followed during the measurement campaign. The chapter is closed with a selection of the obtained experimental results and a discussion on the main conclusions after the experiments. This chapter has produced the following publications:

- [12] C.M. Yetis, J. Fanjul, J.A. García-Naya, N.N. Moghadam and H. Farhadi, “Interference alignment testbeds,” *IEEE Communications Magazine (Com-Mag)*, vol. 55, no. 10, pp. 120-126, Oct. 2017.
- [13] J. Fanjul, R.D. Fernández, J. Ibáñez, J.A. García-Naya and I. Santamaria, “Experimental evaluation of flexible duplexing in small cell multi-tier MIMO networks,” submitted to *EURASIP Journal on Wireless Communications and Networking*.
- [14] J. Fanjul, C. Lameiro, I. Santamaria, J.A. García-Naya and L. Castedo, “An experimental evaluation of broadband spatial IA for uncoordinated MIMO-OFDM systems,” in *Proceedings of the International Conference on Digital Signal Processing (DSP)*, Singapore, Jul. 2015, pp. 570-574.

- Finally, Part V presents the conclusion of the thesis, including future research lines. The main concepts that we have studied throughout this work are illustrated in Fig. 1.1.



# Interference in multi-tier networks

All wireless communication systems have an important aspect in common: multiple users accessing the same service must share the propagation medium. When those user equipments work within the same time, frequency, and spatial domains, their corresponding signals are mixed. This phenomenon is known as *interference*.

All throughout the history of radio and wireless communications, interference has been typically handled in a passive manner. If the level of unintended signals is sufficiently lower than the desired signal, interference is assumed to be harmless for the performance of our system. On the contrary, if the magnitude of such interference is comparable to the desired signals, sharing the access medium is conventionally avoided by orthogonalizing the radio resources. For higher interference levels, in addition, it is possible to decode the interfering signals, then subtract them from the desired message.

The orthogonalization approaches mentioned above lead to an unefficient use of the radio spectrum. Therefore, more advanced techniques are required for the sake of an improved spectral efficiency. This chapter reviews the fundamental concepts related to interference management and how cooperation between users can enhance the performance of next-generation communication systems. Section 2.1 describes the interference channel (IC), and displays the different interference regimes that can be found in wireless networks. Additionally, the DoF are presented as a theoretical approximation for the number of independent data streams that can be transmitted in such deployments. Also, a brief introduction to the concept of interference alignment is provided. For further purposes, small-cell multi-tier networks are described in Section 2.2 and the flexible duplexing approach is introduced in Section 2.3.

## 2.1 Fundamentals of interference management

In the modern era of communications, most of the wireless and cellular networks standards were developed to avoid that the magnitude of the interference reaches that of the desired signals. Interference avoidance is conventionally achieved by orthogonalization of the radio resources, either in the time domain (TDMA) or in the frequency domain (FDMA). Orthogonalization approaches combined with frequency

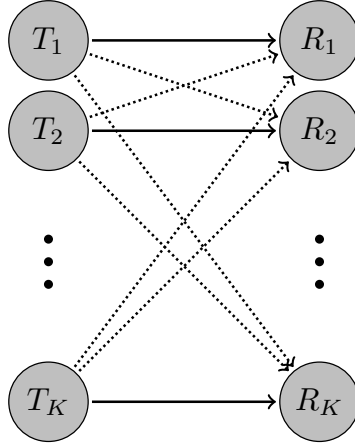


**Figure 2.1:** Interference channel. Solid line arrows represent desired information, and dashed line arrows are associated to interference.

reuse guarantee that the interference level is low enough to treat interference as noise.

However, treating interference as noise (TIN) is not optimal in general scenarios. Whereas noise has, by definition, a random nature, interference is in essence information, even though it is intended for another receiver. Therefore, important knowledge about the interfering signals can be exploited by allowing *cooperation* between the different users in the wireless network. The aforementioned cooperation may require channel state information sharing, or splitting the messages into public and private parts [15, 16], among others.

### 2.1.1 Interference channel

The MIMO interference channel model is of utmost importance in the study of interference in wireless networks. Due to its simplicity with respect to other topologies, the IC has attracted significant attention. In this section, we briefly describe the system model, whereas further details can be found in Chapter 3.

A  $K$ -user IC is comprised of  $K$  transmitter/receiver pairs, as depicted in Fig. 2.1. Each transmitter  $k$  is equipped with  $M$  antennas and wishes to send  $d_k$  independent data streams to its corresponding  $N$ -antenna receiver. In addition, we are assuming that a linear precoding/decoding scheme is implemented. In this regard,  $\mathbf{V}_k \in \mathbb{C}^{M \times d_k}$  represents the precoding matrix applied at transmitter  $k$ , whilst  $\mathbf{U}_k \in \mathbb{C}^{N \times d_k}$  is the decoder for the  $k$ -th receiver. Consequently, since all users share the propagation medium, the desired signals at each receiver are mixed with those from the rest of the users. Therefore, the signal at the input of receiver  $k$  is given by

$$\mathbf{r}_k = \mathbf{U}_k^H \left( \mathbf{H}_{kk} \mathbf{V}_k \mathbf{s}_k + \sum_{\ell \neq k} \mathbf{H}_{k\ell} \mathbf{V}_\ell \mathbf{s}_\ell + \mathbf{n}_k \right), \quad (2.1)$$

where  $\mathbf{s}_k \in \mathbb{C}^{d_k}$  contains the information that transmitter  $k$  is sending to receiver  $k$ ,  $\mathbf{H}_{k\ell} \in \mathbb{C}^{N \times M}$  is the flat-fading MIMO channel from transmitter  $\ell$  to receiver  $k$  and  $\mathbf{n}_k \in \mathbb{C}^N$  is the additive white Gaussian noise (AWGN) at receiver  $k$ . Finally, depending on the ratio between the desired signal level and the interference at the input of the receivers, we can distinguish different regimes, as briefly described below in Section 2.1.2.

### 2.1.2 Interference regimes

As mentioned previously, knowledge about the interfering signals can be exploited to enhance the system performance. A crucial aspect in this sense is the ratio between the magnitudes of interference and desired signals. For each different regime, a variety of approaches can be considered to handle interference in an efficient manner. We summarize the main possible situations as follows:

- **Weak interference:** The energy of the unintended signals is negligible with respect to the desired signal magnitude. Therefore, interference may be treated as noise with no impact on performance [17], and single-user schemes are sufficient. Despite being a counterintuitive approach from an information theoretic standpoint, treating interference as noise (TIN) has been applied for years in cellular networks with frequency-reuse. Theoretical validations of TIN for the weak interference regime can be found in [18, 19, 17, 20].
- **Strong interference:** Interfering signals with a strong presence at the receiver bring an unexpected advantage: their interference-to-noise ratio is sufficient for them to be decoded and cancelled. In cases with a strong interference level, the unintended signals can be decoded and then subtracted from the signal of interest in order to retrieve the desired message. For the standard 2-user IC, the capacity in the high-interference regime is known [21, 22, 23]. However, the capacity in the presence of strong interference is still unknown for more general topologies, such as the heterogeneous networks on which this thesis is focused.
- **Moderate interference:** As in the previous case with strong interference, closed-form expressions to characterize the performance of the HetNets under study are not available in the literature. However, remarkable results have been already published for the IC, with a special mention to the well-known Han-Kobayashi scheme in [15]. This scheme is further applied in [24, 16] with optimal results, but extensions to more general settings and topologies have been discarded for optimal capacity in such scenarios. In cases with a general number of users and a single data stream per user, a simple approach that could be applied is the interference rejection combining (IRC) scheme [25]. The IRC method can be seen as an adaptation of the minimum-mean square error (MMSE) technique that takes into account the knowledge of the channels

from interferers to the intended receiver. This strategy is also known as multicell MMSE (M-MMSE) in the literature [26, 27], and is based on receiving filters given by

$$\mathbf{u}_k^{M-MMSE} = \mathbf{w}_k^H \hat{\mathbf{H}}_{kk}^H \left( \hat{\mathbf{H}}_{kk} \mathbf{w}_k P_k \left( \frac{d_{kk}}{d_0} \right)^{-\alpha} \mathbf{w}_k^H \hat{\mathbf{H}}_{kk}^H + \mathbf{R}_k + \sigma_k^2 \mathbf{I} \right)^{-1} \quad (2.2)$$

where  $\mathbf{w}_k \in \mathbb{C}^{N \times 1}$  is the precoding vector at the  $k$ -th transmitter,  $P_k$  is the transmit power, and  $\mathbf{R}_k = \sum_{\ell \neq k}^K \hat{\mathbf{H}}_{k\ell} \mathbf{w}_\ell P_\ell \left( \frac{d_{k\ell}}{d_0} \right)^{-\alpha} \mathbf{w}_\ell^H \hat{\mathbf{H}}_{k\ell}^H$  is the covariance matrix of the inter-cell interference. The estimated channel from transmitter  $\ell$  to receiver  $k$  is denoted by  $\hat{\mathbf{H}}_{k\ell}$ ,  $d_{k\ell}/d_0$  is the corresponding normalized pairwise distance, and  $\alpha$  is the path-loss exponent. Finally,  $\sigma_k^2$  stands for noise variance.

Once we have described the main interference regimes that can be found in practice, it is worth mentioning that the moderate interference regime is the most common among wireless communication systems, thus this case will be the main focus of this dissertation.

### 2.1.3 Degrees of freedom

As first introduced in [28, 29], the channel capacity in the presence of additive white Gaussian noise, as a function of the signal-to-noise ratio (SNR), is expressed as

$$C(\text{SNR}) = D \log_2(\text{SNR}) + o(\log_2(\text{SNR})). \quad (2.3)$$

The pre-log factor  $D$ , known as degrees of freedom (DoF), characterizes how the capacity scales with the SNR. From (2.3), we can define the DoF as

$$D = \lim_{\text{SNR} \rightarrow \infty} \frac{C(\text{SNR})}{\log_2(\text{SNR})} \quad (2.4)$$

The definition of the capacity given by (2.3) can be extended to a  $K$ -user scenario. In such cases, instead of a scalar, the capacity must be regarded as a  $K$ -dimensional region, defined by the achievable rates tuples

$$\mathcal{R} = \{R_1(\text{SNR}), R_2(\text{SNR}), \dots, R_K(\text{SNR})\}, \quad (2.5)$$

where  $R_k(\text{SNR})$  denotes the rate achieved by the  $k$ -th user. The sum-rate achieved at any point of the capacity region is

$$R_{\text{sum}} = \sum_k R_k.$$

Moreover, when working at high-SNR regimes, we can approximate the sum-rate as  $D \log_2 \text{SNR} + r$  with

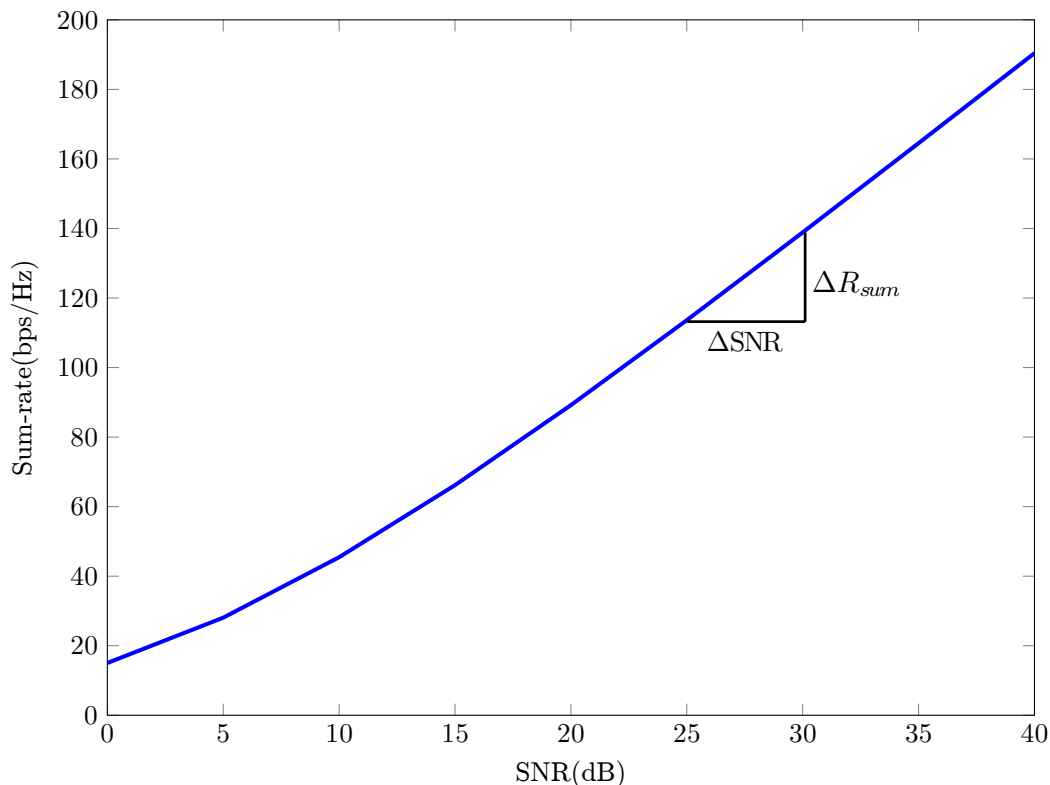


**Figure 2.2:** Relationship between SNR and DoF.

$$r = \lim_{\text{SNR} \rightarrow \infty} R_{sum} - D \log_2 \text{SNR}. \quad (2.6)$$

As illustrated in Fig. 2.2,  $r$  denotes the rate offset of the high-SNR asymptote of the achievable rate, whereas the pre-log factor  $D$  given by (2.4) is the sum-rate slope at high-SNR. Therefore,  $D$  corresponds to the number of independent, interference-free data streams that can be handled in the network. Further definitions on the concept of DoF are provided in [30] and [31].

In addition, noticeable research efforts have been focused on a generalization of the DoF called the generalized degrees of freedom (GDoF). As we can observe from (2.4), (2.5) and (2.6), the DoF are defined with a normalized SNR for all users. The GDoF are an extension of the concept of DoF, considering different SNR values for the different users in the system. Remarkable results on the GDoF optimality of TIN in interference networks can be found in [20, 32, 33, 34, 35]. More recently, GDoF characterizations of networks with imperfect channel estimates have been addressed in [36, 37, 38].

### 2.1.4 Interference alignment in the interference channel

The  $K$ -user interference channel has attracted significant research interest, and the DoF characterization of the IC has been one of the most popular topics over the last decade. In this scenario, we can straightforwardly state that orthogonalization-based approaches can only allocate a  $1/K$  portion of the access resources. However, authors in [39] proved that the optimal DoF per user in such scenarios is  $1/2$ , and that this optimal amount is achieved by means of interference alignment.

The main idea behind interference alignment is to transmit the signals in such a way that they remain confined in a dimensionality-reduced subspace at the unintended receivers, whilst being still distinguishable at the desired receivers. In the general case, this level of cooperation requires a global CSI knowledge for all nodes in the network. For a better understanding, authors in [39] illustrate their result with the *half-the-cake* analogy in the interference channel. They consider the total network resources as a cake to be shared by all users in the system. When relying on orthogonal access, every user gets a  $1/K$ -size piece of cake. Equivalently, the sum-DoF will be always 1 regardless of how large the number of users grows. However, when applying IA, every user gets half of the cake. This translates into a total of  $K/2$  sum-DoF, or in other words, the total number of data streams in the network grows linearly with the amount of active users. The result is stated for the asymptotic case where an infinite number of symbol extensions are allowed.

Applying the main intuition above to the MIMO signal model (2.1) in Section 2.1.1, we can write the IA conditions as

$$\mathbf{U}_k^H \mathbf{H}_{k\ell} \mathbf{V}_\ell = \mathbf{0}, \quad \forall k, \ell \neq k \quad (2.7a)$$

$$\text{rank} \left( \mathbf{U}_k^H \mathbf{H}_{kk} \mathbf{V}_k \right) = d_k, \quad \forall k, \quad (2.7b)$$

where condition (2.7a) describes the interference cancellation requirements, whereas (2.7b) ensures the preservation of the desired signals.

Even before V. Cadambe and S.A. Jafar introduced the applicability of IA to interference channels [39], the first studies originated out in [40, 41]. Specifically, overlapping interfering signals onto a common subspace was proposed for the 2-user X channel with  $M$ -antenna nodes. Whereas  $M$  maximum DoF could be attained in the 2-user IC [42],  $\lfloor 4M/3 \rfloor$  DoF are achieved in the case of the 2-user X channel. Shortly afterwards, the first closed-form solution for perfect alignment is provided in [43] by means of linear beamforming at the transmitters combined with zero forcing at the receiver end. The solution in [42] is further applied for performance evaluation in [44]. In parallel, the first advances are made for the multiple-input single-output (MISO) broadcast channel (BC) [45], and already in 2008, Jafar and Shamai are the first researchers using the denomination of *interference alignment* when referring to this technique [46].

Once the path was set by the literature above, the results were extended to the  $K$ -user IC in [39]. Since then, a large number of IA algorithms have been proposed for the IC when the channels are generic, which happens for instance when the channel

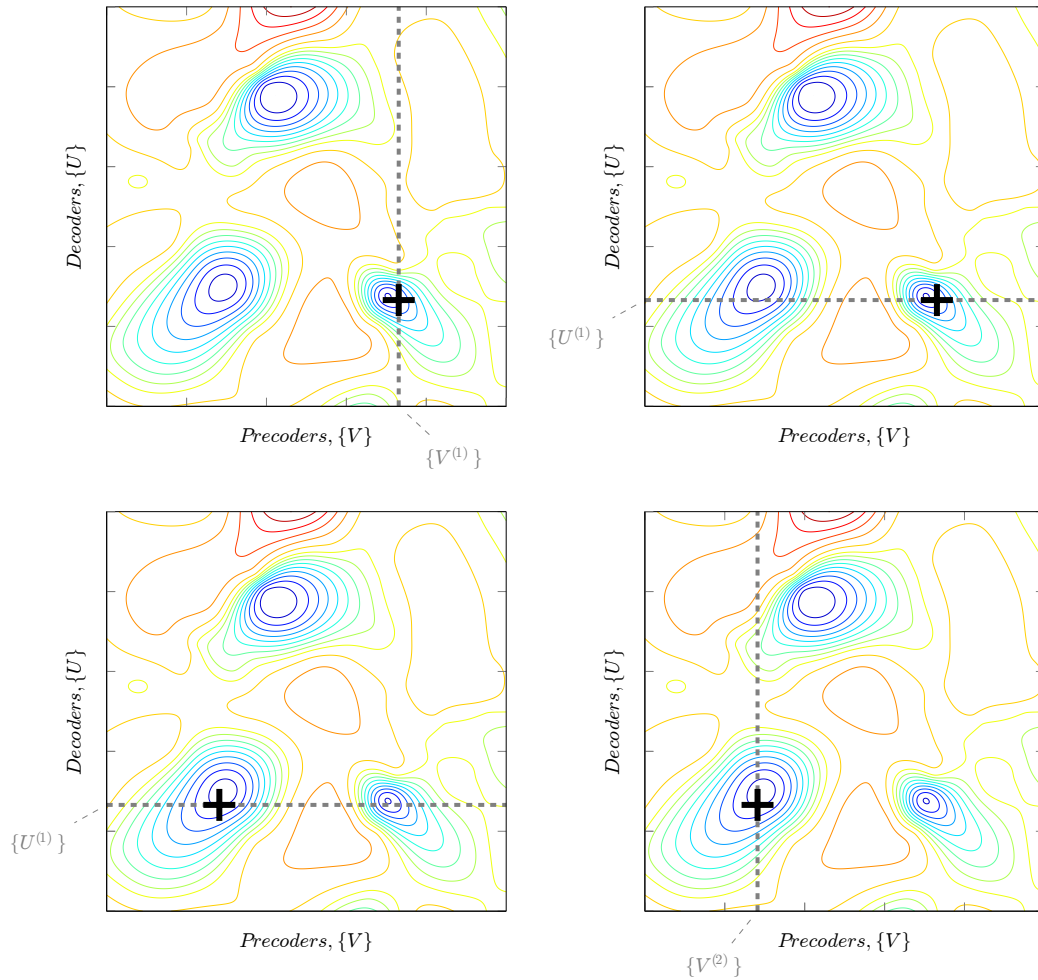


**Figure 2.3:** MinIL for the calculation of IA solutions.

coefficients are drawn from a continuous distribution and hence the MIMO channel matrices have no particular structure. Widely known examples are the alternating minimization algorithm in [47, 48], as well as the rank minimization method in [49]. The alternating minimization algorithm, which is used for comparison throughout this work, is described at the end of this section. Many other algorithms using different cost functions (mean-squared error, average sum-rate) [50, 51], or applying different optimization criteria have been proposed for this particular network topology [52, 53, 54, 55]. More recently, a Gauss-Newton IA method was proposed in [56] to improve the convergence speed of previous approaches.

### Interference alignment via alternating minimization

The alternating minimization algorithm in [48], also known as minimum interference leakage (MinIL) in the literature, has been extensively used in IA research due to its

simplicity. The main idea behind this method consists of minimizing the interference leakage (IL) given by

$$\text{IL} = \sum_{\ell \neq k} \left\| \mathbf{U}_k^H \mathbf{H}_{k\ell} \mathbf{V}_\ell \right\|^2 \quad \forall k, \ell \neq k. \quad (2.8)$$

In other words, the MinIL scheme intends to satisfy conditions (2.7a). For this purpose, the decoding matrices  $\{\mathbf{U}_k\}$  are calculated for a set of fixed precoders  $\{\mathbf{V}_k\}$  to minimize the cost function in (2.8). The resulting  $\{\mathbf{U}_k\}$  are then fixed and a new set of precoders  $\{\mathbf{V}_k\}$  is obtained. This alternating sequence is repeated iteratively, as illustrated in Fig 2.3.

In the case of the IC with generic channels (no symbol extensions), conditions (2.7b) are automatically satisfied as long as constraints (2.7a) hold, and the precoders  $\{\mathbf{V}_k\}$  and decoders  $\{\mathbf{U}_k\}$  are full-rank. However, as we will discuss in Chapter 3, this is not true for more sophisticated network topologies, and therefore more advanced algorithms are required in order to satisfy the whole set of IA conditions, i.e., both (2.7a) and (2.7b).

## 2.2 Heterogeneous networks

As aforementioned, the requirements for the different generations in the history of wireless communication have followed an exponential growth. Consequently, the nature of information and services has evolved together with the size and features of the corresponding user devices. This state of affairs has been dramatically emphasized over the last decade, with data traffic overpassing voice traffic in 2009 and the whole diversity that data communication has generated during the LTE era. For this reason, conventional topologies no longer reflect the model of a contemporary wireless communication network [57].

Providing services such as high-quality video streaming or real-time car-to-car communication requires high data transmission rates and reliability. Such rates inevitably translate into more stringent radio requirements, especially in terms of spectrum allocation. Together with the diversity of user size, transmit power (with possible battery life constraints) and hierarchy, the need for more efficient topologies arises when taking the leap towards the 5-th generation of mobile networks. On top, not only user equipments are evolving, but base stations and access points are getting smaller and less expensive in infrastructure terms. In this sense, several cell sizes had been already considered for 4G, depending on the coverage range and transmitted power, among other features [58]:

- **Macrocells:** The conventional cell for mobile communication, with base station transmitting up to 20W and a coverage range from 1 to 20km. Macrocells usually serve roaming devices.
- **Microcells:** Conventional base stations transmitting 1 to 5W and covering 500m to 2km. This hierarchy level is usually assigned to slow traffic, such

as pedestrian and indoor users. The microtier can be subsequently classified as:

- **Hot Spots:** These areas usually correspond to small, crowded places, with high traffic demands.
  - **Downtown clustered microcells:** Dense urban areas with pedestrian and mobile users. Antennas in such cases are considerably below building height.
  - **In-Building, 3-D cells:** Associated to office buildings in most cases. These coverage areas are characterized by a high user density, as well as strict power consumption constraints.
- **Picocells:** This cell sub-class works with small-scale versions of a base station, having user equipment-sized access points. Picocells are commonly used to enhance voice and data capacity with limited cost, hence being suitable for special events such as conferences or conventions. Additionally, picocells are used to extend the coverage range to indoor environments where outdoor signals cannot reach the in-building users.
  - **Femtocells:** Suitable for home and small business. Access points in femtocells are usually connected via cable to a provider backhaul, and extend the provider service coverage to the indoor environment. As in the case of picocells, this task is necessary when direct access to the outdoor signal coverage is limited. The main benefits of femtocells are:
    - The capacity is increased, since the short-distance links between the users and the access points allow for high signal-to-interference-plus-noise ratio (SINR).
    - Short distance additionally translates into lower transmit power levels, which not only reduces interference, but also contributes to extend the battery life of the wireless devices.
    - As cell size is reduced, the number of users per cell is limited. Therefore, femtocells directly address the spectrum scarcity problem and each user has access to a larger portion of the total bandwidth.

As we will describe in the subsequent chapters, the hierarchical structure of Het-Nets provides significant gains such as improved quality of service (QoS) and remarkable benefits in terms of power efficiency. Also, despite the diversity that the concept of HetNets encompasses, in this thesis we specifically focus on multi-tier networks, that is, we analyze how the different hierarchy levels in the network (e.g. macrocells, picocells, etc) may be taken into account in order to enhance the system performance.

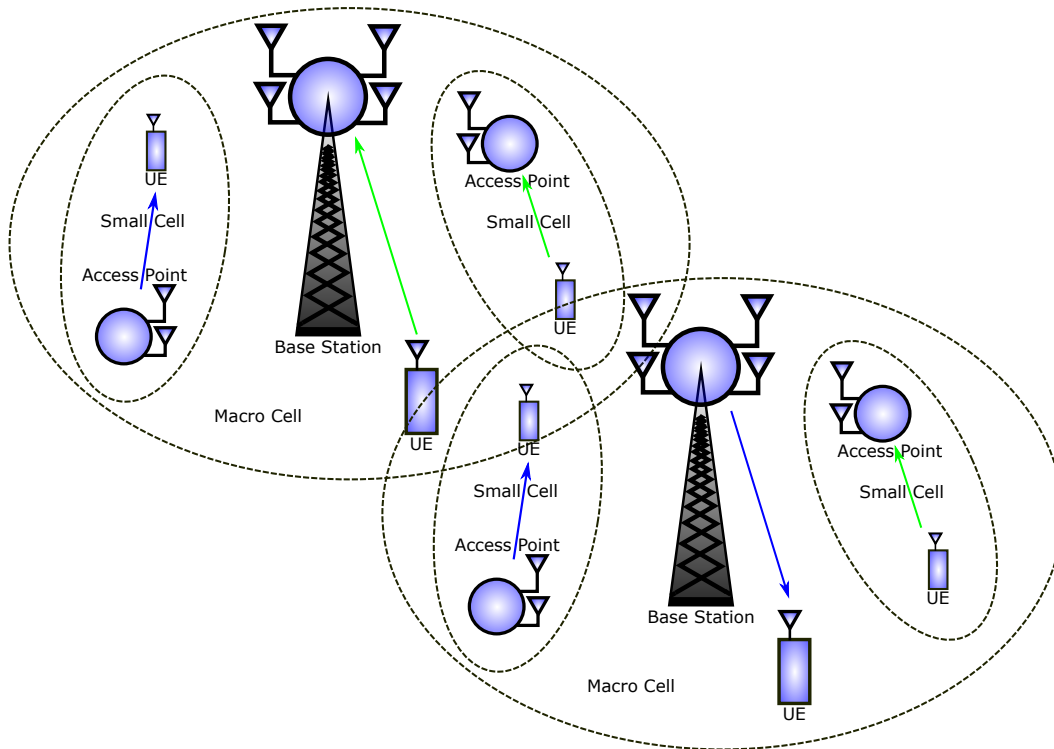


Figure 2.4: 2-tier heterogeneous network implementing flexible duplexing.

### 2.3 Flexible duplexing for multi-tier networks

With the advances in terms of network topology and the deployment of HetNets, several technologies have been proposed in order to address the increasingly demanding features of mobile communications to come. Searching for larger bandwidths, one of the most important changes has been the shift to the mmWave band [59, 60]. Also, advances in MIMO communications has evolved towards devices with a larger amount of antennas (massive MIMO). Besides discussing on efficient applications of massive MIMO, authors in [61] are among the first considering the following question: *Why have we always set all cells in the network either in uplink or in downlink synchronously?* In other words, *why not allowing some of the cells to be in UL, while the rest of them are set in DL mode?* The flexible duplexing access technique, also known as reverse time-division duplex (R-TDD) [62] or dynamic-TDD [63] in the literature, is the answer to this question. The main idea consists in allowing the coexistence of uplink and downlink cells within the same time and frequency slots. Each UL/DL combination generates different interference levels at the receivers, hence having an impact on QoS. This technique plays an important role when focusing on multi-tier networks, where the different hierarchy levels may establish different access approaches. A representation of a 2-tier network implementing flexible duplexing is depicted in Fig. 2.4.

In [61], authors consider a fixed R-TDD scheme for a 2-tier HetNet, and evaluate the potential performance benefits with respect to conventional TDD. Afterwards, several studies on the benefits of flexible duplexing have been recently carried out, most of them, as in [61], assuming that a fixed UL/DL combination is given. In the following, we provide a brief review of the prior works that have been carried out, distinguishing three different performance metrics.

### 2.3.1 Degrees of freedom benefits

Regarding the DoF performance of flexible duplexing in cellular systems, the number of existing works in the literature is still scant. Nevertheless, authors in [64] present an analysis of 2-cell MIMO networks when IA is applied. They provide a necessary condition and a sufficient condition for the feasibility of IA in such scenarios. Additionally, an IA algorithm is proposed to calculate the precoding and decoding matrices at the corresponding base stations and user equipments. The algorithm is a combination of a closed-form solution for a subset of the equations, together with an adaptation of the MinIL technique for the rest of the alignment conditions.

Part II in this thesis is dedicated to the evaluation of the potential DoF benefits that flexible duplexing provides in generic multi-cell networks. We review the main results in [64] for 2-cell networks, and we present sufficient conditions for multi-cell mobile systems. The impact of network asymmetry in the DoF improvement achieved by flexible duplexing is studied, and we provide numerical validation of the presented results.

### 2.3.2 Throughput benefits

Although the study of flexible duplexing is recent, some existing works address the analysis of the potential improvements in terms of data rate. In [65], 2-tier networks are considered and the rate benefits when the small cells are reversed with respect to the macro-tier are investigated. Also, the authors provide additional results regarding coverage probability and spectral efficiency.

On the other hand, the number of works addressing the task of finding the best UL/DL combination is still scarce. Nevertheless, a joint user scheduling, precoding and UL/DL selection framework is presented in [66]. The complete analysis provided in [66] covers user scheduling, the design of the precoders, and the selection of the UL/DL configuration at each cell. The presented framework also takes into account the traffic asymmetries for a better characterization of the flexible TDD schemes intended for 5G mobile communications. Finally, the authors conclude that the throughput gains are more significant for high interference regimes with a reduced number of antennas per node.

In Chapter 5, we follow the same line as in [65] and study the rate improvements achieved by means of flexible duplexing in 2-tier networks. Unlike [65], where all the small cells were simultaneously reversed with respect to the macrocell, we allow

generic UL/DL combinations. In addition, we propose suboptimal approaches in order to reduce the computational cost of UL/DL selection.

### 2.3.3 Power efficiency benefits

Regarding power efficiency, most of the works are still focused on orthogonal TDD access techniques [67, 68, 69, 70, 71]. However, a power optimization method with flexible UL/DL sets is provided in [72]. The particular aspect about this work is that full-duplex base stations are considered, unlike most of the existing works considering independent UL/DL slots for all the nodes in the network. Afterwards, authors in [73] analyze the coexistence of UL and DL cells in terms of downlink transmit power. Specifically, the frequency-division duplex (FDD) uplink band may be used for downlink transmission. In this scenario, a closed-form solution is proposed for downlink power control. Finally, a remarkable study is performed in [74], where a variation of flexible duplexing called  $\alpha$ -duplex is introduced. In this model, a partial bandwidth overlap is allowed among uplink and downlink FDD slots. The data rate is optimized subject to power constraints, so as to determine user scheduling as well. Such an optimization problem is decomposed into several sub-problems. Authors in [74] solve user scheduling by means of an iterative Hungarian algorithm and optimize power and spectrum overlap by successive convex approximation for a single-tier network.

Chapter 6 is focused on the improvements that flexible duplexing attains in terms of power efficiency for multi-tier networks. Specifically, we provide an algorithm to minimize the total transmit power for a fixed UL/DL combination. As in the case of throughput, we present a suboptimal scheme that reduces the computational cost of finding the appropriate UL/DL configuration.

# Part II

## **DoF benefits of flexible duplexing in multi-cell networks**



# Chapter 3

## Network model and interference alignment

Heterogeneous networks are sophisticated topologies that encompass a diversity of services, user characteristics, and access points size/power. In such a rich environment, the models that have been conventionally used to theoretically characterize interference-dominated networks, e.g. the interference channel, are no longer sufficient for this task. In this chapter, we describe the X network model, which is a generic topology that encompasses several particular cases. Some well known examples of these particular networks are the IC itself, the conventional interference multiple-access channel (IMAC) and interference broadcast channel (IBC), as well as the multi-cell flexible duplexing networks under study. First, we provide the general X network model. Since flexible duplexing and interference alignment have been considerably related throughout this entire work, we briefly explain how IA is extended to operate over X networks, including some literature on the matter. With the general model and the interference management technique being introduced, we follow by explaining how the X network can be particularized into the topologies that we will analyze in the rest of this thesis. Finally, we present an homotopy continuation-based algorithm to calculate IA precoders and decoders for these sophisticated scenarios. The proposed method is validated over general X networks, whereas further simulations for flexible duplexing multi-cell networks are left for the DoF analysis in Chapter 4.

### 3.1 System model and interference alignment

This section introduces the X network model, which will serve later on as a generic baseline to describe the topologies under study. The description of such model is strongly related to the interference alignment technique, and for this reason we include a brief review on the most celebrated IA background.

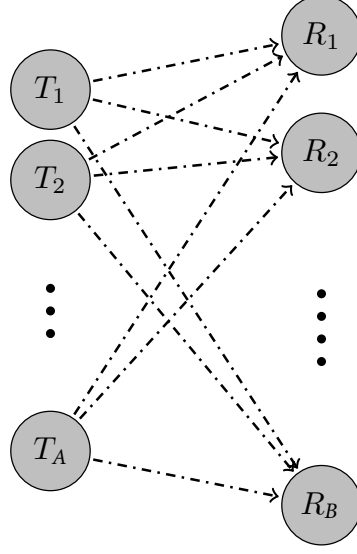


**Figure 3.1:** General MIMO X network model. Dash-dotted lines indicate that both desired signal and interference coexist in the corresponding link.

### 3.1.1 X Network

An  $A \times B$  user MIMO X network is a single-hop communication network with  $A$  transmitters and  $B$  receivers, where transmitter  $\ell$  and receiver  $k$  are equipped with  $M_\ell$  and  $N_k$  antennas, respectively. Let us introduce the *demands matrix*,  $\mathbf{D}$ , defined as follows:

$$\mathbf{D} = \begin{bmatrix} D_{11} & D_{12} & \cdots & D_{1A} \\ D_{21} & \ddots & & \\ \vdots & & D_{k\ell} & \vdots \\ & & & \ddots \\ D_{B1} & \cdots & & D_{BA} \end{bmatrix},$$

where  $D_{k\ell}$  determines the number of independent data streams that transmitter  $\ell$  wishes to send to receiver  $k$ , with  $\ell \in \{1, 2, \dots, A\}$ ,  $k \in \{1, 2, \dots, B\}$ . This setting is depicted in Figure 3.1, where dash-dotted lines indicate that both desired signal and interference coexist in the corresponding link.

Let  $\mathbf{V}_{j\ell} \in \mathbb{C}^{M_\ell \times D_{j\ell}}$  be the precoding matrix used by transmitter  $\ell$  to send its  $D_{j\ell}$  independent data streams to receiver  $j$ . At the other side of the link, receiver  $k$  applies a decoding matrix  $\mathbf{U}_k \in \mathbb{C}^{N_k \times D_k^{\text{Rx}}}$ , where  $D_k^{\text{Rx}} = \sum_\ell D_{k\ell}$  is the total number of streams that receiver  $k$  wants to decode. Thus, the signal after decoding at the  $k$ -th receiver can be expressed as

$$\mathbf{r}_k = \mathbf{U}_k^H \left( \sum_\ell \mathbf{H}_{k\ell} \mathbf{v}_{k\ell} \mathbf{s}_{k\ell} + \sum_\ell \sum_{j \neq k} \mathbf{H}_{k\ell} \mathbf{v}_{j\ell} \mathbf{s}_{j\ell} + \mathbf{n}_k \right),$$

where  $\mathbf{s}_{k\ell} \in \mathbb{C}^{D_{k\ell}}$  contains the information that transmitter  $\ell$  is sending to receiver  $k$ ,  $\mathbf{H}_{k\ell} \in \mathbb{C}^{N_k \times M_\ell}$  is the flat-fading MIMO channel from transmitter  $\ell$  to receiver  $k$  and  $\mathbf{n}_k \in \mathbb{C}^{N_k}$  is the additive and spatially white Gaussian noise at receiver  $k$ .

### 3.1.2 Interference alignment in X networks: Conditions and feasibility

Despite its broad scope, existing theoretical results for X networks are scarce, most of them focusing on the 2-user X channel. Nevertheless, some advances have been made for the X networks described in Section 3.1.1. In [46], the total number of DoF is obtained for a 2-user X channel where all users are equipped with the same number of antennas. Additionally, an upper bound is provided for the asymmetric case, and more recently, the upper bound is achieved by the scheme in [75]. Further results are provided in [76, 77, 78, 79] for more generic user demands and antenna configurations.

A few algorithms for computing IA solutions have also been proposed for the 2-user X channel. First, Jafar and Shamai [46] proposed the so-called JS-scheme for the 2-user MIMO X channel, which is able to achieve the outer bound for some antenna configurations. Later, Agustín and Vidal [75, 80] presented an algorithm based on the generalized singular value decomposition (GSVD) that attains the outer DoF bound for any antenna configuration. However, these algorithms are again limited to the 2-user X channel and are not easily generalizable to arbitrary X networks. Similarly, IA algorithms originally developed for other topologies such as the IC, interference multiple-access channel (IMAC) or interference broadcast channel (IBC), cannot be straightforwardly adapted to X networks. The reason for this is that in the X network every link acts as both a desired and an interfering link and, due to this coupling, these algorithms are not able to guarantee the rank of the signal in the desired links at the same time they null out the interference.

On the other hand, spatial IA with no symbol extensions is limited to integer values of DoF. This is due to the fact that each stream is associated to one transmit direction, hence the number of transmitted streams per channel use must be integer. When the number of available spatial dimensions is not sufficient, symbol extensions are required to achieve higher DoF. This is the case of the single-input single-output (SISO) IC, in which just 1 DoF per channel use is achievable due to the lack of dimensional limitation. On the contrary,  $\frac{1}{2}$  DoF per user and channel use is attained by using IA over an infinite number of channel extensions. However, when time or frequency symbol extensions are used together with the spatial dimension, the resulting MIMO channels are not generic anymore and therefore specific IA algorithms that preserve the rank of the desired signal subspaces are needed. A couple of examples are the methods in [81, 82, 83], which are applicable to the MIMO IC. Also, the GSVD-based scheme in [80] is capable of achieving the optimal DoF in the 2-user X channel with symbol extensions.

As previously mentioned, the key idea of interference alignment consists in designing precoding matrices to reduce the dimension of the interference subspace at

each receiver. In this way, the interference can be zero-forced by the decoders at the corresponding receivers, but at the same time the desired signals at each receiver should be linearly independent. More formally, solving the IA problem for a generic X network amounts to finding a set of precoders and decoders satisfying the following conditions:

$$\mathbf{U}_k^H \mathbf{H}_{k\ell} \mathbf{V}_{k\ell}^- = \mathbf{0}, \quad \forall k, \ell \quad (3.1a)$$

$$\text{rank} \left( \mathbf{U}_k^H \left[ \mathbf{H}_{k1} \mathbf{V}_{k1} \quad \cdots \quad \mathbf{H}_{kM} \mathbf{V}_{kM} \right] \right) = D_k^{\text{Rx}}, \quad \forall k, \quad (3.1b)$$

where  $\mathbf{V}_{k\ell}^-$  represents the horizontal concatenation of all  $\mathbf{V}_{j\ell}$  such that  $j \neq k$ , i.e.,

$$\mathbf{V}_{k\ell}^- \stackrel{\text{def}}{=} \text{cat}_{j \neq k} (\mathbf{V}_{j\ell}).$$

Notice that  $\mathbf{U}_k^H \left[ \mathbf{H}_{k1} \mathbf{V}_{k1} \quad \cdots \quad \mathbf{H}_{kM} \mathbf{V}_{kM} \right]$  in (3.1b) is a  $D_k^{\text{Rx}} \times D_k^{\text{Rx}}$  matrix formed by the concatenation of all equivalent channels (after precoding and decoding) for the  $k$ -th user. Condition (3.1a) guarantees that all interferences are properly zero-forced, while (3.1b) preserves the desired signal dimensionality at the intended receivers.

In order to provide some insight into the necessary conditions for the feasibility of the IA problem, we follow the usual approach in the literature [77, 79]. Note that, given the sets of precoders and decoders,  $\{\mathbf{V}_{j\ell}\}$  and  $\{\mathbf{U}_k\}$ , satisfying (3.1a), we can right-multiply them by arbitrary invertible matrices and (3.1a) still holds. Therefore, a total of  $D_{k\ell}^2 ((D_k^{\text{Rx}})^2)$  elements can be arbitrarily fixed in each precoder (decoder) leaving a total of

$$N_v = \sum_{k=1}^B \sum_{\ell=1}^A (M_\ell - D_{k\ell}) D_{k\ell} + \sum_{k=1}^B (N_k - D_k^{\text{Rx}}) D_k^{\text{Rx}}$$

free variables. The total number of scalar equations in (3.1a) relating those variables is

$$N_e = \sum_{k=1}^B D_k^{\text{Rx}} \left( \sum_{j=1, j \neq k}^B D_j^{\text{Rx}} \right).$$

Hence, a natural condition for (3.1a) to be solvable is  $N_e \leq N_v$ . Given an antenna configuration such that  $M_\ell = M$ ,  $N_k = N$ ,  $\forall k, \ell$ , and assuming symmetric demands,  $D_{k\ell} = D$ ,  $\forall k, \ell$ , we can obtain a simplified condition, as established in [77]:

$$D \leq \frac{M + N}{AB + 1}. \quad (3.2)$$

A network that satisfies  $N_e \leq N_v$  is said to be *proper* [79]. Although proper systems are not always feasible, it has been proved for different topologies that improper systems are always infeasible [77, 79, 84, 85].

### 3.1.3 Particular network topologies

Many well-known network topologies can be viewed as particular cases of the general X network considered in this work. To make this point clear, in this section we specialize the general X network to IC, IMAC and IBC topologies.

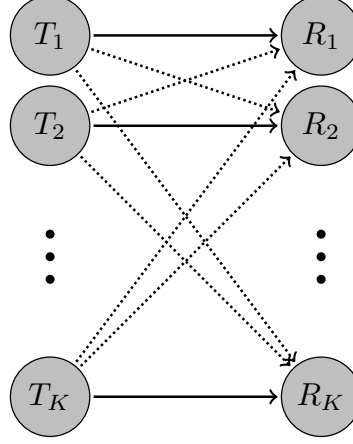


**Figure 3.2:** Interference channel. Solid line arrows represent desired information, and dashed line arrows are associated to interference.

### Interference channel

An interference channel (cf. Fig. 3.2) is a particular case of the MIMO X network in which the following conditions are satisfied:

- The number of transmitters is equal to the number of receivers, i.e.  $A = B = K$ .
- Each transmitter sends its information only to its corresponding receiver. This fact is reflected in the demands matrix,  $\mathbf{D}$ , by making  $D_{k\ell} = 0, \forall k \neq \ell$ .

Consequently, the alignment conditions (3.1a) and (3.1b) simplify to

$$\mathbf{U}_k^H \mathbf{H}_{k\ell} \mathbf{V}_{\ell\ell} = \mathbf{0}, \quad \forall k, \forall \ell \neq k \quad (3.3a)$$

$$\text{rank} \left( \mathbf{U}_k^H \mathbf{H}_{kk} \mathbf{V}_{kk} \right) = D_{kk}, \quad \forall k. \quad (3.3b)$$

Notice that, for generic MIMO interference channels (i.e., without symbol extensions), the rank condition (3.3b) is automatically satisfied with probability one as long as both precoders and decoders are full column rank. This is clear by noticing that the channel matrices involved in (3.3b) are independent from those appearing in (3.3a). The alternating minimization algorithm in [48] relies on this fact to solve (3.3a) by restricting the precoding and decoding matrices to lie in the Stiefel manifold, i.e.  $\mathbf{V}_{\ell\ell}^H \mathbf{V}_{\ell\ell} = \mathbf{I}$  and  $\mathbf{U}_k^H \mathbf{U}_k = \mathbf{I}$ .

### Interference multiple-access and broadcast channels

Cellular networks can also be viewed as particular cases of X networks. More specifically, two dual topologies have been traditionally used to characterize both the uplink and downlink channels in cellular systems, namely the IMAC and IBC models, which are depicted in Figs. 3.3 and 3.4 respectively.

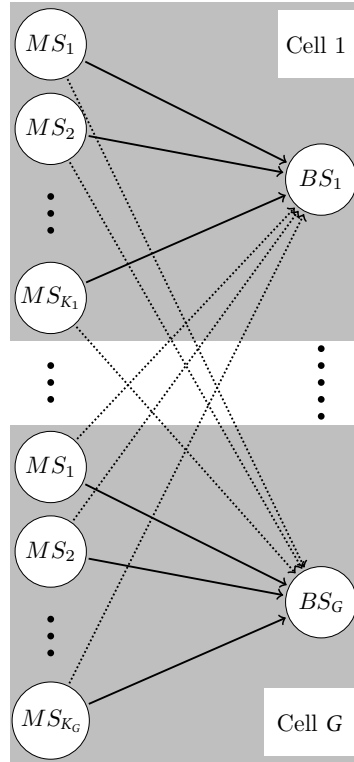


**Figure 3.3:** Interference multiple-access channel. Solid line arrows represent desired information, and dashed line arrows are associated to interference.

Regarding the application of IA schemes to cellular networks, outer bounds for the DoF of IMAC and IBC networks have been derived in [86]. IA algorithms for cellular networks have been proposed in [87, 88]. Also, the sum-rate performance of IA under imperfect CSI for the IBC is studied in [89]. Even further, for broadcast channels where no CSI is available at the transmitters, the blind IA (BIA) strategy is introduced in [90, 91, 92]. More recently, [93] describes a set of schemes that allow to obtain IA precoders and decoders for downlink MIMO HetNets with partial connectivity, and BIA is considered for 2-tier cellular networks in [94, 95].

An IMAC with  $G$  cells and  $K = \sum_k K_k$  users per cell can be viewed as an X network with the following characteristics:

- The demands matrix,  $\mathbf{D} = \mathbf{D}_{IMAC}$ , has a block-diagonal structure, as shown in (3.4).
- The number of transmitters will be equal to the total number of mobile stations within the network, and the number of receivers will correspond to the number of base stations.

Analogously, an IBC with the same cell and user distribution can be particularized from an X network as follows:

$$\mathbf{D}_{IMAC} = \begin{bmatrix} \mathbf{D}_{1,1:K_1} & \mathbf{0}_{1,K_2} & \mathbf{0} & \cdots & \mathbf{0} & \mathbf{0}_{1,K_G} \\ \mathbf{0}_{1,K_1} & \mathbf{D}_{2,K_1+1:K_2} & \mathbf{0} & \cdots & \mathbf{0} & \mathbf{0}_{1,K_G} \\ & & \ddots & & & \vdots \\ \vdots & & \mathbf{0} & \mathbf{D}_{k,\sum_{\ell=1}^{k-1} K_\ell+1:\sum_{\ell=1}^k K_\ell} & \mathbf{0} & \vdots \\ \mathbf{0}_{1,K_1} & \mathbf{0}_{1,K_2} & \mathbf{0} & \cdots & \mathbf{0} & \mathbf{D}_{G,K-K_G+1:K} \end{bmatrix} \quad (3.4)$$

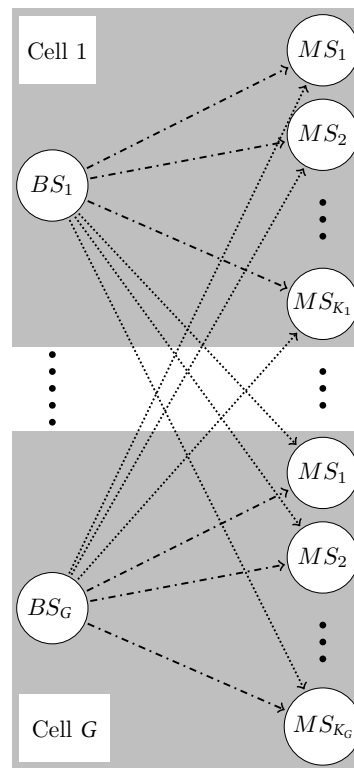


**Figure 3.4:** Interference broadcast channel. Dashed line arrows are associated to interference, and dash-dotted lines indicate that both desired and interfering signals coexist in the same link.

- The demands matrix,  $\mathbf{D} = \mathbf{D}_{IBC}$ , has a block-diagonal structure, as shown in (3.5).
- The number of transmitters coincides with the number of base stations, and the number of receivers is the number of mobile stations.

$$\mathbf{D}_{IBC} = \begin{bmatrix} \mathbf{D}_{1:K_1,1} & \mathbf{0}_{K_1,1} & \mathbf{0} & \cdots & \mathbf{0} & \mathbf{0}_{K_1,1} \\ \mathbf{0}_{K_2,1} & \mathbf{D}_{K_1+1:K_2,2} & \mathbf{0} & \cdots & \mathbf{0} & \mathbf{0}_{K_2,1} \\ & & \ddots & & & \\ \vdots & & \mathbf{0} & \mathbf{D}_{\sum_{\ell=1}^{k-1} K_{\ell+1} : \sum_{\ell=1}^k K_{\ell},k} & \mathbf{0} & \vdots \\ \mathbf{0}_{K_G,1} & \mathbf{0}_{K_G,1} & \mathbf{0} & \cdots & \mathbf{0} & \mathbf{D}_{K-K_G+1:K,G} \end{bmatrix} \quad (3.5)$$

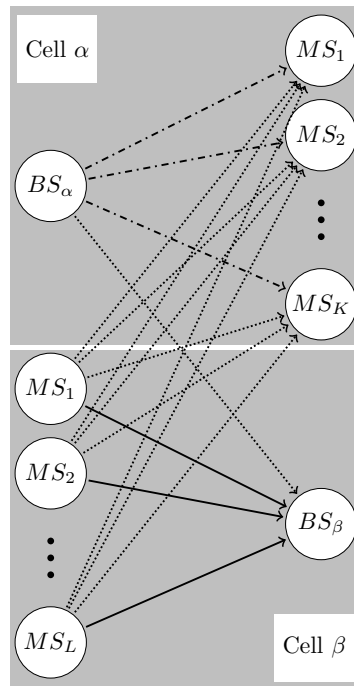


**Figure 3.5:** Reverse TDD model. Solid line arrows represent desired information, and dashed line arrows are associated to interference. Dash-dotted lines indicate that both desired and interfering signals coexist in the same link.

### Flexible duplexing cellular networks

Whereas in traditional cellular systems all cells operate synchronously either in uplink or downlink mode, in this work we also consider networks in which some cells may operate in uplink mode while the rest of them operate in downlink. An example of a flexible duplexing 2-cell network is shown in Fig. 3.5.

- Since this type of networks consists of both multiple-access channels and broadcast channels, the demands matrix,  $\mathbf{D}$ , will be a combination of (3.4) and (3.5), depending on the particular uplink/downlink configuration.

- The number of transmitters will be the number of downlink base stations plus the uplink mobile stations. The number of receiving nodes will be the sum of base stations in uplink mode and mobile stations in downlink mode.

## 3.2 Homotopy continuation

Homotopy continuation (HC) is a numerical method for solving systems of nonlinear equations: the basic idea consists in gradually deforming a trivially solvable system or *start* system into the original problem or *target* system [96, 97, 98, 99]. Basically, the methodology comprises the following stages:

1. Identifying the target system with a family of problems depending on parameters. This is made by combining both start and target systems by means of a *continuation parameter* which allows to control the tracking procedure.
2. Solving the system for an appropriate set of parameters, in such a way that the start system has a straightforward solution (or set of solutions).
3. Conducting a tracking procedure, following the solutions as the parameters evolve from the start system onto the original problem that we wish to solve. In other words, we begin the procedure setting the continuation parameter to a value that makes the combination equivalent to the start system. Afterwards, the value of the continuation parameter is gradually modified until the combination has been tracked towards the target systems so that the corresponding solutions are obtained.

The most conventional way to define the aforementioned family of problems is building a convex combination of the start system  $\mathbf{q}(\mathbf{w})$  and the original problem  $\mathbf{p}(\mathbf{w})$ , given by

$$\mathbf{g}(\mathbf{w}, t) \triangleq (1 - t) \mathbf{q}(\mathbf{w}) + t \mathbf{p}(\mathbf{w}), \quad (3.6)$$

being  $\mathbf{w}$  in the general case a vector of polynomials, and where  $t$  is the continuation parameter. From (3.6),  $t = 0$  leads to  $\mathbf{g}(\mathbf{w}, 0) = \mathbf{q}(\mathbf{w})$ , whilst  $t = 1$  leaves us with  $\mathbf{g}(\mathbf{w}, 1) = \mathbf{p}(\mathbf{w})$ . Equivalently, the combination in (3.6) is transformed from the straightforward problem  $\mathbf{q}(\mathbf{w})$  towards the target system  $\mathbf{p}(\mathbf{w})$  as the continuation parameter  $t$  varies from  $t = 0$  to  $t = 1$  with a *continuation step*  $\Delta t$ .

### 3.2.1 The pentagon example

In order to illustrate this procedure with a toy example, let us consider a degree  $d$  polynomial,  $p(w) = w^d + a_1 w^{d-1} + \dots + a_d$ , where  $d$  is a positive integer and the terms  $a_i$  are constant coefficients. The roots for polynomial  $p(w)$  can be obtained by means of homotopy continuation. Let us begin with the start system  $w^d - 1 = 0$ , whose solutions are

$$w_k^* = e^{2\pi k j/d} \quad \text{con } k = 1, 2, \dots, d. \quad (3.7)$$

Therefore, the family of problems is defined as

$$g(w, t) \triangleq (1 - t) (w^d - 1) + t p(w), \quad (3.8)$$

in such a way that, for  $t = 0$ , we have the straightforward  $g(w, 0) = w^d - 1$ , whereas  $t = 1$  corresponds to the problem we wish to solve,  $g(w, 1) = p(w)$ .

Assuming that the solutions for the target system were unknown, the continuation method allows us to track these solutions all along the paths  $w_k^*$  defined in (3.7). The next question is how to perform the tracking process from  $t = 0$  to  $t = 1$ . First, we rely on the fact that the paths  $w_k^*$  satisfy the Davidenko differential equation [100, 101]. Let us denote as  $g_w(w, t)$  and  $g_t(w, t)$  the partial derivatives of  $g(w, t)$  with respect to  $w$  and  $t$ . Applying the chain rule, we obtain

$$0 \equiv \frac{dg(w_k^*(t), t)}{dt} = g_w(w_k^*(t), t) \frac{dw_k^*(t)}{dt} + g_t(w_k^*(t), t),$$

where, for the family in (3.8), we obtain

$$\frac{dw_k^*(t)}{dt} = -\frac{g_t(w_k^*(t), t)}{g_w(w_k^*(t), t)} = \frac{w_k^*(t)^d - 1 - p(w_k^*(t))}{(1 - t) dw_k^*(t)^{d-1} + t p'(w_k^*(t))}.$$

Therefore, we are left with an ordinary differential equation in  $w_k^*(t)$ , with initial conditions given by  $w_k^*(0)$  and roots  $w_k^*(1)$ , being the latter the roots of the target system. Let us now illustrate the continuation procedure with a particular case of (3.8). Specifically, we calculate the solutions for  $w^d - a = 0$ . Substituting in (3.8) results in

$$g(w, t) = (1 - t) (w^d - 1) + t (w^d - a) = w^d + (1 - a)t - 1. \quad (3.9)$$

After these steps, and for  $t \in [0, 1]$ , the solutions for  $g(w, t) = 0$  can be defined as

$$w_k^*(t) = \sqrt[d]{1 - (1 - a)t}.$$

These expressions are consequently associated to the paths through which the solutions for the family of problems evolve as the continuation parameter  $t$  varies from  $t = 0$  to  $t = 1$ .

The previously detailed example is represented in Fig. 3.6, calculating the roots of  $p(w) = w^5 + 32e^{j(\epsilon)}$  by means of homotopy continuation with start system  $w^5 - 1 = 0$ . Figure 3.6 shows that, as  $\epsilon$  tends to 0, the solution paths approach the origin  $(0, 0)$ . As a matter of fact, for  $\epsilon = 0$ , all the paths  $w_k^*$  would reach the origin, leading to a singularity and hence failing to reach the target solution. Such singularities are a crucial handicap for the Davidenko approach, considering how sensitive the solution paths are with respect to slight variations in the initial problem definition. In addition, it is worth remarking that solving such problems with the Davidenko approach can originate numerical inaccuracies.

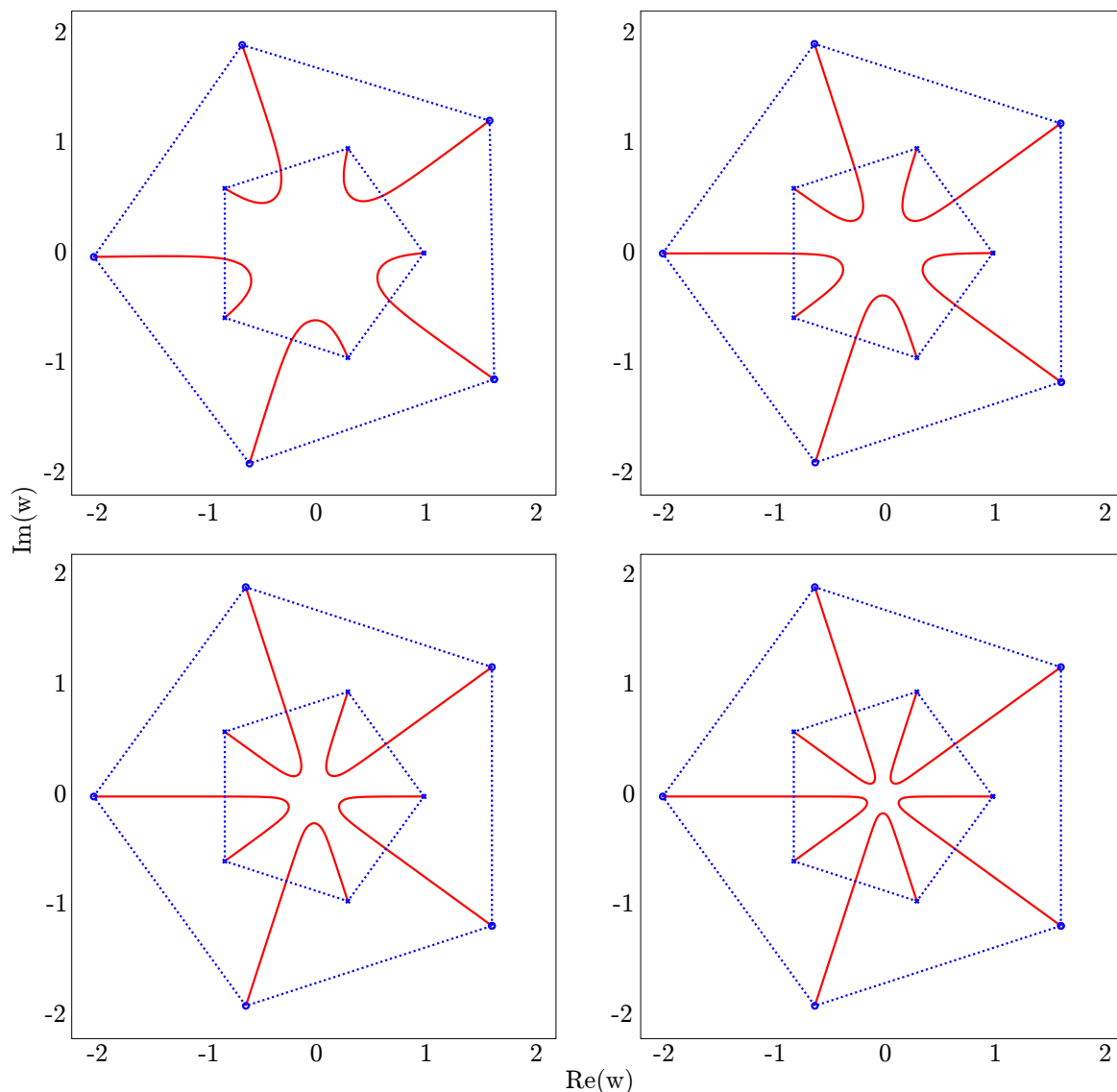


**Figure 3.6:** Example of an homotopy continuation of the family (3.9) for  $d = 5$ ,  $a = 32e^{j(\epsilon)}$ , and with  $\epsilon = \{1, 10^{-1}, 10^{-2}, 10^{-3}\}$

### 3.2.2 Path tracking procedures

As we have observed in the example above, a robust numerical approach to complete the continuation process is required. A possible candidate would be the so-called *simple path tracker*, based on a prediction + correction scheme. By applying the simple path tracker to our homotopy continuation, we ensure that there is almost surely a continuation step which is small enough so that convergence is guaranteed [98]. However, a fixed-step approach would be computationally inefficient in practice. Therefore, in our algorithm we have included a variation of the simple path tracker, considering the possibility to adapt the step size depending on the progression of the tracking procedure. The main structure of this method is as follows:

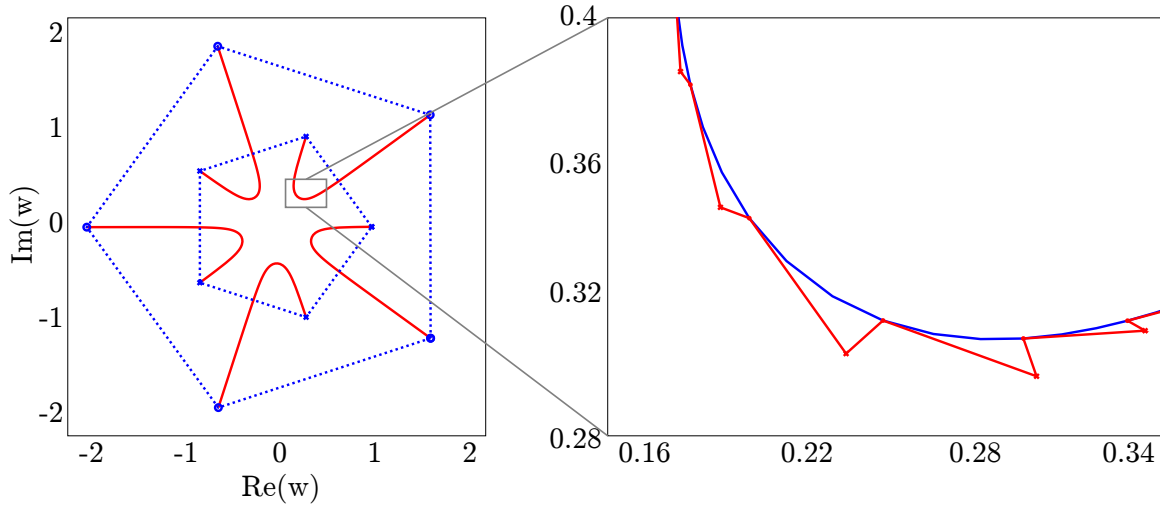


**Figure 3.7:** Simple path tracking for the example in Fig. 3.6 with  $\epsilon = 10^{-1}$ .

1. **Initialization:** A start system is defined in such a way that we begin with a straightforward solution. An initial step size shall be determined as well.
2. **Prediction:** The update of the problem for the next value of the continuation parameter  $t$  is estimated as

$$g(w + \Delta w, t + \Delta t) = g(w, t) + g_w(w, t) \Delta w + g_t(w, t) \Delta t + \dots,$$

i.e., by means of the Euler predictor. If the point  $(w_1, t_1)$  is sufficiently close to the path, i.e.  $g(w_1, t_1) \approx 0$ , we can approximate the solution for  $t_1 + \Delta t$  making  $g(w_1 + \Delta w, t_1 + \Delta t) = 0$ , and neglecting terms beyond first order:

$$\Delta w = -\Delta t \frac{g_t(w_1, t_1)}{g_w(w_1, t_1)},$$

3. **Correction:** We apply the Newton corrector to the previous estimate. In case that, after the Euler prediction,  $g(w_1, t_1)$  is not sufficiently small, we can hold  $t$  constant, i.e.  $\Delta t = 0$ , resulting in

$$\Delta w = -\frac{g(w_1, t_1)}{g_w(w_1, t_1)}.$$

The Newton correction step can be performed several times in order to approximate back to the path with as much accuracy as possible.

4. **Step size adaptation:** Depending on the success of the previous points, the continuation step size is either enlarged or reduced.

Figure 3.7 displays the behaviour of the Euler+Newton-based continuation described in the lines above. As observed in the figure, a first estimate of the next update is obtained for the new value of  $t$ ,

$$\Delta w = -\Delta t \frac{w_j^5 - 1 - (w_j^5 - a)}{5tw_j^4 + 5(1-t)w_j^4} = -\Delta t \frac{a-1}{5w_j^4} \Rightarrow w = w_j + \Delta w,$$

being  $w_j$  the solution for the previous value of the continuation parameter, and  $w$  the updated value of the solution for  $t + \Delta t$ . Immediately afterwards, the required corrections are performed in order to bring the solution back to the corresponding path,

$$\Delta w = \frac{(t-1)(w^5 - a) - t(w^5 - 1)}{5tw^4 + 5(1-t)w^4} = \frac{a - w^5 - t(a+1)}{5w^4} \Rightarrow w_{j+1} = w + \Delta w,$$

where  $w_{j+1}$  is the solution to the problem after applying the Newton method with initial value  $w$ .

### 3.3 HC-based algorithm for interference alignment

Once we have provided some fundamentals about homotopy continuation as a numerical method, we present a general IA algorithm which can be applied to arbitrary MIMO X networks, possibly including symbol extensions. Recall that we aim to start from an easy-to-solve system, and then transform such problem onto our original system. In the particular case of IA, our goal is to start from a system composed of channels, precoders and decoders that trivially satisfy (3.1a) and (3.1b), and then track the IA solution until the desired precoding and decoding matrices for the target channel. We characterize our scheme regarding implementation and convergence, and we finally validate the presented approach by means of Monte Carlo simulations over several instances of X networks.

In previous works, the proposed algorithms were based solely on the interference cancellation conditions (3.1a). However, when generic X networks with arbitrary demands are considered, we have to explicitly enforce the rank conditions (3.1b) as well. To this end, we propose an homotopy function that reformulates the rank conditions as a new set of bilinear equations which then can be easily combined with the alignment bilinear equations (3.1a). We start by changing (3.1b) to

$$\mathbf{U}_k^H [\mathbf{H}_{k1} \mathbf{V}_{k1} \quad \cdots \quad \mathbf{H}_{kM} \mathbf{V}_{kM}] = \mathbf{I}_{D_k^{\text{rx}}}, \quad \forall k. \quad (3.10)$$

Note that a solution to (3.1a), (3.10) is a solution of (3.1a), (3.1b), and reciprocally if a solution to (3.1a), (3.1b) is known then a solution to (3.1a), (3.10) is produced by right-multiplying each precoder by an appropriate invertible square matrix<sup>1</sup>. We can

<sup>1</sup>This trick is used later in (3.17) to obtain a start system for the homotopy continuation method. Notice that the decoders obtained this way are not necessarily given by matrices with orthogonal columns.

therefore substitute (3.1b) by (3.10), and in this way the IA problem now amounts to solving an extended set of bilinear equations. In order to combine both (3.1a) and (3.10), this extended set of equations can be written more compactly as follows:

$$\mathbf{U}_k^H \mathbf{H}_{kl} \mathbf{V}_{kl} = \mathbf{P}_{kl} \quad \forall k, \ell, \quad (3.11)$$

where  $\mathbf{P}_{kl}$  is a block of  $D_{kl}$  columns extracted from the  $D_k^{\text{Rx}} = \sum_{\ell} D_{kl}$  identity matrix,  $\mathbf{I}_{D_k^{\text{Rx}}}$ , i.e.,

$$\mathbf{P}_{kl} = [ \mathbf{e}_{i+1} \quad \mathbf{e}_{i+2} \quad \cdots \quad \mathbf{e}_{i+D_{kl}} ],$$

where  $\mathbf{e}_i$  is a column vector with all zero elements except for a 1 in the  $i$ -th position, and  $i = \sum_{n=1}^{k-1} D_{n\ell}$ .

Let  $D_{\ell}^{\text{Tx}} = \sum_k D_{k\ell}$  be the total number of messages that the  $\ell$ -th user wishes to transmit, and let  $\mathbf{V}_{\ell}$  be the horizontal concatenation of all  $\mathbf{V}_{j\ell}$ ,

$$\mathbf{V}_{\ell} \stackrel{\text{def}}{=} \underset{j}{\text{cat}}(\mathbf{V}_{j\ell}).$$

With this notation, the alignment equations in (3.11) can be rewritten as

$$\mathbf{U}_k^H \mathbf{H}_{kl} \mathbf{V}_{\ell} = \mathbf{A}_{kl} \quad \forall k, \ell, \quad (3.12)$$

where, again,  $\mathbf{U}_k \in \mathbb{C}^{N_k \times D_k^{\text{Rx}}}$  is the decoding matrix for receiver  $k$ ,  $\mathbf{H}_{kl} \in \mathbb{C}^{N_k \times M_{\ell}}$  is the flat-fading MIMO channel from transmitter  $\ell$  to receiver  $k$ , and  $\mathbf{V}_{\ell} \in \mathbb{C}^{M_{\ell} \times D_{\ell}^{\text{Tx}}}$  is the precoding matrix applied by transmitter  $\ell$ . Additionally,  $\mathbf{A}_{kl} = [ \mathbf{0} \quad \cdots \quad \mathbf{P}_{kl} \quad \cdots \quad \mathbf{0} ]$  is a  $D_k^{\text{Rx}} \times D_{\ell}^{\text{Tx}}$  matrix such that  $\mathbf{P}_{kl}$  is the only block in  $\mathbf{A}_{kl}$  containing non-zero elements. Therefore,  $\mathbf{A}_{kl}$  includes all interference cancellation and rank preservation equations related to channel  $\mathbf{H}_{kl}$ .

According to these compacted bilinear equations, we define the function that will allow us to obtain the precoders,  $\mathbf{V}_{\ell}$ , and decoders,  $\mathbf{U}_k^H$ . Let us first consider a parametrized channel matrix,  $\mathbf{H}_{kl}(t)$ , as a convex combination of a *start* channel,  $\bar{\mathbf{H}}_{kl}$ , and the *target* channel,  $\mathbf{H}_{kl}$ . This combination is controlled by the continuation parameter,  $t$ , leading to a homotopy function given by

$$\mathbf{G}_{kl}(\mathbf{U}_k^H, \mathbf{V}_{\ell}, t) = \mathbf{U}_k^H \underbrace{((1-t)\bar{\mathbf{H}}_{kl} + t\mathbf{H}_{kl})}_{\mathbf{H}_{kl}(t)} \mathbf{V}_{\ell} - \mathbf{A}_{kl}, \quad (3.13)$$

$\forall k, \ell$  and  $t \in [0, 1]$ . Our goal is to move the solution along the path  $\mathbf{G}_{kl}(\mathbf{U}_k^H, \mathbf{V}_{\ell}, t) = \mathbf{0} \quad \forall k, \ell$  from  $t = 0$  to  $t = 1$  in a finite number of steps  $\Delta t$ . Usually, this path tracking procedure is accomplished by an iterative predictor/corrector method [99], as introduced in Section 3.2. In particular, a first order approximation of the homotopy function in (3.13), which is given by

$$\begin{aligned} \mathbf{G}_{kl}(\mathbf{U}_k^H + \Delta \mathbf{U}_k^H, \mathbf{V}_{\ell} + \Delta \mathbf{V}_{\ell}, t + \Delta t) &= \mathbf{U}_k^H \mathbf{H}_{kl}(t) \mathbf{V}_{\ell} \\ &\quad + \Delta \mathbf{U}_k^H \mathbf{H}_{kl}(t) \mathbf{V}_{\ell} \\ &\quad + \mathbf{U}_k^H \mathbf{H}_{kl}(t) \Delta \mathbf{V}_{\ell} \\ &\quad + \mathbf{U}_k^H (\mathbf{H}_{kl} - \bar{\mathbf{H}}_{kl}) \mathbf{V}_{\ell} \Delta t - \mathbf{A}_{kl}, \quad \forall k, \ell \end{aligned}$$

gives rise to the basic Euler prediction and Newton correction steps. Assuming that there is a point  $(\{\mathbf{U}_k^H\}, \{\mathbf{V}_\ell\}, t)$  close enough to the path (i.e.,  $\mathbf{U}_k^H \mathbf{H}_{k\ell}(t) \mathbf{V}_\ell \approx \mathbf{A}_{k\ell} \forall k, \ell$ ), we may predict an approximate solution at  $t + \Delta t$  by setting  $\mathbf{G}_{k\ell}(\mathbf{U}_k^H + \Delta \mathbf{U}_k^H, \mathbf{V}_\ell + \Delta \mathbf{V}_\ell, t + \Delta t) = \mathbf{0}$ :

$$\Delta \mathbf{U}_k^H \mathbf{H}_{k\ell}(t) \mathbf{V}_\ell + \mathbf{U}_k^H \mathbf{H}_{k\ell}(t) \Delta \mathbf{V}_\ell = -\mathbf{U}_k^H (\mathbf{H}_{k\ell} - \bar{\mathbf{H}}_{k\ell}) \mathbf{V}_\ell \Delta t \quad \forall k, \ell. \quad (3.14)$$

Updates  $\Delta \mathbf{V}_\ell$  and  $\Delta \mathbf{U}_k^H \forall k, \ell$  are obtained by solving –if possible– the system of linear equations in (3.14). Further details on this point are relegated to Subsection 3.3.2.

Additionally, if the current point  $(\{\mathbf{U}_k^H\}, \{\mathbf{V}_\ell\}, t)$  is not as close to the path as required, i.e., the elements in  $\mathbf{G}_{k\ell}(\mathbf{U}_k^H, \mathbf{V}_\ell, t)$  are greater than a predefined tolerance, we may hold  $t$  constant by setting  $\Delta t = 0$  and obtain the Newton correction step:

$$\Delta \mathbf{U}_k^H \mathbf{H}_{k\ell}(t) \mathbf{V}_\ell + \mathbf{U}_k^H \mathbf{H}_{k\ell}(t) \Delta \mathbf{V}_\ell = \mathbf{A}_{k\ell} - \mathbf{U}_k^H \mathbf{H}_{k\ell}(t) \mathbf{V}_\ell, \quad \forall k, \ell. \quad (3.15)$$

Analogously to the prediction procedure, precoder and decoder updates,  $\Delta \mathbf{V}_\ell$  and  $\Delta \mathbf{U}_k^H \forall k, \ell$ , are calculated by solving –if possible– the system of linear equations in (3.15). This step leads to a new set of precoding and decoding matrices,  $\{\mathbf{V}_\ell + \Delta \mathbf{V}_\ell\}$  and  $\{\mathbf{U}_k^H + \Delta \mathbf{U}_k^H\}$ , which are expected to lie closer to the tracked path.

### 3.3.1 Start system

As we have already mentioned, one important step in homotopy continuation methods is the choice of a start system composed of a set of precoders  $\{\bar{\mathbf{V}}_\ell\}$ , decoders  $\{\bar{\mathbf{U}}_k\}$  and channels  $\{\bar{\mathbf{H}}_{k\ell}\}$ , which satisfies (3.12) and that it is easy to compute.

A first idea is to look at (3.12) as if we were given  $\{\bar{\mathbf{U}}_k\}$  and  $\{\bar{\mathbf{V}}_\ell\}$  (for instance, we might use randomly generated precoders and decoders) and we had to solve it for  $\{\bar{\mathbf{H}}_{k\ell}\}$ . This is naturally called the inverse IA problem in [85], and it is an easily solvable linear problem for some network topologies such as the MIMO-IC without symbol extensions. However, for general MIMO X networks it is unlikely that a randomly chosen collection of precoders and decoders will satisfy (3.12) for *some* channel. The three objects (channel, precoders and decoders) must be chosen simultaneously. To this end, in this work we propose an alternative procedure that first obtains a start system composed of precoders, decoders and channels satisfying the zero-forcing alignment conditions (3.1a), and then modifies this start system to fulfill the extended set of equations in (3.12).

First, we randomly generate a set of precoders and decoders; second, we obtain the channels as follows

$$\bar{\mathbf{H}}_{k\ell} = \mathbf{X}_{k\ell} - \mathbf{F}_k \mathbf{F}_k^H \mathbf{X}_{k\ell} \mathbf{C}_{k\ell}^- \mathbf{C}_{k\ell}^{H-}, \quad \forall k, \ell \quad (3.16)$$

where  $\mathbf{F}_k$  and  $\mathbf{C}_{k\ell}^-$  are orthonormal bases of  $\bar{\mathbf{U}}_k$  and  $\bar{\mathbf{V}}_{k\ell}^-$ , respectively, and  $\mathbf{X}_{k\ell}$  is a non-zero arbitrary random matrix. Notice that by calculating  $\bar{\mathbf{H}}_{k\ell}$  as in (3.16), the

interference cancellation conditions (3.1a) are trivially satisfied. Now, we can right-multiply either the precoders or the decoders by arbitrary invertible matrices and (3.1a) still holds. Therefore, by applying the transformation

$$\bar{\mathbf{U}}'_k = \bar{\mathbf{U}}_k \left( \left( \bar{\mathbf{U}}_k^H \begin{bmatrix} \bar{\mathbf{H}}_{k1} \bar{\mathbf{V}}_{k1} & \cdots & \bar{\mathbf{H}}_{kM} \bar{\mathbf{V}}_{kM} \end{bmatrix} \right)^H \right)^{-1}, \quad \forall k, \quad (3.17)$$

(if the inverse exists) the new system comprised of the sets  $\{\bar{\mathbf{V}}_{k\ell}\}$ ,  $\{\bar{\mathbf{U}}'_k\}$  and  $\{\bar{\mathbf{H}}_{k\ell}\}$  satisfies (3.1a) and (3.10), and thus (3.12). We can then use it as a start system for the homotopy continuation procedure.

### 3.3.2 Implementation details

In this section, we discuss some important implementation aspects of the proposed algorithm.

The expressions for the Euler prediction and Newton correction steps are given by (3.14) and (3.15), respectively. Now, in order to simplify the algorithm implementation, it is convenient to define a new vector

$$\mathbf{w} = \left[ \text{cat}_\ell((\text{vec } \mathbf{V}_\ell)^T), \text{cat}_k((\text{vec } \mathbf{U}_k^H)^T) \right]^T$$

by stacking all precoding and decoding matrices. Both (3.14) and (3.15) represent systems of linear equations which can be conveniently solved as large sparse linear systems. Starting with the prediction step, our goal is to write the set of linear equations in (3.14) as a single linear equation,  $D\mathbf{G}(\mathbf{w}) \Delta \mathbf{w} = -D\mathbf{G}(t)$ . Applying the identity

$$\text{vec}(\mathbf{ABC}) = (\mathbf{C}^T \otimes \mathbf{A}) \text{vec}(\mathbf{B}),$$

we first vectorize (3.14) as

$$\begin{aligned} & \underbrace{\left( (\mathbf{V}_\ell^T \mathbf{H}_{k\ell}^T(t)) \otimes \mathbf{I}_{D_k^{Rx}} \right)}_{D\mathbf{G}_{k\ell}(\mathbf{U}_k^H)} \Delta \text{vec } \mathbf{U}_k^H \\ & + \underbrace{\left( \mathbf{I}_{D_\ell^{Tx}} \otimes (\mathbf{U}_k^H \mathbf{H}_{k\ell}(t)) \right)}_{D\mathbf{G}_{k\ell}(\mathbf{V}_\ell)} \Delta \text{vec } \mathbf{V}_\ell \\ & = - \underbrace{\text{vec} \left( \mathbf{U}_k^H (\mathbf{H}_{k\ell} - \bar{\mathbf{H}}_{k\ell}) \mathbf{V}_\ell \right)}_{D\mathbf{G}_{k\ell}(t)} \Delta t, \quad \forall k, \ell. \end{aligned}$$

Once the equations have been vectorized, we can stack them together to represent the Euler prediction step:

$$D\mathbf{G}(\mathbf{w}) \Delta \mathbf{w} = -D\mathbf{G}(t) \Delta t \Rightarrow \Delta \mathbf{w} = -D\mathbf{G}(\mathbf{w})^+ D\mathbf{G}(t) \Delta t, \quad (3.18)$$

where  $D\mathbf{G}(\mathbf{w})$  is the Jacobian matrix of the system of matrix equations in (3.12), comprising all the derivatives with respect to the variables  $\{\mathbf{V}_{j\ell}\}$  and  $\{\mathbf{U}_k^H\}$  in the order specified in

$$D\mathbf{G}(\mathbf{w}) = \left[ \begin{array}{cccc|ccc} D\mathbf{G}_{11}(\mathbf{V}_{11}) & D\mathbf{G}_{11}(\mathbf{V}_{21}) & \cdots & D\mathbf{G}_{11}(\mathbf{V}_{NM}) & D\mathbf{G}_{11}(\mathbf{U}_1^H) & \cdots & D\mathbf{G}_{11}(\mathbf{U}_N^H) \\ D\mathbf{G}_{21}(\mathbf{V}_{11}) & & & & \vdots & & \vdots \\ \vdots & & D\mathbf{G}_{k\ell}(\mathbf{V}_{jp}) & \vdots & \vdots & D\mathbf{G}_{k\ell}(\mathbf{U}_j^H) & \vdots \\ D\mathbf{G}_{NM}(\mathbf{V}_{11}) & \cdots & & D\mathbf{G}_{NM}(\mathbf{V}_{NM}) & D\mathbf{G}_{NM}(\mathbf{U}_1^H) & \cdots & D\mathbf{G}_{NM}(\mathbf{U}_N^H) \end{array} \right].$$

It is a block partitioned matrix with as many row partitions as channel matrices and as many column partitions as precoding and decoding matrices. Sparsity comes from the fact that each equation involves a subset of the variables and, therefore, many blocks in  $D\mathbf{G}(\mathbf{w})$  are zero. Specifically,  $D\mathbf{G}_{k\ell}(\mathbf{V}_{jp}) = \mathbf{0}$  when  $p \neq \ell$ , and  $D\mathbf{G}_{k\ell}(\mathbf{U}_j^H) = \mathbf{0}$  when  $j \neq k$ . The solution vector  $\Delta\mathbf{w}$  contains the updates for all the variables in both precoders and decoders, and the derivative with respect to the continuation parameter is built from all partial derivatives as  $D\mathbf{G}(t) = \text{cat}_{(k,\ell)} \left( D\mathbf{G}_{k\ell}(t)^T \right)^T$ .

Following the same steps, the Newton correction expressions can be rewritten as the solution of a linear equation,  $D\mathbf{G}(t)\Delta\mathbf{w} = \mathbf{g}$ , obtained by vectorizing all the equations in (3.15),

$$D\mathbf{G}_{k\ell}(\mathbf{U}_k^H)\Delta\text{vec } \mathbf{U}_k^H + D\mathbf{G}_{k\ell}(\mathbf{V}_\ell)\Delta\text{vec } \mathbf{V}_\ell = \underbrace{\text{vec} \left( \mathbf{A}_{k\ell} - \mathbf{U}_k^H \mathbf{H}_{k\ell}(t) \mathbf{V}_\ell \right)}_{\mathbf{g}_{k\ell}}, \quad \forall k, \ell,$$

and then stacking up all the equations together,

$$D\mathbf{G}(\mathbf{w})\Delta\mathbf{w} = \mathbf{g} \Rightarrow \Delta\mathbf{w} = D\mathbf{G}(\mathbf{w})^+ \mathbf{g}, \quad (3.19)$$

where  $\mathbf{g} = \text{cat}_{k,\ell}(\mathbf{g}_{k\ell}^T)^T$ .

Theoretically, the Newton step should be executed iteratively for a fixed  $t$  until a point below the predefined tolerance has been obtained. Since the Newton method converges quadratically to a point in the path, a common strategy is to run the correction step a few times establishing a limit on the number of executions to a maximum of `MaxNwtIter` or until all the entries of  $\mathbf{g}$  are below a predefined tolerance `NwtTol`, whatever happens first. Nevertheless, in those cases in which the step size,  $\Delta t$ , is too large, the precoders and decoders after the Euler prediction might be so far from the path that the Newton correction step could require several iterations to reach the tolerance value, or it might escape from the basin of attraction of Newton's operator and thus be unable to follow the correct path. In this sense, although there is theoretical evidence proving that there is always a step size,  $\Delta t$ , small enough to assure convergence [98], a fixed step size strategy might not be efficient in practice.

To deal with this issue, we have provided the simple path tracker with an additional feature, allowing our algorithm to adapt the continuation step size depending

---

**Algorithm 1:** Interference alignment via homotopy continuation in MIMO X networks.

---

**Input:**  $\{\mathbf{H}_{kl}\}$ ,  $\Delta t$ ,  $NwtTol$ ,  $MaxNwtIter$ ,  $MinStepSize$ ,  $NumHitsToDoubleStep$   
**Output:**  $\{\mathbf{V}_\ell\}$  and  $\{\mathbf{U}_k\}$  satisfying (3.1a) and (3.1b), and a convergence indicator,  $PathFailed$

```

/* Inverse IA */
Obtain  $\{\bar{\mathbf{V}}_{kl}\}$ ,  $\{\bar{\mathbf{U}}'_k\}$ ,  $\{\bar{\mathbf{H}}_{kl}\}$  as shown in (3.16), (3.17);  $t = 0$ ,  $NumHits = 0$ ,
   $PathFailed = false$ 
 $\mathbf{w} = [\text{cat}((\text{vec } \mathbf{V}_\ell)^T), \text{cat}((\text{vec } \mathbf{U}_k^H)^T)]^T$ 
 $t^* = t$ ,  $\mathbf{w}^* = \mathbf{w}$  // backup variables
while  $t < 1$  do
   $t = \min(t + \Delta t, 1)$ 
  /* Euler prediction */
   $\mathbf{w} = \mathbf{w} - D\mathbf{G}(\mathbf{w})^+ D\mathbf{G}(t)\Delta t$  as indicated in (3.18)
  /* Newton correction */
   $NewtonFailed = true$ 
  for  $iter = 1$  to  $MaxNwtIter$  do
     $\mathbf{w} = \mathbf{w} + D\mathbf{G}(\mathbf{w})^+ \mathbf{g}$  as shown in (3.19)
    if  $\|\mathbf{g}\|^2 < NwtTol$  then
       $NumHits = NumHits + 1$ 
       $NewtonFailed = false$ 
      break
  /* Step size adaptation routine */
  if  $NumHits == NumHitsToDoubleStep$  then
     $\Delta t = 2\Delta t$ 
     $t^* = t$ ,  $\mathbf{w}^* = \mathbf{w}$ ,  $NumHits = 0$ 
  else if  $NewtonFailed$  then
     $\Delta t = \Delta t / 2$ 
     $t = t^*$ ,  $\mathbf{w} = \mathbf{w}^*$ ,  $NumHits = 0$ 
    if  $\Delta t < MinStepSize$  then
       $PathFailed = true$ 
      return
  Find orthonormal basis for the precoders and decoders satisfying  $\mathbf{V}_{kl}^H \mathbf{V}_{kl} = \mathbf{I}$ ,
   $\mathbf{U}_k^H \mathbf{U}_k = \mathbf{I}$ ,  $\forall k, \ell$ 
return

```

---

on the Newton corrector success or failure. A common practice is to halve the step size if we detect that the Euler prediction has failed, and then repeat it. If a number of repeated failed predictions occur –i.e. if the step size becomes smaller than a pre-defined minimum step size,  $MinStepSize$ – we stop the path tracking procedure and no output is produced. Conversely, if the correction step is successful for  $NumHit$ –

sToDoubleStep consecutive iterations, we can double the step size in order to reduce the total number of iterations of the path tracking routine. Algorithm 1 describes the proposed method in full detail<sup>2</sup>.

### 3.3.3 Convergence analysis

In this section, we analyze the convergence of the homotopy continuation method and provide some important details regarding the implementation of the algorithm.

Let us define the two following spaces:

$$\mathcal{I} = \{(\mathbf{H}_{k\ell}) : \ell \in \{1, \dots, A\}, k \in \{1, \dots, B\}\},$$

$$\mathcal{O} = \{(\mathbf{U}_k, \mathbf{V}_{j\ell}) : \ell \in \{1, \dots, A\}, j, k \in \{1, \dots, B\}\},$$

which can be thought of as the space of possible “inputs” (channel matrices) and the set of possible “outputs” (precoders and decoders) of the algorithm. Note that an element of  $\mathcal{I}$  or  $\mathcal{O}$  is just a concatenation of complex matrices. We assume that the order of such concatenation is fixed and we can thus identify

$$\mathcal{I} \equiv \mathbb{C}^a, \quad \mathcal{O} \equiv \mathbb{C}^b,$$

where

$$a = \sum_{k,\ell} M_\ell N_k, \quad b = \sum_k N_k D_k^{\text{Rx}} + \sum_\ell M_\ell D_\ell^{\text{Tx}}.$$

Note that alternatively to (3.12) we can consider the same equations but changing Hermitian transpose to transpose:

$$\mathbf{U}_k^T \mathbf{H}_{k\ell} \mathbf{V}_\ell = \mathbf{A}_{k\ell} \quad \forall k, \ell. \quad (3.20)$$

Mathematically, it is more simple to deal with this case since the functions involved are then (complex) analytic, so we consider these equivalent equations in this section. Obviously, a solution to (3.20) produces an answer to (3.12) and viceversa, so there is no harm in this change. In the rest of this section, we will focus on the most challenging case that happens when the solution set for any given  $\mathbf{H} = (\mathbf{H}_{k\ell}) \in \mathcal{I}$  (out of some zero-measure set) is finite [102]. In words, this is the situation of a tightly-feasible scenario in which removing a single antenna at any transmitter or receiver turns the system unfeasible [103].

Recall that, for fixed  $\mathbf{H} \in \mathcal{I}$ , a point  $(\mathbf{U}_k, \mathbf{V}_{j\ell}) \in \mathcal{O}$  is a *nonsingular* solution of (3.20) if the linear mapping given by the derivative:

$$(\dot{\mathbf{U}}_k, \dot{\mathbf{V}}_{k\ell}) \rightarrow \dot{\mathbf{U}}_k^T \mathbf{H}_{k\ell}(t) \mathbf{V}_\ell + \mathbf{U}_k^T \dot{\mathbf{H}}_{k\ell}(t) \mathbf{V}_\ell \quad \forall k, \ell \quad (3.21)$$

is invertible. It is thus easy to check if a solution of (3.20) is nonsingular (up to numerical errors).

We now state our convergence result

<sup>2</sup>For our actual implementation of the proposed method, the input parameters of the algorithm take the following values:  $\Delta t = 10^{-3}$ ,  $\text{NwtTo1} = 10^{-10}$ ,  $\text{MaxNwtIter} = 5$ ,  $\text{MinStepSize} = 10^{-15}$  and  $\text{NumHitsToDoubleStep} = 3$ .

**Theorem 3.1.** Let  $\bar{\mathbf{H}} \in \mathcal{I}$  and let  $(\bar{\mathbf{U}}_k, \bar{\mathbf{V}}_{j\ell})$  be a nonsingular solution of

$$\bar{\mathbf{U}}_k^T \bar{\mathbf{H}}_{k\ell} \bar{\mathbf{V}}_{j\ell} = \mathbf{A}_{k\ell} \quad \forall k, \ell. \quad (3.22)$$

Then, for almost all  $\mathbf{H} \in \mathcal{I}$ , the solution  $(\bar{\mathbf{U}}_k, \bar{\mathbf{V}}_{j\ell})$  can be smoothly continued using the homotopy  $\mathbf{H}(t) = (1-t)\bar{\mathbf{H}} + t\mathbf{H}$  to a nonsingular solution of (3.20).

**Proof.** See Appendix A.1.

In general, we cannot guarantee in advance that the start system in Section 3.3.1 satisfies the nonsingularity hypothesis of Theorem 3.1. However, as pointed out above, checking whether it satisfies the hypothesis is an elementary task, which implies that there are two possibilities regarding the starting pair described in Section 3.3.1

1. Case 1: our starting alignment solution  $(\bar{\mathbf{U}}_k, \bar{\mathbf{V}}_{j\ell})$  defines a nonsingular solution of (3.22). Then, with probability 1 a channel  $\mathbf{H} \in \mathcal{I}$  admits at least one nonsingular alignment solution and we can consider the problem as feasible. Moreover, we can construct a solution for almost all possible inputs by continuing the known one.
2. Case 2: our starting alignment solution  $(\bar{\mathbf{U}}_k, \bar{\mathbf{V}}_{j\ell})$  defines a singular solution of (3.22). In this case, the derivative (3.21) is singular and hence we cannot continue the solution to the target system using the generated start system. Although the singularity of (3.21) does not determine if the problem is feasible or unfeasible, in this work we assume that the networks under study are feasible systems. Therefore, it may suffice to perform the procedure in Section 3.3.1 again in order to generate a new start system which might define a nonsingular solution of (3.22) (see Case 1).

Consequently, in the worst scenario we may just have to discard the start system after a simple linear algebra test, and then generate a new starting point as described in Section 3.3.1. This contrasts with other iterative methods such as Alternating Minimization or simply applying Newton's method where one must make a (possibly very long) number of iterations on an initial guess with no a priori guarantee on the convergence of the method.

Of course, the algorithm being a numerical method, there is a chance that, even knowing that a continuation exists, it cannot be found in reasonable time or the homotopy step is too small to be used in practice (see the discussion in Section 3.3.2). Theorem 3.1 gives however a strong theoretical support to the use of homotopy techniques for the problem under study.

### 3.3.4 Simulation results

In this section we evaluate the performance of the homotopy continuation IA algorithm by means of Monte Carlo simulations in a generic X network topology. More

**Table 3.1:** Prob[DoF =  $K^2d = 16$ ] or probability of achieving the requested number of degrees of freedom for  $K = 4$  and  $d = 1$ .

Scenario	1	2	3
$(M, N) =$	$(8, 9)$	$(9, 9)$	$(10, 10)$
HC	0.98	0.99	1.00
MinIL	0.00	0.00	0.44

specifically, the performance of the method is evaluated on a 4-user MIMO X network including three different antenna configurations (Scenarios 1, 2, and 3). Afterwards, the proposed scheme is applied over structured IC and X channels (Scenarios 4 and 5), such as those arising when symbol extensions are allowed. For each configuration, the results of 1000 independent Rayleigh channel realizations were averaged.

In order to evaluate the performance of the proposed method (denoted as HC), we consider for comparison the minimum interference leakage (MinIL) alternating minimization algorithm proposed in [48], which has been conveniently adapted to operate in MIMO X networks.

### Generic channels

The first comparison scenario is a MIMO X network comprised of  $A = 4$  transmitters and  $B = 4$  receiver nodes, satisfying  $A = B = K$ , equipped with  $M$  and  $N$  antennas, respectively. Each transmitter wishes to send one stream to each receiver, i.e.,  $D_{k\ell} = D = 1 \forall k, \ell$ . As shown in Table 3.1, three different antenna configurations were simulated. Notice that the bound in (3.2) holds with equality for Scenario 1, which has the minimum number of antennas to ensure feasibility.

Although there exists numerical evidence that for feasible systems the MinIL method always converges to the global minimum for generic interference channels, it does not guarantee the rank conditions in (3.1b) for an X network. This is due to the fact that, as it was mentioned before, in an X network every link acts as both a desired and an interfering link. Since the proposed algorithm takes both interference cancellation and rank preservation conditions into account, it clearly outperforms the results achieved by MinIL in terms of degrees of freedom, especially in the tightest scenarios, as Fig. 3.8 shows. Note that the sum-rate slope in the high signal-to-noise-ratio (SNR) regime attained by HC in Scenario 1 is even higher than that achieved by MinIL in Scenario 3, with the advantage of HC using fewer antennas than MinIL. As the number of antennas is increased, the performance of MinIL improves, requiring at least 10 antennas at both ends of the link to obtain the requested DoF.

Of course, the probability of attaining the requested DoF affects the average sum-rate performance. As shown in Table 3.1, we observe that the probability of achieving the maximum of  $K^2d = 16$  DoF is significantly higher for the HC algorithm, being close to 1 for the 3 considered scenarios. This is in agreement with the theoretical

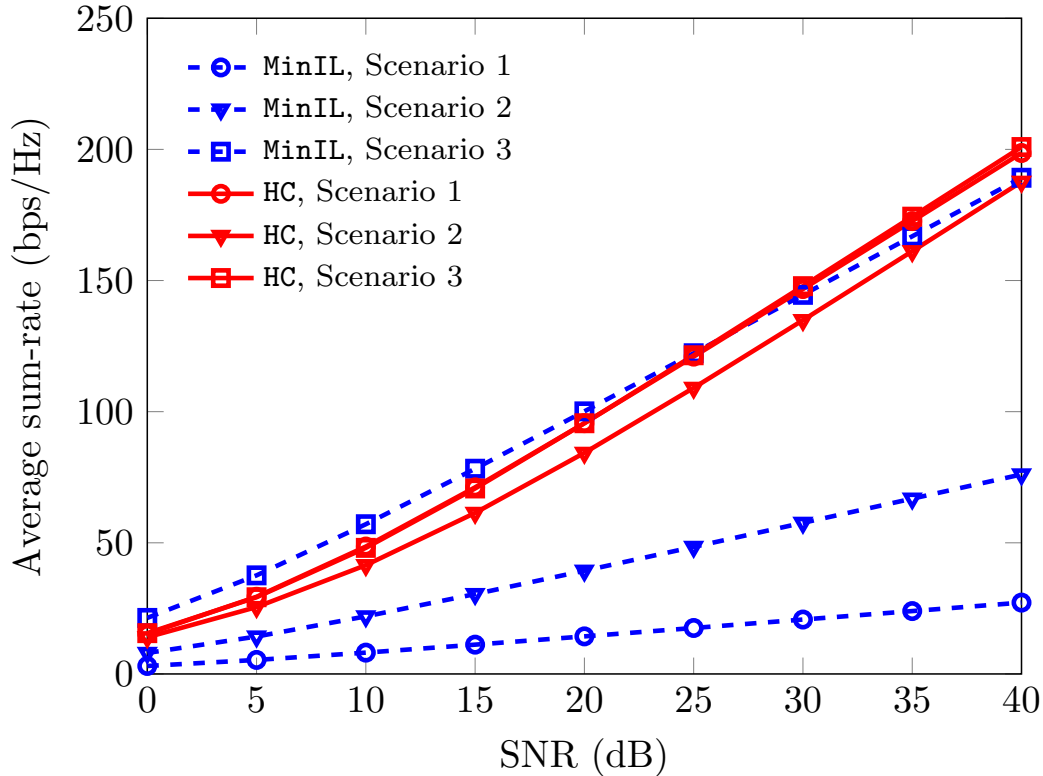


**Figure 3.8:** Average sum-rate achieved by MinIL and HC in the three considered scenarios.

convergence result proved in Theorem 3.1, and provides strong support for the use of the homotopy continuation algorithm in MIMO X networks.

### Structured channels

In Scenarios 4 and 5, we evaluate the performance of the HC algorithm when symbols extensions are used. To this end, two different network configurations, namely, an interference channel and a 2-user X channel are considered.

Scenario 4 is comprised of  $K = 6$  users, each transmitter is equipped with  $M = 2$  antennas, and each receiver has a single antenna, i.e.,  $N = 1$ . The first three transmitter nodes wish to send 2 independent messages to their corresponding receivers, whereas the remaining three want to send 3 messages, leading to a demands matrix given by  $\mathbf{D} = \text{diag} [ 2 \ 2 \ 2 \ 3 \ 3 \ 3 ]$ . Moreover, 6 channel extensions are used, giving rise to a block-diagonal channel matrix. Following the notation introduced in [79],[83], the scenario of interest corresponds to a  $[(2 \times 1, 2)^3, (2 \times 1, 3)^3, 6]$  interference network with a total of 15 independent streams.

Since the aforementioned system model has been previously studied in [83], we compare the sum-rate slope achieved by homotopy continuation to that obtained by the algorithm in [83], which is denoted here as StructMinIL. This method is a

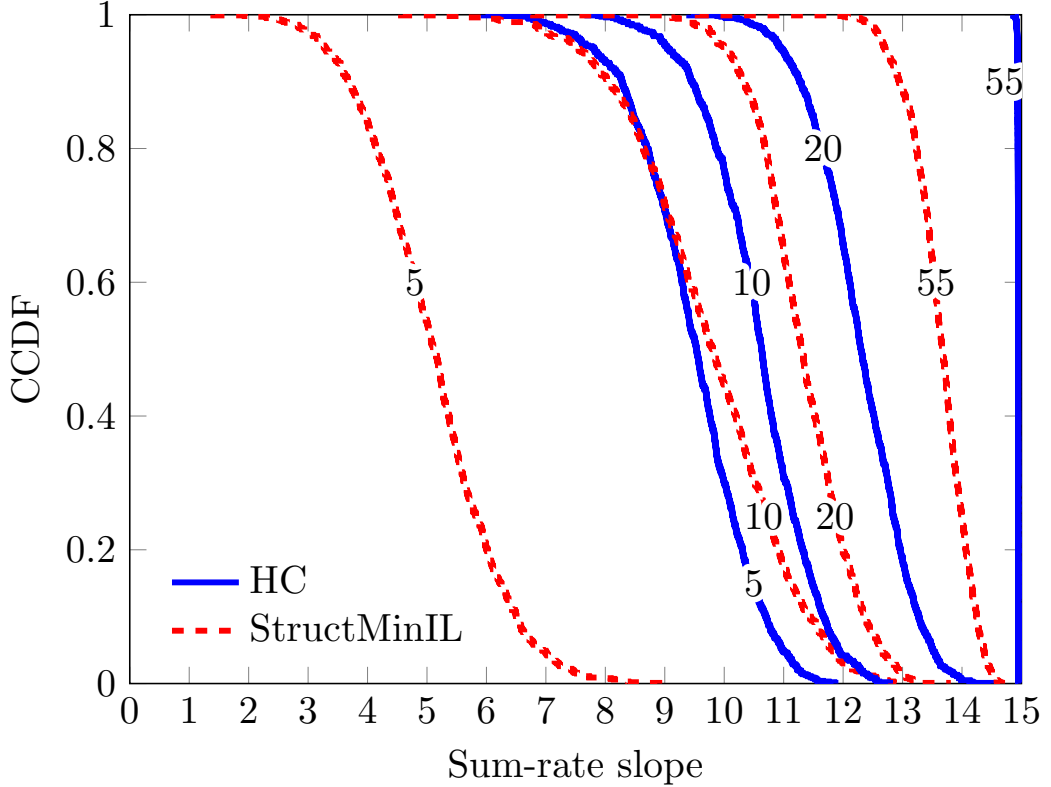


**Figure 3.9:** CCDF of the sum-rate slope at  $\text{SNR} = \{5, 10, 20, 55\}$  dB in Scenario 4.

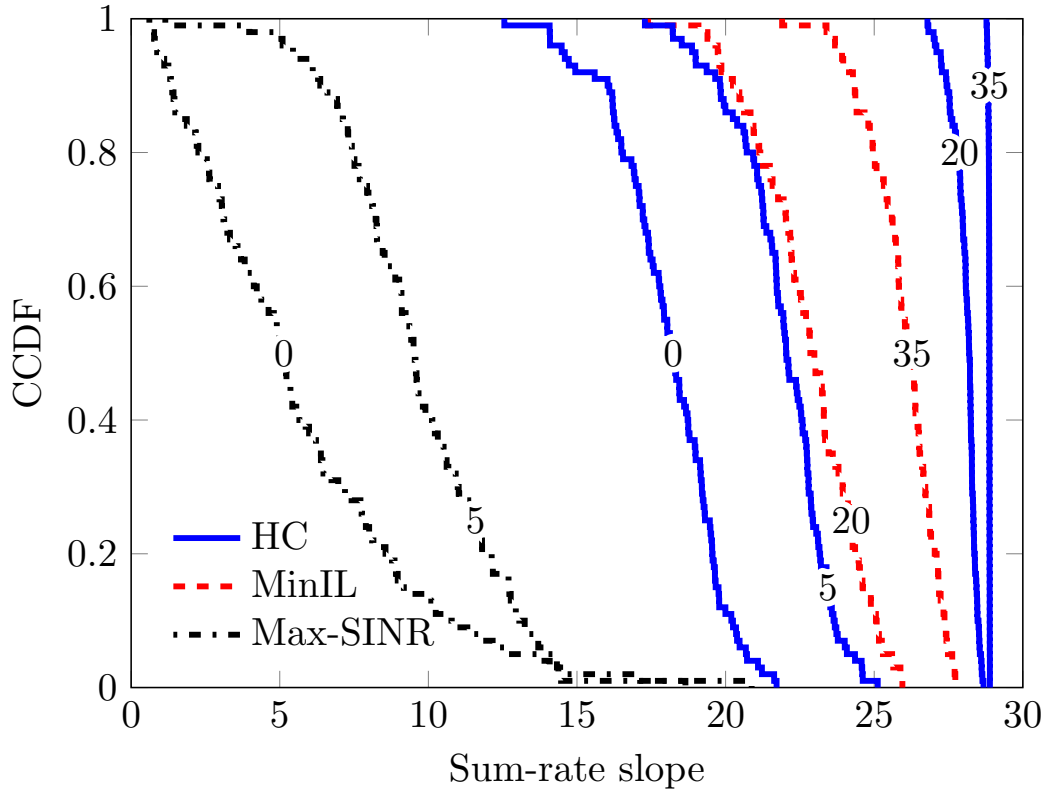
modification of the `MinIL` algorithm that explicitly enforces a given rank for the signal subspaces while the transmitters satisfy a power budget constraint. Although the `StructMinIL` method improves the performance of `MinIL` with symbol extensions, the optimization problem in [83] is non-convex and therefore convergence to the desired solution cannot be guaranteed.

Figure 3.9 shows the complementary cumulative distribution function (CCDF) of the sum-rate slope achieved by both algorithms at several SNR values. From this figure, it is clear that the DoF performance of HC is better than that of the `StructMinIL`.

Now, we focus on a 2-user X channel, with transmitters having  $M_1 = 5$  and  $M_2 = 8$  antennas, and with receivers equipped with  $N_1 = 6$  and  $N_2 = 7$  antennas, respectively. According to [80], this network configuration is capable of transmitting a maximum of 29 independent data streams when using a total of 3 channel extensions. Hereinafter, we will refer to this setting as Scenario 5. The only feasible demands allocation was numerically found to be given by

$$\mathbf{D} = \begin{bmatrix} 5 & 8 \\ 5 & 11 \end{bmatrix}.$$

The CCDF of the sum-rate slope achieved by HC at different SNR values in Scenario 5 is represented in Fig. 3.10, which shows that the proposed algorithm always obtains the maximum DoF for SNRs larger than 35 dB, in agreement with



**Figure 3.10:** CCDF of the sum-rate slope at  $\text{SNR} = \{0, 5, 20, 35\}$  dB in Scenario 5.

the results in [80]. Additionally, we have compared the HC method with two alternative algorithms: for high SNR values (20 and 35 dB) we used again the MinIL method, whereas for low SNR regimes (0 and 5 dB) we used the maximum signal-to-interference-plus-noise ratio (Max-SINR) algorithm [48][104] adapted to work in MIMO X networks. Note that, given the characteristics of Max-SINR algorithm, it fits well within the low SNR regime whilst providing a performance similar to MinIL for the rest of SNR values. As shown in Fig. 3.10, the proposed algorithm outperforms both Max-SINR and MinIL methods, hence being the most appropriate choice for the whole range of SNR values.

### Computational complexity

We finally compare the computational complexity of the HC and MinIL algorithms. For this comparison, we have considered the X network in Scenario 3. Table 3.2 shows the average number of iterations required by each algorithm to achieve convergence in the considered scenario, as well as the average time per iteration. We can see that the number of iterations for the HC method is significantly lower than that of the

**Table 3.2:** Average number of iterations and average time per iteration in Scenario 3.

Algorithm	Number of iterations	Time per iteration (ms)
HC	40.55	43.228
MinIL	356.15	5.788

MinIL. However, the average time per iteration is considerably higher<sup>3</sup>, resulting in a similar overall convergence time for both algorithms.

<sup>3</sup>The average number of Newton corrections for Scenario 3 is 3.37.



## DoF analysis of flexible duplexing

Once we have described the IA algorithm to be applied, in this chapter we characterize flexible duplexing in terms of DoF. As mentioned in previous sections, the works addressing the implementation of interference alignment in HetNets together with flexible duplexing are still scarce. However, remarkable results regarding DoF can be found in [64] for 2-cell settings.

In Section 4.1, we particularize the interference alignment conditions to the case of cellular networks implementing flexible duplexing. Then, the IA feasibility test for 2-cell deployments in [64] is introduced in Section 4.2 as a background for further study. In Section 4.3, a necessary condition for the feasibility of alignment is provided in the multi-cell case, and finally the DoF improvements achieved by flexible UL/DL scheduling are numerically evaluated by means of the HC algorithm described in 3.3.

### 4.1 IA for flexible duplexing schemes

Although a general model for the interference alignment conditions is detailed in Section 3.1, a reformulation is required in order to describe the HetNets under evaluation. For this purpose, in the following we decouple the uplink and downlink signal models in such a way that flexible duplexing is fully characterized.

In this work, we consider a MIMO cellular network as in Section 3.1.3 composed of  $G$  cells, where the  $g$ -th cell contains a base station (BS) and  $K_g$  user equipments (UE). There is a total of  $G_u$  uplink cells and  $G_d$  downlink cells, such that  $G = G_u + G_d$ . Each base station is equipped with  $N_g$  antennas, whereas the  $k$ -th user of cell  $g$ , which we will denote as user  $k_g$ , has  $M_{k_g}$  antennas, with  $g \in \{1, 2, \dots, G\}$  and  $k_g \in \{1, 2, \dots, K_g\}$ .

Since a cellular network in flexible duplexing configuration comprises cells in both uplink and downlink mode, we split the notation into signal models (4.1) and (4.2), one for each type of cell.

Regarding the uplink cells, base station  $g$  applies the decoding matrices  $\mathbf{U}_{k_g} \in \mathbb{C}^{N_g \times D_{k_g}}$  to receive  $D_{k_g}$  independent data streams from each user  $k_g$ , leading to a set of received signals given by (4.1), where  $\mathbf{H}_{g,k_g} \in \mathbb{C}^{N_g \times M_{k_g}}$  represents the channel matrix from user  $k_g$  to base station  $g$ ;  $\mathbf{s}_{k_g} \in \mathbb{C}^{D_{k_g} \times 1}$  is the symbol vector transmitted

$$\mathbf{r}_{k_g} = \mathbf{U}_{k_g}^H \left( \underbrace{\mathbf{H}_{g,k_g} \mathbf{V}_{k_g} \mathbf{s}_{k_g}}_{\text{desired information}} + \underbrace{\sum_{\substack{\ell_g=1 \\ \ell_g \neq k_g}}^{K_g} \mathbf{H}_{g,\ell_g} \mathbf{V}_{\ell_g} \mathbf{s}_{\ell_g}}_{\text{intra-cell interference}} + \underbrace{\sum_{\substack{j=1 \\ j \neq g}}^{G_u} \sum_{i_j=1}^{K_j} \mathbf{H}_{g,i_j} \mathbf{V}_{i_j} \mathbf{s}_{i_j}}_{\text{uplink cells}} + \underbrace{\sum_{j=G_u+1}^G \sum_{i_j=1}^{K_j} \mathbf{H}_{g,j} \mathbf{V}_{i_j} \mathbf{s}_{i_j}}_{\text{downlink cells}} + \mathbf{n}_g \right) \quad (4.1)$$

$$\mathbf{r}_{\ell_j} = \mathbf{U}_{\ell_j}^H \left( \underbrace{\mathbf{H}_{\ell_j,j} \mathbf{V}_{\ell_j} \mathbf{s}_{\ell_j}}_{\text{desired information}} + \underbrace{\sum_{\substack{k_j=1 \\ k_j \neq \ell_j}}^{K_j} \mathbf{H}_{\ell_j,j} \mathbf{V}_{k_j} \mathbf{s}_{k_j}}_{\text{intra-cell interference}} + \underbrace{\sum_{g=1}^{G_u} \sum_{i_g=1}^{K_g} \mathbf{H}_{\ell_j,i_g} \mathbf{V}_{i_g} \mathbf{s}_{i_g}}_{\text{uplink cells}} + \underbrace{\sum_{\substack{g=G_u+1 \\ g \neq j}}^G \sum_{i_g=1}^{K_g} \mathbf{H}_{\ell_j,g} \mathbf{V}_{i_g} \mathbf{s}_{i_g}}_{\text{downlink cells}} + \mathbf{n}_{\ell_j} \right) \quad (4.2)$$

by user  $k_g$  and precoded by applying the precoding matrix  $\mathbf{V}_{k_g} \in \mathbb{C}^{M_{k_g} \times D_{k_g}}$ .  $\mathbf{n}_g \in \mathbb{C}^{N_g \times 1}$  is the additive white Gaussian noise (AWGN) at the input of BS  $g$ .

Analogously, in the case of downlink cells, the UE  $\ell_j$  applies a decoder  $\mathbf{U}_{\ell_j} \in \mathbb{C}^{M_{\ell_j} \times D_{\ell_j}}$ , giving a received signal represented by (4.2), where  $\mathbf{H}_{\ell_j,j} \in \mathbb{C}^{M_{\ell_j} \times N_j}$  is the channel matrix from BS  $j$  to UE  $\ell_j$ .  $\mathbf{s}_{\ell_j} \in \mathbb{C}^{D_{\ell_j} \times 1}$  denotes the symbol vector transmitted between base station  $j$  and user  $\ell_j$  and precoded with  $\mathbf{V}_{\ell_j} \in \mathbb{C}^{N_j \times D_{\ell_j}}$ . Finally,  $\mathbf{n}_{\ell_j} \in \mathbb{C}^{M_{\ell_j} \times 1}$  represents the AWGN at the input of user  $\ell_j$ .

Given the received signals in (4.1) and (4.2), the interference cancellation conditions can be expressed as

$$\mathbf{U}_{k_g}^H \mathbf{H}_{g,i_j} \mathbf{V}_{i_j} = \mathbf{0}, \quad \forall k, g, j, i \neq k \quad (4.3a)$$

$$\mathbf{U}_g^H \mathbf{H}_{g,j} \mathbf{V}_{i_j} = \mathbf{0}, \quad \forall g, i, j \neq g \quad (4.3b)$$

$$\mathbf{U}_{\ell_j}^H \mathbf{H}_{\ell_j,i_g} \mathbf{V}_{i_g} = \mathbf{0}, \quad \forall \ell, j, i, g \neq j \quad (4.3c)$$

$$\mathbf{U}_{\ell_j}^H \mathbf{H}_{\ell_j,g} \mathbf{V}_{i_g} = \mathbf{0}, \quad \forall \ell, j, g, i \neq \ell, \quad (4.3d)$$

being  $D_g = \sum_{k_g} D_{k_g}$  the total data streams transmitted within the  $g$ -th cell and  $\mathbf{U}_g \in \mathbb{C}^{N_g \times D_g}$  the horizontal concatenation of all  $\mathbf{U}_{k_g} \in \mathbb{C}^{N_g \times D_{k_g}}$ , i.e.,

$$\mathbf{U}_g \stackrel{\text{def}}{=} \text{cat}_{k_g} \left( \mathbf{U}_{k_g} \right).$$

Condition (4.3a) corresponds to the interference generated by every UE in uplink mode at the input of a base station in an uplink cell, whereas (4.3b) is associated to the interference from a base station in downlink mode at the input of a BS in uplink.

Analogously, conditions (4.3c) and (4.3d) take into account the interference at a UE in downlink configuration, coming from both users in uplink and base stations in downlink cells, respectively.

Furthermore, we have to guarantee that the DoF of the desired signals are preserved by satisfying the following rank conditions

$$\text{rank} \left( \mathbf{U}_g^H \left[ \mathbf{H}_{g,1_g} \mathbf{V}_{1_g}, \dots, \mathbf{H}_{g,K_g} \mathbf{V}_{K_g} \right] \right) = D_g, \quad \forall g \quad (4.4a)$$

$$\text{rank} \left( \mathbf{U}_{\ell_j}^H \mathbf{H}_{\ell_j,j} \mathbf{V}_{\ell_j} \right) = D_{\ell_j}, \quad \forall j, \ell_j. \quad (4.4b)$$

Note that conditions (4.4a) and (4.4b) refer to the rank preservation for both uplink and downlink cells, respectively.

## 4.2 IA feasibility for 2-cell networks

Authors in [64] presented a remarkable result in the context of flexible duplexing. More specifically, they proposed a necessary condition and a sufficient condition for the feasibility of IA in 2-cell networks, being one of the cells in DL and the other in UL. In this section, we review these conditions, and we rely on the algorithm in Section 3.3 to illustrate their result with a 2-cell example.

Let us consider a MIMO cellular network such as described in Section 4.1, with  $G = 2$ ,  $G_u = 1$  and  $G_d = 1$ . The downlink cell comprises  $K$  users whereas the UL cell includes  $L$  users. The base stations are equipped with  $N_d$  and  $N_u$  antennas, respectively. Additionally, user  $k$  in downlink is equipped with  $N_{k_d}$  antennas and user  $\ell$  in uplink has  $N_{\ell_u}$  antennas, with  $k \in [1, 2, \dots, K]$  and  $\ell \in [1, 2, \dots, L]$ . Finally, the BS in downlink sends  $D_{k_d}$  streams to user  $k$  in the DL cell, whereas the  $\ell$ -th UE in uplink transmits  $D_{\ell_u}$  streams to their corresponding BS<sup>1</sup>.

**Theorem 4.1.** *For a MIMO 2-cell network applying flexible duplexing, the DoF tuple  $(D_{1_d}, \dots, D_{K_d}, D_{1_u}, \dots, D_{L_u})$  must satisfy the following conditions:*

<sup>1</sup>Since flexible duplexing in 2-cell setups always includes a DL and a UL cell, we use subindices  $d$  and  $u$  instead of numeric indexing to improve readability.

$$\sum_{k=1}^K D_{k_d} \leq N_d, \quad (4.5a)$$

$$\sum_{\ell=1}^L D_{\ell_u} \leq N_u, \quad (4.5b)$$

$$\sum_{k=1}^K D_{k_d} + \sum_{\ell=1}^L D_{\ell_u} \leq \max(N_d, N_u), \quad (4.5c)$$

$$\sum_{k \in I_d} D_{k_d} + \sum_{\ell \in I_u} D_{\ell_u} \leq \max\left(\sum_{k \in I_d} N_{k_d}, \sum_{\ell \in I_u} N_{\ell_u}\right) \quad \forall I_d, I_u, \quad (4.5d)$$

$$\sum_{k \in I_d} \sum_{\ell \in I_u} D_{\ell_u} D_{k_d} \leq \sum_{k \in I_d} D_{k_d} (N_{k_d} - D_{k_d}) + \sum_{\ell \in I_u} D_{\ell_u} (N_{\ell_u} - D_{\ell_u}) \quad \forall I_d, I_u, \quad (4.5e)$$

where  $I_d \subseteq [1, 2, \dots, K]$  and  $I_u \subseteq [1, 2, \dots, L]$ .

*Proof.* See [64]. □

Conditions (4.5a) and (4.5b) are straightforward. Also, conditions (4.5c) and (4.5d) can be obtained from the 2-user MIMO IC bound in [42] by assuming full cooperation between all the user equipments. Finally, condition (4.5e) results from counting the number of free variables and linear equations required to solve the IA problem in (4.3). More details on variable and equation counting for IA properness and feasibility can be found in [85, 77].

In order to complete the necessary condition in Theorem 4.1 with a sufficient condition, authors in [64] consider a partition of the inter-cell channel matrices  $\mathbf{H}_{k_d \ell_u}$  into four blocks, such that

$$\mathbf{H}_{k_d \ell_u} = \begin{bmatrix} \mathbf{H}_{k_d \ell_u}^{(1)} & \mathbf{H}_{k_d \ell_u}^{(2)} \\ \mathbf{H}_{k_d \ell_u}^{(3)} & \mathbf{H}_{k_d \ell_u}^{(4)} \end{bmatrix}, \quad (4.6)$$

where  $\mathbf{H}_{k_d \ell_u}^{(1)} \in \mathbb{C}^{D_{k_d} \times D_{\ell_u}}$ ,  $\mathbf{H}_{k_d \ell_u}^{(2)} \in \mathbb{C}^{D_{k_d} \times (N_{\ell_u} - D_{\ell_u})}$ ,  $\mathbf{H}_{k_d \ell_u}^{(3)} \in \mathbb{C}^{(N_{k_d} - D_{k_d}) \times D_{\ell_u}}$ , and finally  $\mathbf{H}_{k_d \ell_u}^{(4)} \in \mathbb{C}^{(N_{k_d} - D_{k_d}) \times (N_{\ell_u} - D_{\ell_u})}$ .

**Theorem 4.2.** *In a MIMO 2-cell network applying flexible duplexing, the DoF tuple  $(D_{1_d}, \dots, D_{K_d}, D_{1_u}, \dots, D_{L_u})$  is feasible almost surely if (4.5a) to (4.5c) are satisfied and the matrix  $\mathbf{H}_d$  in (4.7) is full rank.*

$$\mathbf{H}_d = \left[ \begin{array}{cccccc|cccc} \mathbf{H}'_{1_d 1_u} & \mathbf{0} & \cdots & \mathbf{0} & \cdots & \mathbf{0} & \mathbf{H}''_{1_d 1_u} & \mathbf{0} & \cdots & \mathbf{0} \\ \mathbf{H}'_{1_d 2_u} & \mathbf{0} & \cdots & \mathbf{0} & \cdots & \mathbf{0} & \mathbf{0} & \mathbf{H}''_{1_d 2_u} & \cdots & \mathbf{0} \\ \vdots & \vdots & \ddots & \vdots & \ddots & \vdots & \vdots & \ddots & \vdots & \vdots \\ \mathbf{H}'_{1_d L_u} & \mathbf{0} & \cdots & \mathbf{0} & \cdots & \mathbf{0} & \mathbf{0} & \mathbf{0} & \cdots & \mathbf{H}''_{1_d L_u} \\ \mathbf{0} & \mathbf{H}'_{2_d 1_u} & \cdots & \mathbf{0} & \cdots & \mathbf{0} & \mathbf{H}''_{2_d 1_u} & \mathbf{0} & \cdots & \mathbf{0} \\ \mathbf{0} & \mathbf{H}'_{2_d 2_u} & \cdots & \mathbf{0} & \cdots & \mathbf{0} & \mathbf{0} & \mathbf{H}''_{2_d 2_u} & \cdots & \mathbf{0} \\ \vdots & \vdots & \ddots & \vdots & \ddots & \vdots & \vdots & \ddots & \vdots & \vdots \\ \mathbf{0} & \mathbf{H}'_{2_d L_u} & \cdots & \mathbf{0} & \cdots & \mathbf{0} & \mathbf{0} & \mathbf{0} & \cdots & \mathbf{H}''_{2_d L_u} \\ \vdots & \vdots & \ddots & \vdots & \ddots & \vdots & \vdots & \vdots & \ddots & \vdots \\ \mathbf{0} & \mathbf{0} & \cdots & \mathbf{0} & \cdots & \mathbf{H}'_{K_d 1_u} & \mathbf{H}''_{K_d 1_u} & \mathbf{0} & \cdots & \mathbf{0} \\ \mathbf{0} & \mathbf{0} & \cdots & \mathbf{0} & \cdots & \mathbf{H}'_{K_d 2_u} & \mathbf{0} & \mathbf{H}''_{K_d 2_u} & \cdots & \mathbf{0} \\ \vdots & \vdots & \ddots & \vdots & \ddots & \vdots & \vdots & \vdots & \ddots & \vdots \\ \mathbf{0} & \mathbf{0} & \cdots & \mathbf{0} & \cdots & \mathbf{H}'_{K_d L_u} & \mathbf{0} & \mathbf{0} & \cdots & \mathbf{H}''_{K_d L_u} \end{array} \right], \quad (4.7)$$

where

$$\mathbf{H}'_{k_d \ell_u} = \mathbf{I}_{D_{k_d}} \otimes \left( \mathbf{H}_{k_d \ell_u}^{(3)T} \right),$$

$$\mathbf{H}''_{k_d \ell_u} = \begin{bmatrix} \mathbf{I}_{D_{\ell_u}} \otimes \left( \mathbf{H}_{k_d \ell_u}^{(2)} [1] \right)_{1,1:N_{\ell_u}-D_{\ell_u}} \\ \mathbf{I}_{D_{\ell_u}} \otimes \left( \mathbf{H}_{k_d \ell_u}^{(2)} [2] \right)_{2,1:N_{\ell_u}-D_{\ell_u}} \\ \vdots \\ \mathbf{I}_{D_{\ell_u}} \otimes \left( \mathbf{H}_{k_d \ell_u}^{(2)} [D_{k_d}] \right)_{D_{k_d},1:N_{\ell_u}-D_{\ell_u}} \end{bmatrix},$$

whilst  $\mathbf{H}_{k_d \ell_u}^{(2)}$  and  $\mathbf{H}_{k_d \ell_u}^{(3)}$  are defined in (4.6).

*Proof.* See [64]. □

**Remark 4.3.** When building the matrix  $\mathbf{H}_d$  in (4.7), only the user equipments are implied. Therefore, the sufficient feasibility condition given by Theorem 4.2 can be straightforwardly extended for multi-cell cases with only one downlink cell.

### 4.3 Extension to multi-cell networks

In this section, we extend the network model in Section 4.2 to general multi-cell networks. In this context, we provide necessary conditions for the feasibility of alignment, as previously presented in Theorem 4.1 for 2-cell networks. Additionally, we particularize the aforementioned condition to the case of symmetric DoF and equal distribution of antennas, showing that, in some particular cases, flexible duplexing is

not capable of improving the DoF performance of conventional TDD systems. Let us remember that authors in [105] showed that the existence of DoF benefits depends on the network configuration. Finally, we rely on numerical evaluation to discuss on the impact of network asymmetry on the DoF benefits achieved by flexible duplexing.

### 4.3.1 Necessary condition for the feasibility of IA

As stated in [64], there is a first condition that needs to be satisfied in every cell within the network:

$$\sum_k D_{k_g} = D_g \leq N_g, \quad \forall g.$$

Additionally, we establish the following result:

**Theorem 4.4.** *A necessary condition for the feasibility of IA in multi-cell networks implementing flexible duplexing is represented by*

$$\sum_{g=G_u+1}^G \sum_{k_g=1}^{K_g} \left[ D_{k_g} \left( \sum_{\substack{\ell_g=1 \\ \ell_g \neq k_g}}^{K_g} D_{\ell_g} + \sum_{\substack{j=1 \\ j \neq g}}^G D_j \right) \right] + \sum_{g=1}^{G_u} \left( g \sum_{\substack{j=1 \\ j \neq g}}^G D_j \right) \leq N_v, \quad (4.8)$$

where the left side of the inequality quantifies the total number of scalar equations and

$$N_v = \sum_{g=1}^{G_u} \left[ (N_g - D_g) D_g + \sum_{k_g=1}^{K_g} (M_{k_g} - D_{k_g}) D_{k_g} \right] + \sum_{g=G_u+1}^G \sum_{k_g=1}^{K_g} (N_g + M_{k_g} - 2D_{k_g}) D_{k_g},$$

is the number of free variables in the system.

*Proof.* Since  $\mathbf{U}_{k_g}$  and  $\mathbf{V}_{k_g}$  must be full column rank matrices for all  $g, k_g$  (see conditions (4.4a) and (4.4b)), we can right-multiply them by arbitrary invertible matrices, and both (4.3) and (4.4) will still hold. Hence, following the lines established in [77] for X networks and in [64] for 2-cell flexible duplexing networks, we can rewrite the precoding and decoding matrices as

$$\mathbf{U}_{k_g} = \begin{bmatrix} \mathbf{I}_{D_{k_g}} \\ \tilde{\mathbf{U}}_{k_g} \end{bmatrix} \mathbf{P}_{k_g}^{-1}, \quad \mathbf{V}_{k_g} = \begin{bmatrix} \mathbf{I}_{D_{k_g}} \\ \tilde{\mathbf{V}}_{k_g} \end{bmatrix} \mathbf{Q}_{k_g}^{-1}. \quad (4.9)$$

where  $\mathbf{P}_{k_g} = \mathbf{U}_{k_g}(1 : D_{k_g}, :)$  and  $\mathbf{Q}_{k_g} = \mathbf{V}_{k_g}(1 : D_{k_g}, :)$  are submatrices of  $\mathbf{U}_{k_g}$  and  $\mathbf{V}_{k_g}$ , respectively.

By transforming the precoders  $\mathbf{V}_{k_g}$  and decoders  $\mathbf{U}_{k_g}$  as in (4.9),  $D_{k_g}^2$  elements are fixed for each precoding/decoding matrix, thus leaving a total of  $N_v$  free variables,

where the first line corresponds to the uplink cells and the second term is associated to the downlink cells. Given that, for a system of equations to be proper, the number of equations must be less than or equal to the number of free variables, the inequality in (4.8) is a necessary condition for the feasibility of IA.  $\square$

### Necessary condition for symmetric networks

Let us consider now a network with symmetric demands and equal distribution of users and antennas for all cells, that is,  $D_{k_g} = d$ ,  $K_g = K$ ,  $N_g = N$ ,  $M_{k_g} = M \forall g, k_g$ . In this context, the following result holds.

**Corollary 4.5.** *In multi-cell networks with the same demands, users, and antenna configuration for all cells, no benefit in terms of maximum DoF can be achieved by means of flexible duplexing.*

*Proof.* The expressions in Section 4.3.1 for the number of variables and equations in this case leads to

$$\begin{aligned} N_v &= Kd [G_u [M + N - (K + 1)d] + G_d (M + N - 2d)], \\ N_e &= Kd^2 [G_u K(G - 1) + G_d [(K - 1) + K(G - 1)]]. \end{aligned}$$

As in (4.8), the condition  $N_e \leq N_v$  needs to be satisfied, thus yielding

$$d \leq \frac{M + N}{GK + 1}, \quad (4.10)$$

which is, in fact, exactly the same condition provided in [106] for conventional TDD systems.  $\square$

Therefore, if (4.10) holds with equality in a cellular network using a regular TDD configuration, flexible duplexing will not be able to improve the DoF performance of the system. Nevertheless, there exist many different topologies where flexible duplexing yields significant DoF benefits, as originally proved in [105, 64] for 2-cell cases and as we corroborate in Section 4.3.2 for other asymmetric multi-cell networks.

### 4.3.2 Numerical evaluation and results

In order to analyze the DoF benefits of flexible duplexing in multi-cell networks, we apply the homotopy continuation algorithm in Section 3.3 to two different simulation scenarios. For each scenario, the results of 1000 independent trials have been averaged.

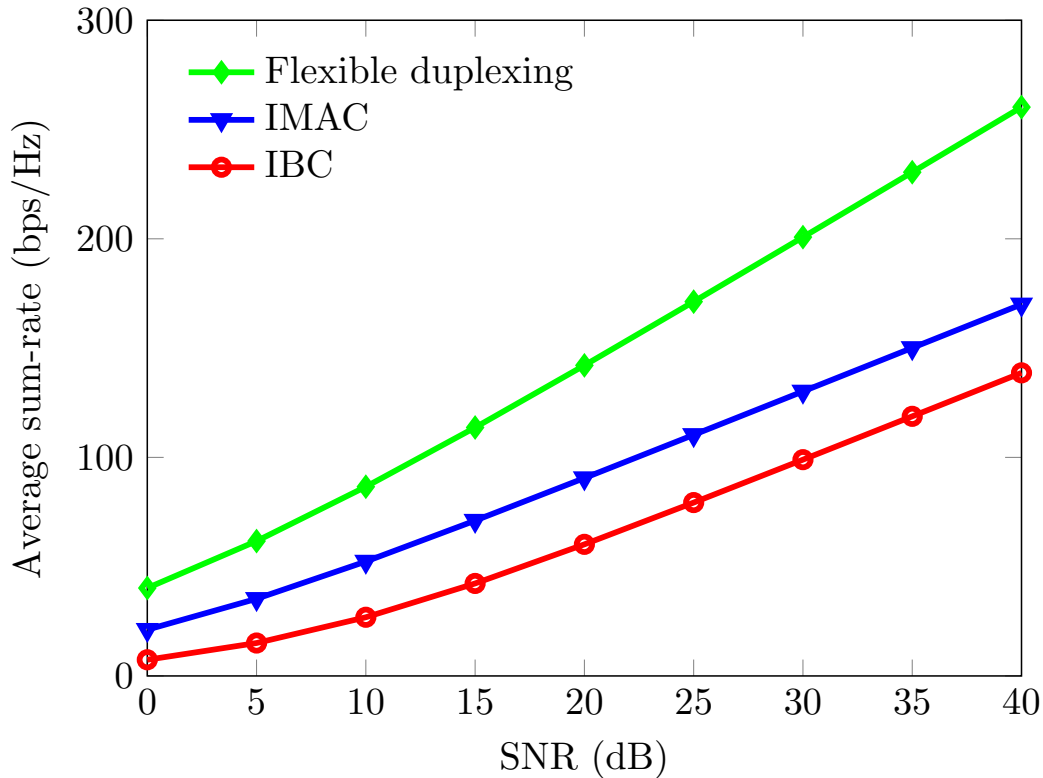


**Figure 4.1:** Average sum-rate achieved by the HC method in three different network configurations.

## 2-cell networks

The first scenario, denoted as Network 1, is intended to corroborate the results in [64], which have been previously explained in Section 4.2. It comprises  $G = 2$  cells, containing  $K_u = 4$  and  $N_2 = 3$  users, respectively. In cell 1, the base station (BS) has 12 antennas, whereas each mobile station (MS) is equipped with 8 antennas. Regarding the second cell, its base station has 18 antennas and the mobile stations have 4 antennas each.

In Figure 4.1, we compare the average sum-rate achieved by the homotopy continuation algorithm in three different configurations of the cellular network: two cells in downlink (IBC), two cells in uplink (IMAC), or cell 1 in downlink and cell 2 in uplink (R-TDD). For both the IBC and IMAC scenarios, in which the two cells operate synchronously as downlink or uplink channels, a maximum of 12 independent, interference-free data streams can be transmitted. However, according to [64], a total of 18 DoF can be achieved by applying the reverse TDD scheme, in which one of the cells operates in downlink mode while the other cell operates in uplink mode. This result is corroborated by our experiments, thus confirming that reverse TDD can enlarge the DoF region in some scenarios.

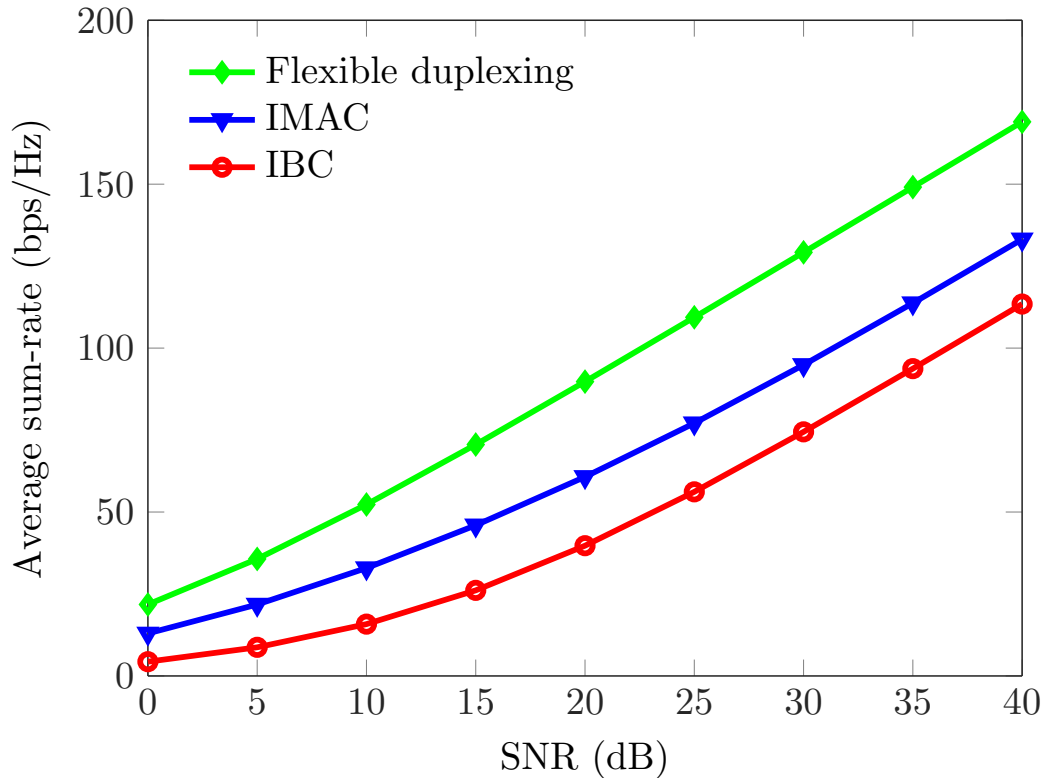


**Figure 4.2:** Average sum-rate achieved by the IBC, IMAC and flexible duplexing configurations in Network 2.

### Symmetric DoF and antenna configuration

The next network, denoted as Network 2, comprises  $G = 4$  cells whose base stations are equipped with  $N = 10$  antennas. Each cell contains  $K = 3$  users with  $M = 3$  antennas each. According to the notation introduced in [64], this is equivalent to a  $(10, (3, 3, 3))^4$  MIMO cellular network. In the case of flexible duplexing, there are two cells in uplink and two cells in downlink mode.

Figure 4.2 shows the average sum-rate achieved for the three considered configurations in Network 2, i.e., all cells in uplink (IMAC), all cells in downlink (IBC), and flexible duplexing, as a function of the SNR. Due to the duality properties of MIMO networks, both IMAC and IBC will attain the same DoF.

Since Network 2 satisfies the condition described in (4.10), and as we corroborated in Fig. 4.2, the sum-rate slope at the high SNR regime is the same for the three operating modes. More specifically, a maximum of 12 interference-free, independent data streams can be transmitted over this network configuration. This is due to the fact that (4.10) holds with equality for Network 2, and consequently flexible duplexing is not capable of improving the number of DoF obtained by conventional TDD configurations.

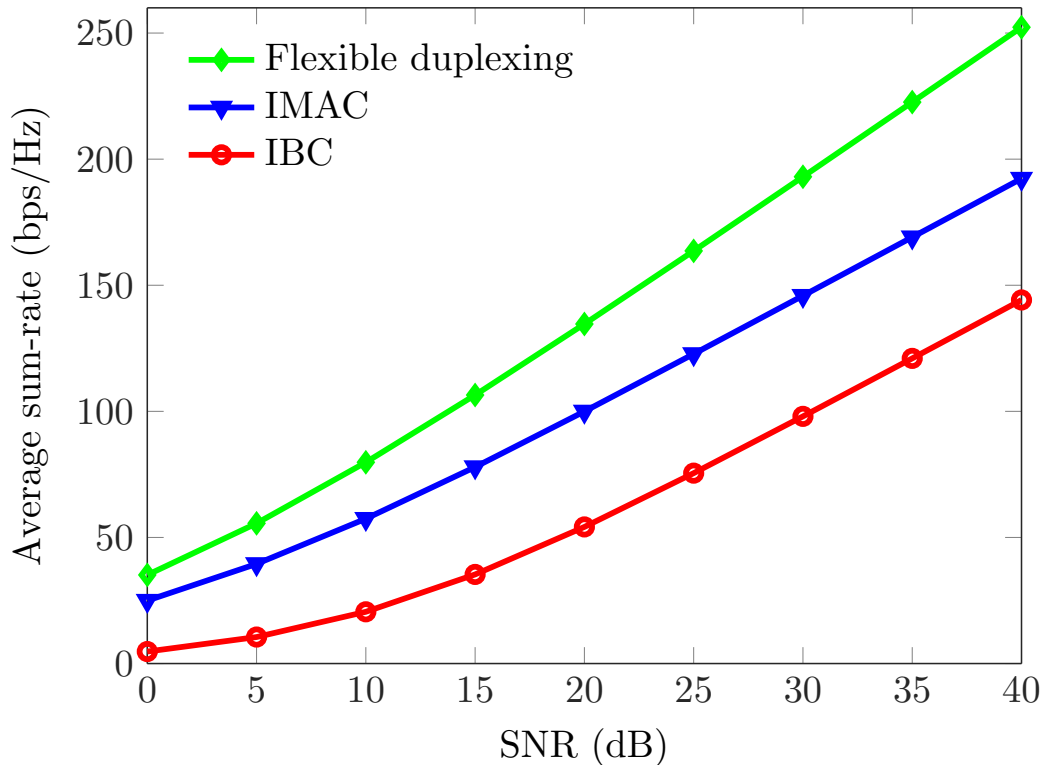


**Figure 4.3:** Average sum-rate achieved by the IBC, IMAC and flexible duplexing configurations in Network 3.

Nevertheless, improvements might be achieved by flexible UL/DL scheduling regarding other techniques and figures of merit. For instance, even though the number of DoF does not increase, there might be sum-rate benefits with symmetric distribution of data streams and number of antennas, as shown in [61] for a two-tier flexible duplexing network.

### General asymmetric configuration

We have considered a third example, composed of  $G = 3$  cells. Specifically, Network 3 is a  $(12, (8, 8, 8, 8)) \times (17, (4, 4, 4))^2$  MIMO cellular network, i.e., there is a BS equipped with  $N_1 = 12$  antennas, which wants to communicate with  $K_1 = 4$  users having  $M_{k_1} = 8$  antennas each. The other two base stations have  $N_2 = N_3 = 17$  antennas and are assigned to  $K_2 = K_3 = 3$  users with  $M_{k_2} = M_{k_3} = 4$  antennas each. In the case of flexible duplexing, the first cell is in downlink, whereas the remaining cells are configured in uplink. Notice that, for the complementary configuration (i.e., cell 1 in uplink, cells 2 and 3 in downlink), the duality is guaranteed according to [64].

As shown in Fig. 4.3, flexible duplexing provides noticeable DoF benefits for this asymmetric network configuration, extending the conclusions of [105, 64] to

the multi-cell context. Specifically, only 14 DoF are obtained by conventional TDD modes, whereas a total of 18 DoF can be achieved by applying flexible duplexing.

### Discussion on the asymmetry of multi-cell networks

In order to provide some insights into the implications of asymmetry in the networks under study, we analyze the configuration of Network 3 in more detail. As mentioned in the previous section, a total of 14 DoF are achieved by applying conventional TDD modes. More specifically, this amount of degrees of freedom is obtained with  $D_{k_1} = 2 \forall k_1$ ,  $D_{k_2} = 1 \forall k_2$  and  $D_{k_3} = 1 \forall k_3$ , i.e.,  $D_1 = 8$  and  $D_2 = D_3 = 3$ .

In the case of Network 3 with flexible duplexing modes, base stations 2 and 3 are configured as receiving nodes, and, since both BS are equipped with much more antennas than the rest of the nodes in the network, these antenna excess could be exploited to align additional interfering streams transmitted from BS 1. In this case, base station 1 can transmit a total of  $D_1 = 12$  ( $D_{k_1} = 3$  streams per user), leading to a total of 18 interference-free streams in the network, hence providing a 4 DoF benefit.

When considering those networks described in Section 4.3.1 for which (4.10) holds with equality, such antenna excess is not available and hence we cannot choose any cell to support the additional DoF load.

Fortunately, most of the state-of-the-art HetNet topologies comprise, by definition, different tiers including a variety of access points and base stations with different number of users, antennas and communication links. In this context, it is possible to exploit the DoF performance improvements of flexible duplexing to its fullest potential.



Part **III**

**Optimization of flexible duplexing  
configurations**



# Chapter 5

## Sum-rate analysis of flexible duplexing

All throughout Part II, we have characterized the DoF benefits of flexible duplexing in heterogeneous networks, where each cell included an arbitrary number of users. On top, each user equipment was allowed to share multiple independent data streams with the corresponding base station (BS)/access point (AP). For further analysis, however, the following considerations are taken into account regarding the topology of our network model:

- Intra-cell interference is typically handled by means of user scheduling. Independent resource blocks are assigned to different users in order to avoid any potential access collision. Thus, there is no intra-cell interference within the same time and frequency resource block.
- Multiple data streams may be transmitted by the same user over different subcarriers. Nevertheless, since orthogonal frequency-division multiplexing OFDM allows for multiplexing in a per-subcarrier fashion, we assume that a single data stream is transmitted within the same time and frequency slot.

Additionally, in order to better approximate a realistic scenario, we include in our model arbitrary transmit power levels for the nodes in the system. Further, we take into account the pairwise distances between the devices in the network by allowing the different nodes to have arbitrary locations. Consequently, every UL/DL combination in such scenario is associated to an independent MIMO interference channel realization.

For this simplified system model, in this chapter we address the study of flexible duplexing in small cell HetNets in terms of data rate performance. Whilst Part II analyzed the DoF potential of flexible UL/DL combining, in the following we also address the task of finding the optimal UL/DL configuration. Section 5.1 introduces the general problem statement. Interference alignment is used together with flexible duplexing to suppress the inter-cell interference. In Section 5.2, we present a statistical characterization of the IA solutions for interference channels with arbitrary transmit power levels and spatial distribution. Additionally, the statistical model takes into

account the interference leakage due to channel estimation errors, which is one of the most significant sources of misalignment in real-world scenarios. In Section 5.3 we address the selection of the optimal UL/DL setting, and we propose suboptimal approaches intended to reduce computational cost. Simulation results for the aforementioned approaches are presented in Section 5.4.

## 5.1 Problem statement

In the following, we consider a cellular network with general transmit power levels and arbitrary locations for all BS and UE, where the coexistence of both uplink and downlink cells within the same time slot is allowed. Such network is comprised of two tiers, namely, a set of  $G_m$  macrocells, and a set of  $G_s$  small cells located within the coverage area of the different macrocells, being  $G = G_m + G_s$  the total number of cells. Furthermore, the base stations corresponding to the macrocells have  $N_{BS}$  antennas and transmit power  $P_{BS}$ , whilst the access points (AP) associated to the different small cells are equipped with  $N_{AP}$  antennas and have a transmit power level of  $P_{AP}$ . Analogously, user equipments in both macro and small cells have  $N_{UE}$  antennas and transmit power  $P_{UE}$ . Each cell handles its own intra-cell interference internally, thus we can model the scenario under study as a MIMO interference channel where each cell has a single active user and the different interfering links represent inter-cell interference.

In this context, our goal is to determine the uplink/downlink combination that maximizes the total weighted rate of the HetNet over 2 time slots, establishing a downlink-to-uplink time ratio of 1:1, i.e., all cells switch transmit direction in consecutive slots<sup>1</sup>. For this purpose, we propose the following discrete optimization problem:

$$\begin{aligned} \mathcal{P}_1 : \quad & \underset{\substack{\{\mathbf{w}_g\}, \{\mathbf{u}_g\}, \\ \{i_g\}_{\forall g}}}{\text{maximize}} \quad \sum_{g=1}^G \left( a_g R_g^D + (1 - a_g) R_g^U \right) \\ & \text{s. t.} \quad i_g = \begin{cases} 0 & \text{if cell } g \text{ is in uplink} \\ 1 & \text{if cell } g \text{ is in downlink} \end{cases} \quad \forall g \end{aligned} \quad (5.1)$$

where  $R_g^D$  and  $R_g^U$  are, respectively, the downlink and uplink rates for cell  $g$  over the 2 considered time slots. Introducing  $\mathcal{I} \stackrel{\text{def}}{=}} \text{cat}_g(i_g)$ , these rates are represented in general by

<sup>1</sup>For the sake of simplicity, we have considered a ratio 1:1, although more general settings, e.g. 4:1, can be found in practice.

$$\begin{aligned}
R_g^D &= \log \left( 1 + \text{SINR}_g^D (\{\mathbf{w}_j\}, \mathbf{u}_g, \mathcal{I}) \right) \quad \forall g, j, \\
R_g^U &= \log \left( 1 + \text{SINR}_g^U (\{\mathbf{w}_j\}, \mathbf{u}_g, \mathcal{I}) \right) \quad \forall g, j, .
\end{aligned} \tag{5.2}$$

The SINR is highly dependent on the transmission strategy implemented by the users in the network. Further, regardless of the transmission technique, the interference generated by the whole set of interfering cells is strongly related to the UL/DL configuration at any given time slot. For this reason, we include the discrete control variables  $i_g$  in the optimization problem, in such a way that the transmission direction of every cell is taken into account when the SINR is considered.

Although (5.1) is a general problem that encompasses any interference management technique, it can be viewed as a weighted SINR maximization problem. In this sense, we take into account that at sufficiently high SNR the MaxSINR solution can be obtained by means of interference alignment. Therefore, in subsequent sections we explain in detail how the UL/DL configuration of these flexible duplexing scenarios can be optimized when IA is implemented. Additionally, we compare the rate benefits obtained for IA with those achieved by applying the M-MMSE receiving filters in (2.2). This comparison will allow us to analyze the impact of flexible duplexing depending on the interference management scheme under study.

### 5.1.1 UL/DL selection by exhaustive search

In our first evaluation, we intend to study the potential benefits that flexible duplexing enables in terms of rate, when the optimal UL/DL combination is determined by exhaustive search. In order to compute the SINR in (5.2), IA precoders and decoders must be calculated for every channel realization. For this purpose, we consider a 5-cell, 2-tier network with  $G_m = 2$  macrocells and  $G_s = 3$  small cells. All nodes in the network are equipped with  $N_{BS} = N_{AP} = N_{UE} = 3$  antennas. Although power levels in local area network (LAN) standards are usually lower, we take into account the worst case scenario with the maximum transmit power for the UE in long-term evolution (LTE) communications, i.e.,  $P_{UE} = 24\text{dBm}$  for all user equipments. Naturally, base stations and access points have a higher transmitted power, thus we set  $P_{BS} = 34\text{dBm}$  and  $P_{AP} = 31\text{dBm}$ . The spatial distribution of the cells in terms of normalized distance is displayed in Fig. 5.1. For this scenario the rate performance achieved by conventional TDD and the best flexible duplexing configuration have been evaluated over 100 independent channel realizations.

For this network, we analyze the sum-rate improvements for two different values of the weight parameters  $a_g$  in  $\mathcal{P}_1$ . First, we set  $a_g = 0 \forall g$ , i.e., we prioritize the maximization of the uplink rate. As shown in Fig. 5.2, the best up/down setting in this case happens to be the conventional TDD approach. This is due to the network characteristics together with the maximization priority (uplink rate). When all user equipments are transmitting in uplink, their lower power levels generate less interference at the unintended receivers, hence providing the best throughput. Nev-

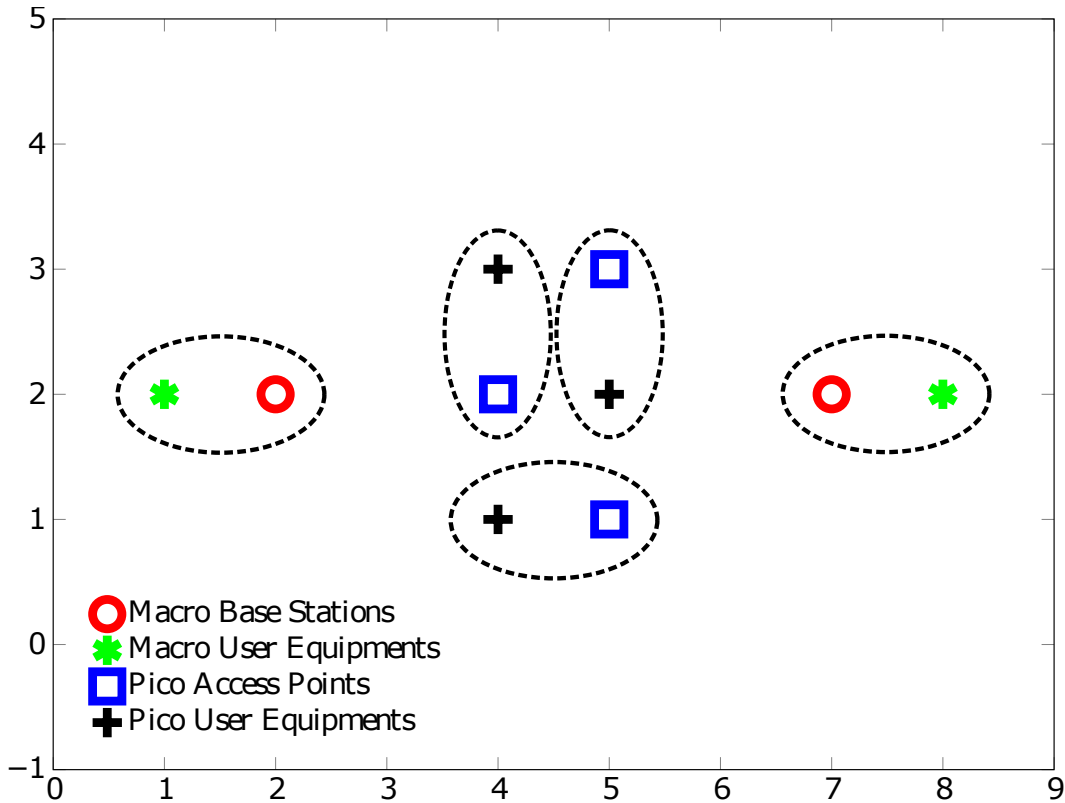


**Figure 5.1:** Normalized locations of the nodes in the system (Network 4).

ertheless, if we maximize the downlink rate, first intuition is that noticeable benefits could be achieved, thus we repeat the simulations now setting  $a_g = 1 \forall g$ .

As corroborated by Fig. 5.3, significant benefits can be attained in terms of sum-rate when flexible duplexing is enabled. In this case, the optimal downlink rate is achieved when both macrocells are transmitting in the same mode as the upper-left small cell, whilst the remaining small cells are reversed. From the schematic representation in Fig. 5.1, it can be noticed that all small cells are located in the coverage edge of both macro BS, as well as significantly close to each other. Hence, when conventional TDD is applied, the inter-cell interference level generated at the input of the small cells users is considerably higher than that of the optimal flexible duplexing mode.

As observed in Fig. 5.3, the best flexible duplexing combination outperforms conventional TDD by approximately 25% in terms of downlink rate performance. Although this improvement comes at the price of a lower uplink rate, the uplink performance difference is still below 15% and thus the selected uplink/downlink combination provides the best overall performance as well.

However, the computational cost of evaluating all the  $2^G$  possible UL/DL combinations grows exponentially with the total number of cells  $G$ . On top, when IA is implemented, going through all UL/DL configurations implies calculating a set of precoding and decoding matrices for each of the  $2^G$  cases. In order to overcome this inconvenient, we investigate two main lines to reduce the computational expense of

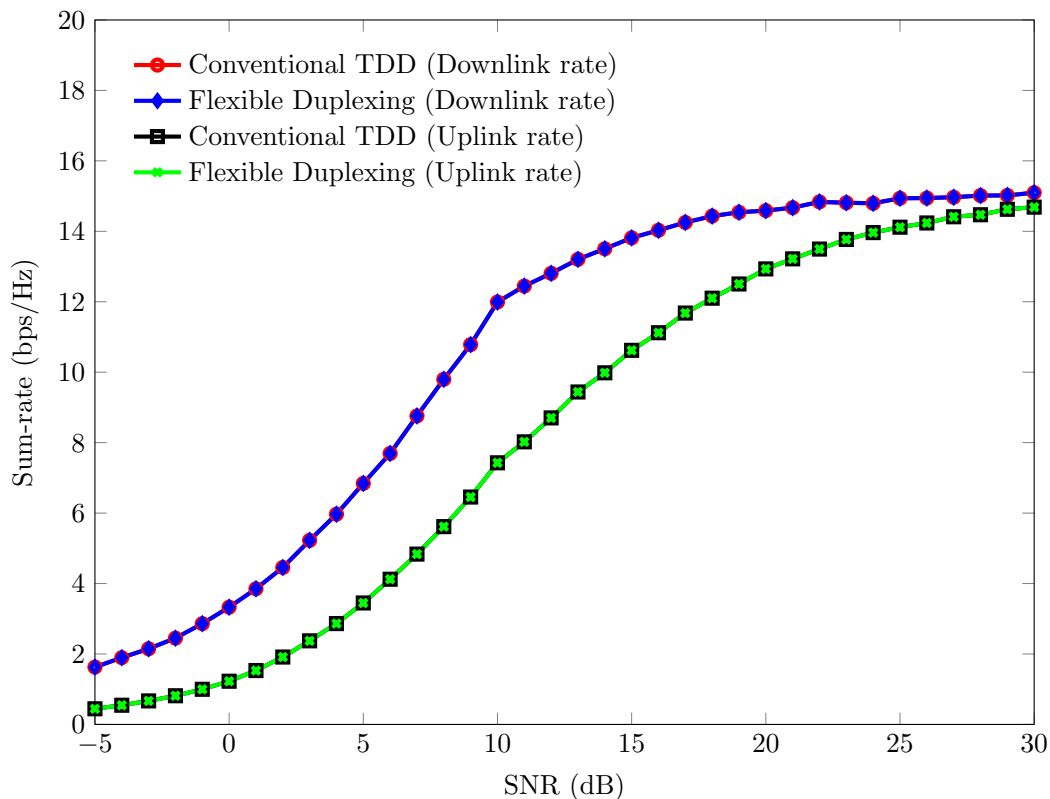


**Figure 5.2:** Average rate over 100 independent channel realizations, obtained by conventional TDD and the UL/DL that maximizes uplink rate.

UL/DL selection. On the one hand, we present a statistical expression that characterizes the average rate achievable by means of IA for a given channel realization, without needing to calculate the actual precoders and decoders. On the other hand, we propose a suboptimal algorithm that reduces the number of UL/DL settings to be evaluated.

## 5.2 Statistical analysis of IA

As mentioned above, the task of computing IA solutions for all different uplink/downlink combinations is computationally expensive, and hence the need for a more efficient way of characterizing the performance of IA arises. To cover that need, we analyze the average sum-rate performance of IA when only an imperfect estimate of the channel state information is available. For the sake of simplicity, in this section we focus on a fixed  $(N \times M, 1)^K$  interference channel configuration.

Consider the well-known IA conditions

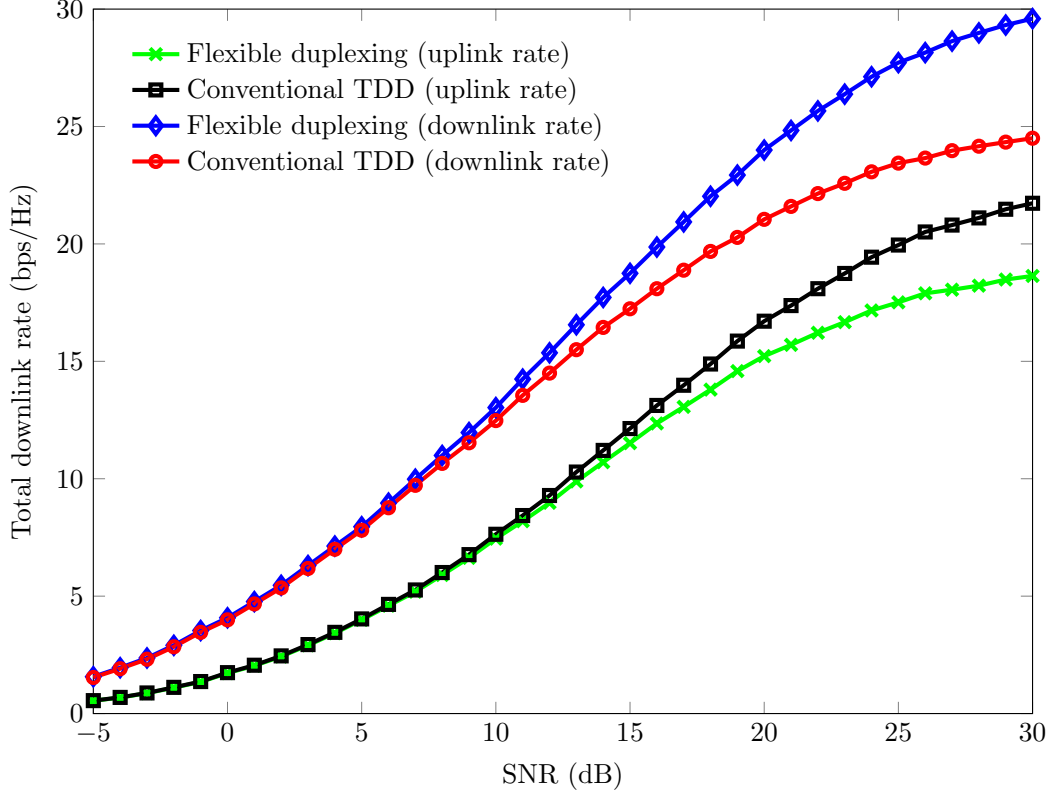


**Figure 5.3:** Average rate over 100 independent channel realizations, obtained by conventional TDD and the UL/DL that maximizes downlink rate.

$$\mathbf{u}_{k,b}^H \mathbf{H}_{k\ell} \mathbf{v}_{\ell,b} = 0 \quad \forall k \neq \ell, \quad (5.3a)$$

$$\mathbf{u}_{k,b}^H \mathbf{H}_{kk} \mathbf{v}_{k,b} \neq 0, \quad \forall k \quad (5.3b)$$

where  $k, \ell \in \{1, 2, \dots, K\}$ ,  $K$  is the number of users, and  $\mathbf{H}_{k\ell}$  represents the  $N \times M$  channel matrix with independent complex entries drawn from a continuous distribution. We also assume that the IA problem is feasible, which can be checked for some particular scenarios using the theoretical results in [79, 107, 108] or, for arbitrary networks, with the polynomial complexity feasibility test proposed in [85].

For feasible systems, it has been recently proven in [109],[102] that the number of different alignment solutions for a given channel realization may be either finite (when  $M + N = K + 1$ ) or infinite (when  $M + N > K + 1$ ). Furthermore, for single-beam systems the exact number of solutions can be easily obtained by the combinatorial counting procedure described in [102]. When perfectly accurate knowledge of the channel is available, condition (5.3a) can be strictly satisfied by the  $b$ -th set of solutions  $\{\mathbf{u}_{k,b}, \mathbf{v}_{\ell,b}\}$ , with  $b \in \{1, 2, \dots, B\}$  out of the total set of  $B$  solutions for the given channel realization. Additionally, when dealing with interference channels, it is known that condition (5.3b) is automatically satisfied as well. Notice that, due to the problem invariances, if  $\mathbf{v}_{k,b}$  is a solution of the IA problem, then  $\mathbf{v}_{k,b} e^{j\theta}$  is also a

solution. In fact, from the point of view of this analysis  $\mathbf{v}_{k,b}$  and  $\mathbf{v}_{k,b}e^{j\theta}$  are exactly the same solution: i.e., the  $B$  solutions are counted in the Grassmann manifold.

Assuming perfect CSI, the average rate achievable by user  $k$ , when a random IA solution from the set  $\mathcal{S}$  of  $B$  different solutions is applied, is given by

$$\mathbb{E}_{\mathcal{S}}[R_k] = \mathbb{E}_{\mathcal{S}} \left[ \log \left( 1 + \frac{P_k \left( \frac{d_{kk}}{d_0} \right)^{-\alpha} \left| \mathbf{u}_{k,b}^H \mathbf{H}_{kk} \mathbf{v}_{k,b} \right|^2}{\sigma_k^2} \right) \right], \quad (5.4)$$

where  $P_k$  is the transmit power level for user  $k$  and  $\sigma_k^2$  is the AWGN variance for receiver  $k$ . Additionally,  $d_{kk}$  is the distance from transmitter  $k$  to receiver  $k$  with respect to a reference distance  $d_0$ . Notice that, unlike prior works focused on the statistical characterization of IA [31, 110], the expectation in (5.4) is not computed over the distribution of the channel coefficients, but over the (possibly finite) set  $\mathcal{S}$  of IA solutions for user  $k$ .

For a feasible system, the SNR after perfect IA at receiver  $k$  can be expressed as

$$\begin{aligned} \text{SNR}_k &= \frac{P_k \left( \frac{d_{kk}}{d_0} \right)^{-\alpha} \left| \mathbf{u}_{k,b}^H \mathbf{H}_{kk} \mathbf{v}_{k,b} \right|^2}{\sigma_k^2} \\ &= \frac{P_k \left( \frac{d_{kk}}{d_0} \right)^{-\alpha} \|\mathbf{h}_{kk}\|^2 \left| \left( \mathbf{v}_{k,b}^* \otimes \mathbf{u}_{k,b} \right)^H \tilde{\mathbf{h}}_{kk} \right|^2}{\sigma_k^2}, \end{aligned} \quad (5.5)$$

where

$$\mathbf{h}_{kk} = \text{vec}(\mathbf{H}_{kk}) = \|\mathbf{h}_{kk}\| \tilde{\mathbf{h}}_{kk}.$$

Let us denote  $\mathbf{b}_{k,b} = \mathbf{v}_{k,b}^* \otimes \mathbf{u}_{k,b}$ . Since the calculation of IA solutions for interference channels does not involve direct channel matrices  $\mathbf{H}_{kk}$ , the unit-norm  $MN \times 1$  vector  $\mathbf{b}_{k,b}$  is independent of  $\tilde{\mathbf{h}}_{kk}$ . At this point, we make the following assumption:

(A1) *For a given channel realization, the vectors  $\mathbf{b}_{k,b}$  corresponding to different IA solutions are independent and isotropically distributed on the  $MN$ -dimensional complex unit sphere.*

To check the validity of this assumption we consider the  $(2 \times 5, 1)^6$  interference channel, for which there are a total of  $B = 265$  different alignment solutions [102]. We obtained all 265 solutions using homotopy continuation, and computed the pairwise angle between vectors  $\mathbf{b}_{k,b}$  and  $\mathbf{b}_{k,p}$  corresponding to two different solutions. Fig. 5.4 compares the estimated cumulative distribution function (cdf) for the pairwise angle with the theoretical cdf of isotropically generated random vectors [111]. We can observe that, for feasible systems and when the number of solutions is sufficiently high, the isotropic assumption is a rather accurate approximation for the distribution of IA solutions.

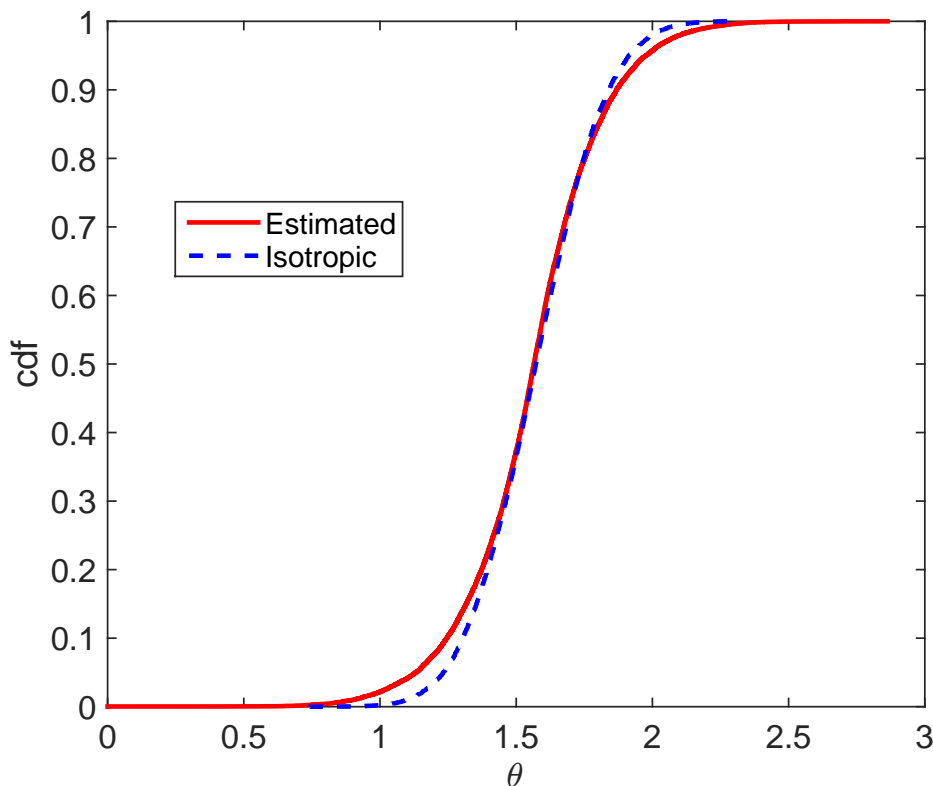


**Figure 5.4:** Comparison of the pairwise angle cdf between two different IA solutions for the  $(2 \times 5, 1)^6$  MIMO IC. The system has a total of  $P = 265$  IA solutions.

In order to validate the isotropic assumption, let  $\mathbf{b}_{k,b}$ ,  $b = 1, \dots, n \leq B$  be a random sample from the set of  $B$  different IA solutions. Without any loss of generality, we assume that the real random vectors formed by stacking the real and imaginary parts of  $\mathbf{b}_{k,b}$  have been drawn according to a  $2MN$ -variate von Mises-Fisher distribution [112]:  $(\Re(\mathbf{b}_{k,b}), \Im(\mathbf{b}_{k,b})) \sim \mathcal{M}(\mu, \kappa)$ , where  $\mu$  indicates the direction along which the unit-norm vectors are clustered and  $\kappa$  is the concentration parameter. The greater is  $\kappa$ , the greater the clustering around the mean direction given by  $\mu$ ; whereas for  $\kappa = 0$  the distribution is isotropic. Now, given  $\mathbf{b}_{k,b}$ ,  $b = 1, \dots, n \leq B$ , we consider the following binary hypothesis testing:

$$\begin{aligned} H_0 &: \kappa = 0 \\ H_1 &: \kappa \neq 0, \end{aligned}$$

where the direction parameter  $\mu$  is unknown. The uniformly most powerful invariant test (UMPIT) for this problem is the Rayleigh test, which is given by [112],[113]

$$\|\bar{\mathbf{b}}_k\|^2 \underset{H_0}{\overset{H_1}{\gtrless}} \eta$$

where the threshold  $\eta$  is fixed for a given probability of false alarm, and  $\bar{\mathbf{b}}_k = \frac{1}{n} \sum_{b=1}^n \mathbf{b}_{k,b}$ . We run the test for 100 different  $(2 \times 5, 1)^6$  MIMO IC channels. More

precisely, we computed all  $B = 265$  IA solutions for each channel realization, and used all solutions in the test ( $n = B$ ). For a  $P_{fa} = 0.1$ , the test always accepted the null hypothesis, thus validating the isotropic assumption. The same result was obtained for other systems with more IA solutions.

### 5.2.1 Average achievable rates

Now, our goal is to characterize the SNR for user  $k$ , when its precoder-decoder pair is randomly taken from the set of  $B$  independent IA solutions. From Assumption 1, vectors  $\mathbf{b}_{k,b}$  are isotropically distributed in the Stiefel manifold, and hence their probability density function (PDF) is

$$p(\mathbf{b}_{k,b}) = \frac{\Gamma(MN)}{2\pi^{MN}} \delta(\mathbf{b}_{k,b}^H \mathbf{b}_{k,b} - 1),$$

where  $\Gamma(n) = (n-1)!$  denotes the Gamma function. Therefore, we have the following result.

**Proposition 5.1.** *The random variable  $\text{SNR}_k$  can be expressed as  $\text{SNR}_k = \rho_k X$ , where*

$$\rho_k = \frac{P_k \left(\frac{d_{kk}}{d_0}\right)^{-\alpha} \|\mathbf{H}_{kk}\|_F^2}{\sigma_k^2}$$

is a deterministic constant, and  $X$  is Beta distributed with parameters 1 and  $MN - 1$ , i.e.,  $X \sim \text{Beta}(1, MN - 1)$ .

*Proof.* From (5.5), we see that  $X \propto \left| \mathbf{b}_{k,b}^H \tilde{\mathbf{h}}_{kk} \right|^2$ . Taking into account that  $\tilde{\mathbf{h}}_{kk}$  is a fixed unit norm vector that points in a direction determined by the direct link MIMO channel, we see that  $X$  is the squared length of the projection of  $\tilde{\mathbf{h}}_{kk}$  onto a vector isotropically distributed on the  $MN$ -dimensional complex hypersphere, which is known to follow a Beta distribution [114, 115, 116], thus  $X \sim \text{Beta}(1, MN - 1)$ .  $\square$

Since  $\text{SNR}_k$  follows a scaled Beta distribution, the average rate achievable by user  $k$  when applying a random IA solution from the set  $\mathcal{S}$  is given by [117]

$$\begin{aligned} \mathbb{E}_{\mathcal{S}}[R_k] &= \mathbb{E}_{\mathcal{S}}[\log(1 + \text{SNR}_k)] \\ &= \left( \frac{\log(e)\rho_k}{MN} \right) {}_3F_2(1, 1, 2; 2, MN + 1; -\rho_k), \end{aligned} \quad (5.6)$$

where  ${}_3F_2(a_1, a_2, a_3; b_1, b_2; x)$  denotes the generalized hypergeometric function. Finally, the average sum-rate can be easily obtained from (5.6) as

$$\mathbb{E}_{\mathcal{S}}[R] = \frac{1}{K} \sum_{k=1}^K \mathbb{E}_{\mathcal{S}}[R_k].$$

As mentioned before, this statistical characterization assumes perfect cancelation of the interference at the unintended receivers. However, perfect channel knowledge is unlikely to be available in practice, and we are usually left with an imperfect estimate of the channel state. In such cases, interference is not completely suppressed at the unintended receivers, leading to the presence of inter-cell interference leakage. Therefore, the average rate achievable by user  $k$ , when a random IA solution from the set  $\mathcal{S}$  of  $B$  different solutions is applied, is represented by

$$\mathbb{E}_{\mathcal{S}}[R_k] = \mathbb{E}_{\mathcal{S}} \left[ \log \left( 1 + \frac{P_k \left( \frac{d_{kk}}{d_0} \right)^{-\alpha} \left| \mathbf{u}_{k,b}^H \mathbf{H}_{kk} \mathbf{v}_{k,b} \right|^2}{\sigma_k^2 + \sum_{\ell \neq k} P_\ell \left( \frac{d_{k\ell}}{d_0} \right)^{-\alpha} \left| \mathbf{u}_{k,b}^H \mathbf{H}_{k\ell} \mathbf{v}_{\ell,b} \right|^2} \right) \right],$$

where  $d_{k\ell}$  is the distance from transmitter  $\ell$  to receiver  $k$  with respect to a reference distance  $d_0$ .

Analogously to the perfect IA case, for a feasible system, the signal-to-interference-plus-noise-ratio (SINR) after applying the IA beamformers and filters under imperfect CSI is expressed as

$$\begin{aligned} \text{SINR}_k &= \frac{P_k \left( \frac{d_{kk}}{d_0} \right)^{-\alpha} \left| \mathbf{u}_{k,b}^H \mathbf{H}_{kk} \mathbf{v}_{k,b} \right|^2}{\sigma_k^2 + \sum_{\ell \neq k} P_\ell \left( \frac{d_{k\ell}}{d_0} \right)^{-\alpha} \left| \mathbf{u}_{k,b}^H \mathbf{H}_{k\ell} \mathbf{v}_{\ell,b} \right|^2} \\ &= \frac{P_k \left( \frac{d_{kk}}{d_0} \right)^{-\alpha} \|\mathbf{h}_{kk}\|^2 \left| \left( \mathbf{v}_{k,b}^* \otimes \mathbf{u}_{k,b} \right)^H \tilde{\mathbf{h}}_{kk} \right|^2}{\sigma_k^2 + \sum_{\ell \neq k} P_\ell \left( \frac{d_{k\ell}}{d_0} \right)^{-\alpha} \left| \mathbf{u}_{k,b}^H \mathbf{H}_{k\ell} \mathbf{v}_{\ell,b} \right|^2}, \end{aligned} \quad (5.7)$$

### 5.2.2 Interference leakage characterization

Once we have presented the expressions associated to the SINR under imperfect alignment, we need to characterize the interference leakage term. For this purpose, and since the leakage is due to an imperfect estimate of the channel information, we rely on the channel estimate variance. The estimate of the channel between transmitter  $\ell$  and receiver  $k$  is

$$\hat{\mathbf{H}}_{k\ell} = \mathbf{H}_{k\ell} + \mathcal{E}_{k\ell} \quad \forall k, \ell, \quad (5.8)$$

where  $\mathcal{E}_{k\ell} \sim \mathcal{CN}(0, \eta \mathbf{I})$  with  $\eta = \beta \left( \frac{1}{\sigma_k^2} \right)^{-\gamma}$ . Regarding parameter  $\gamma$ , we consider a hybrid model:

- For low-mid SNR,  $\gamma = 1$  represent a scenario where the channel estimation errors decrease as the SNR increases.
- For high SNR,  $\gamma = 0$ . We consider that the channel estimate errors are mainly due to quantization impairments, and hence their value remains constant with respect to noise variances.

Several values for parameter  $\beta$  have been evaluated by means of Monte Carlo simulations, being  $\beta = 0.1$  the value that allows to obtain a better representation of the channel estimation errors for the scenarios under study.

From (5.8), with  $\mathbf{H}_{kl}$  and  $\mathcal{E}_{kl}$  being statistically independent Gaussian random variables, then  $\hat{\mathbf{H}}_{kl}$  and  $\mathbf{H}_{kl}$  are jointly Gaussian.  $\mathbf{H}_{kl}$  is Gaussian distributed with mean  $\frac{\hat{\mathbf{H}}_{kl}}{1+\eta}$  and statistically independent elements of variance  $\frac{\eta}{1+\eta}$ . This allows us to rewrite the actual channel as

$$\mathbf{H}_{kl} = \frac{1}{1+\eta} \hat{\mathbf{H}}_{kl} + \boldsymbol{\Upsilon}_{kl}, \quad (5.9)$$

where  $\boldsymbol{\Upsilon}_{kl}$  is independent of  $\hat{\mathbf{H}}_{kl}$ , with distribution

$$\boldsymbol{\Upsilon}_{kl} \sim \mathcal{CN} \left( 0, \frac{\eta}{1+\eta} \mathbf{I} \right).$$

From (5.9) and the IA conditions in (5.3a), we can state that the interference leakage at the input of receiver  $k$  is given by

$$\text{IL}_k = \sum_{\ell \neq k} P_\ell \left( \frac{d_{k\ell}}{d_0} \right)^{-\alpha} \left| \hat{\mathbf{u}}_{k,b}^H \boldsymbol{\Upsilon}_{kl} \hat{\mathbf{v}}_{\ell,b} \right|^2,$$

where  $\hat{\mathbf{u}}_{k,b}$  and  $\hat{\mathbf{v}}_{\ell,b}$  are the decoders and precoders associated to the  $b$ -th IA solution calculated from channel estimate  $\hat{\mathbf{H}}$ , i.e.,  $\left| \hat{\mathbf{u}}_{k,b}^H \hat{\mathbf{H}}_{kl} \hat{\mathbf{v}}_{\ell,b} \right|^2 = 0$ .

Now, in order to obtain an expression defining the SINR for user  $k$ ,  $\text{SINR}_k$ , we need to obtain the interference leakage variance.

$$\text{Lemma 1: } \mathbb{E} \left[ \left| \hat{\mathbf{u}}_{k,b}^H \boldsymbol{\Upsilon}_{kl} \hat{\mathbf{v}}_{\ell,b} \right|^2 \right] = \frac{\eta}{1+\eta}$$

*Proof:* As stated in the model definition,  $\hat{\mathbf{H}}_{kl}$  and  $\boldsymbol{\Upsilon}_{kl}$  are independent, and therefore  $\hat{\mathbf{u}}_{k,b}$  and  $\hat{\mathbf{v}}_{\ell,b}$  (calculated from  $\hat{\mathbf{H}}_{kl}$ ) are independent of  $\boldsymbol{\Upsilon}_{kl}$ . Also,  $\boldsymbol{\Upsilon}_{kl}$  is Gaussian distributed and bi-unitary invariant, thus the terms  $\hat{\mathbf{u}}_{k,b}^H \boldsymbol{\Upsilon}_{kl} \hat{\mathbf{v}}_{\ell,b}$  are Gaussian random variables with zero mean and variance  $\frac{\eta}{1+\eta}$ . Since these terms are zero-mean, their variance is

$$\sigma_{\text{IL}_{kl}}^2 = P_\ell \left( \frac{d_{k\ell}}{d_0} \right)^{-\alpha} \mathbb{E} \left[ \left| \hat{\mathbf{u}}_{k,b}^H \boldsymbol{\Upsilon}_{kl} \hat{\mathbf{v}}_{\ell,b} \right|^2 \right] = P_\ell \left( \frac{d_{k\ell}}{d_0} \right)^{-\alpha} \frac{\eta}{1+\eta} \quad \forall k, \ell \neq k \quad (5.10)$$

### 5.2.3 Average achievable rates for IA with flexible duplexing

Including the control variables  $i_g$  into the SINR expression in (5.7) and taking into account (5.10) leads to  $\text{SINR}_g = \rho_g X$ , where  $X$  is the same Beta random variable as in Section 5.2. On the other hand, for each cell  $g$ ,  $\rho_g$  is now a deterministic constant given by

$$\begin{aligned}
\rho_g &= \|\mathbf{H}_{k_g g}\|_F^2 \left(\frac{d_{k_g g}}{d_0}\right)^{-\alpha} \left( \frac{i_g P_g}{\sigma_{k_g}^2 + \sigma_{IL_{k_g}}^2} + \frac{(1-i_g) P_{k_g}}{\sigma_g^2 + \sigma_{IL_g}^2} \right) \\
&= \|\mathbf{H}_{k_g g}\|_F^2 \left(\frac{d_{k_g g}}{d_0}\right)^{-\alpha} \left( \frac{i_g P_g}{\sigma_{k_g}^2 + \sum_{j \neq g} \left[ i_j P_j \left(\frac{d_{k_g j}}{d_0}\right)^{-\alpha} + (1-i_j) P_{\ell_j} \left(\frac{d_{k_g \ell_j}}{d_0}\right)^{-\alpha} \right] \frac{\eta}{1+\eta}} \right. \\
&\quad \left. + \frac{(1-i_g) P_{k_g}}{\sigma_g^2 + \sum_{j \neq g} \left[ i_j P_j \left(\frac{d_{g j}}{d_0}\right)^{-\alpha} + (1-i_j) P_{\ell_j} \left(\frac{d_{g \ell_j}}{d_0}\right)^{-\alpha} \right] \frac{\eta}{1+\eta}} \right),
\end{aligned}$$

where the channel norms and the distances are common factors since  $\|\mathbf{H}_{k_g g}\|_F^2 = \|\mathbf{H}_{g k_g}\|_F^2$  and  $d_{k_g g} = d_{g k_g}$ . Also, notice that the terms  $\sigma_{IL_{k_g}}^2$  and  $\sigma_{IL_g}^2$  are the variances of the total interference at the input of the UE and BS/AP, respectively. Therefore, the average rate for cell  $g$  when applying IA to mitigate inter-cell interference can be obtained by substituting  $\rho_k$  in (5.6) by the equivalent flexible duplexing notation, that is,

$$\begin{aligned}
\mathbb{E}_{\mathcal{S}}[R_g] &= \mathbb{E}_{\mathcal{S}} [\log(1 + \text{SINR}_g)] \\
&= \left( \frac{\log(e) \rho_g}{NN_{UE}} \right) {}_3F_2(1, 1, 2; 2, NN_{UE} + 1; -\rho_g),
\end{aligned}$$

where  ${}_3F_2(a_1, a_2, a_3; b_1, b_2; x)$  denotes the generalized hypergeometric function. Notice again that analogous expressions are associated to the  $N = N_{AP}$  antennas for access points in the small cells and  $N = N_{BS}$  in the macrocells.

In order to validate the statistical expressions for the average rate performance of IA under imperfect CSI, we consider a  $(3 \times 3, 1)^5$  IC. We have taken  $\beta = 0.1$ , and we assume a channel quantization of 10 bits per MIMO channel matrix. This leads to an SNR threshold of 5 dB as calculated with the expressions in [118], so that  $\gamma = 1$  if  $\text{SNR} < 5$  dB, and  $\gamma = 0$  otherwise.

Figure 5.5 compares the average rate achieved with the actual IA precoders and decoders calculated by the homotopy continuation algorithm in Chapter 3, to the results obtained with the statistical expressions presented above. The results have been averaged over 100 independent channel realizations. As we can observe, the statistical characterization for the average rates achieved by means of interference alignment under imperfect CSI is remarkably accurate. Consequently, we will rely on this approach in the foregoing in order to characterize the rate performance of flexible duplexing together with IA, while avoiding the computational cost of calculating the IA precoders and decoders for every UL/DL combination.

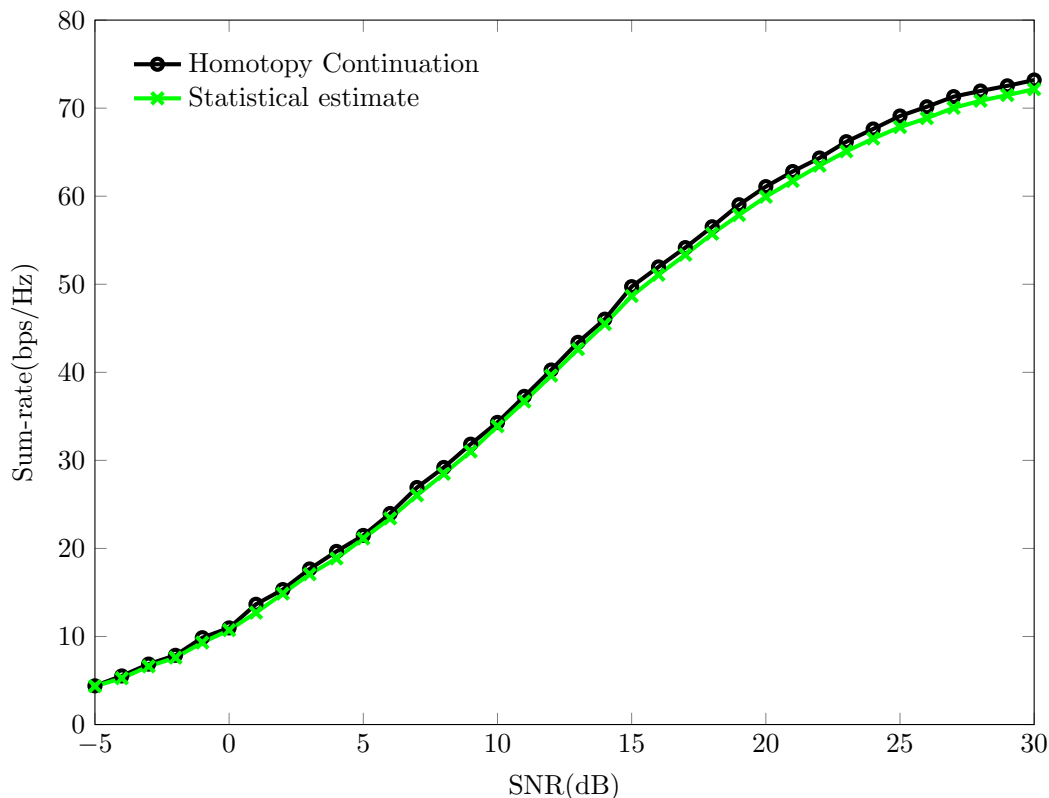


**Figure 5.5:** Average rate over 100 independent channel realizations, obtained by the HC-based algorithm and the proposed statistical approximation.

### 5.3 Determining the best UL/DL configuration

In this section, we present two discrete search techniques to solve the SINR maximization problem with a hierarchical perspective that harmonizes perfectly within the multi-tier context. We propose two different criteria to evaluate a subset of the total number of configurations in a given HetNet. For both of them, the main idea consists in starting with the given network in conventional TDD mode<sup>2</sup>. Then, a cell switches transmit direction with respect to the rest of cells, and the total weighted rate in the network is evaluated over 2 time slots so that all cells have transmitted in both directions at least once. If the weighted rate has been improved, the cell keeps the direction change, whereas if there is no improvement, the cell returns to the previous state. The same procedure is repeated sequentially until every cell has evaluated the potential of the transmit direction switching. The switching sequence is described in Alg. 2 for maximum downlink rate.

The difference between the two proposed strategies originates from the hierarchical structure of the 2-tier HetNet under study. On the one hand, we can carry out the switching sequence in Alg. 2 starting with the macrocells (HS-Macro), and then con-

<sup>2</sup>Recall that conventional TDD is actually a particular case out of the total  $2^G$  uplink/downlink settings in the network

---

**Algorithm 2:** Hierarcical switching for maximum downlink rate.

---

**Input:**  $\mathbf{H}_{gj}, P_{BS}, P_{AP}, P_{UE}, N_{BS}, N_{AP}, N_{UE}, \frac{d_{gj}}{d_0}$   
**Output:** UpLinkFlag  
UpLinkFlag = zeros(1, G); // cat( $i_g$ )  
MaxDownRate =  $\sum_g R_g^D$   
**for**  $g = 1$  **to**  $G$  **do**  
    /\* Cell  $g$  switches \*/  
    UpLinkFlag( $g$ ) =  $\neg$ UpLinkFlag( $g$ )  
    /\* Evaluate the new setting \*/  
    DownRate =  $\sum_g R_g^D$   
    **if**  $DownRate > MaxDownRate$  **then**  
        | MaxDownRate = DownRate  
    **else**  
        | UpLinkFlag( $g$ ) =  $\neg$ UpLinkFlag( $g$ )  
**return**

---

tinue with the small cells once macrocells have determined their best configuration. Nevertheless, as numerically observed by means of Monte Carlo simulations, small cells usually obtain the most significant benefit from flexible duplexing in terms of per-cell rate. Therefore, we also consider performing the sequence in Alg. 2 starting with the small cells first (HS-Small). Both approaches are compared to the optimal solution obtained by exhaustive search in Section 5.4.

## 5.4 Simulation results

Despite the rate improvements of flexible duplexing being already shown for different values of  $a_g$ , practical communication systems tend to prioritize the downlink traffic. For this reason, in this section we evaluate the benefits of flexible duplexing in terms of downlink rate ( $a_g = 1$ ) for 2-tier HetNets with imperfect CSI. For this purpose, we consider two case studies:

- First, we have generated 100 independent spatial distributions for the nodes in the network, being the base stations at a deterministic location, whereas small cell access points and users of both tiers are distributed following a Poisson Point Process (PPP) around each BS location within its coverage area. Over this scenario, we test the validity of the suboptimal HS-Macro and HS-Small approaches for UL/DL selection.
- Afterwards, we analyze the downlink rate improvements of flexible duplexing for a specific scenario which has been generated in order to observe how the different uplink/downlink settings affect the network behaviour.

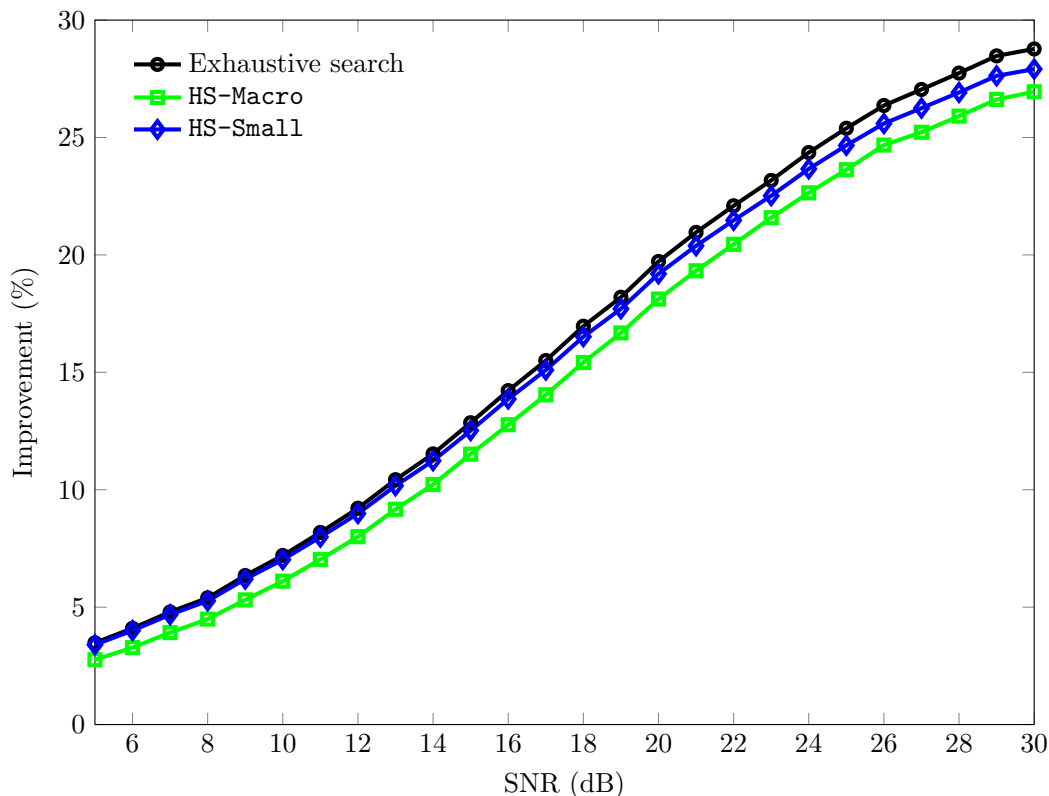


**Figure 5.6:** Downlink rate improvement (%) of flexible duplexing over conventional TDD.

Throughout all our simulations, as in Section 5.2.3 we have taken  $\beta = 0.1$ , and a channel quantization of 10 bits per channel. This results in an SNR threshold of 5 dB [118], so that  $\gamma = 1$  if  $\text{SNR} < 5$  dB, and  $\gamma = 0$  otherwise. Finally, notice that all the selected scenarios satisfy the IA feasibility conditions in (4.3), (4.4).

### 5.4.1 Hierarchical approaches for PPP distributed deployments

As mentioned in Section 5.3, the computational cost of evaluating all the possible flexible duplexing combinations by exhaustive search is significantly high, even when the use of statistical rate expressions allow to avoid the calculation of IA solutions for every single uplink/downlink setting. In this section, we evaluate the two proposed hierarchical heuristic approaches introduced in Section 5.3, and we compare them to the optimal solution. For that purpose, we generate 100 independent PPP spatial distributions of a 2-tier HetNet with 2 macrocells and 4 small cells, each one associated to an independent channel realization. BS and AP are equipped with  $N_{BS} = N_{UE} = 5$  antennas, whereas every UE has  $N_{UE} = 2$  antennas. We consider  $P_{UE} = 24$  dBm for all user equipments, and we set  $P_{BS} = 34$  dBm and  $P_{AP} = 31$  dBm for base stations and access points, respectively.

Figure 5.6 shows the downlink rate improvement of the three strategies with respect to conventional TDD, averaged over the 100 independent PPP realizations.

From the black curve, representing the improvement attained with exhaustive search among all the possible combinations, we can establish that flexible duplexing outperforms conventional transmission by up to almost 30% at high-SNR regimes. As expected, the HS-Small approach slightly outperforms its analogous HS-Macro. Notice that, as discussed in Section 5.1.1, the small cells of the network get the most benefit of flexible duplexing when compared to the macro tier. Finally, it can be observed that both hierarchical approaches provide rates significantly close to the results obtained by means of exhaustive search, with the additional advantage of their reduced computational cost.

### 5.4.2 IA vs M-MMSE

Once we have validated the HS-based approaches, we compare the results obtained by IA to those provided by the multi-cell minimum-mean square error (M-MMSE) receiver. In this case, dominant eigenmode transmission (DET) is implemented at the transmitter side. Therefore, the M-MMSE filter at a given receiver  $g$ ,  $\mathbf{u}_g^{M-MMSE}$  is calculated as

$$\mathbf{u}_g^{M-MMSE} = \mathbf{w}_g^H \hat{\mathbf{H}}_{gg}^H \left( \hat{\mathbf{H}}_{gg} \mathbf{w}_g P_g \left( \frac{d_{gg}}{d_0} \right)^{-\alpha} \mathbf{w}_g^H \hat{\mathbf{H}}_{gg}^H + \mathbf{R}_g + \sigma_g^2 \mathbf{I} \right)^{-1}$$

where  $\mathbf{w}_g \in \mathbb{C}^{N \times 1}$  is the principal eigenvector of channel estimate  $\hat{\mathbf{H}}_{gg}$ , and  $\mathbf{R}_g = \sum_{j \neq g}^G \hat{\mathbf{H}}_{gj} \mathbf{w}_j P_j \left( \frac{d_{gj}}{d_0} \right)^{-\alpha} \mathbf{w}_j^H \hat{\mathbf{H}}_{gj}^H$  is the covariance matrix of the inter-cell interference.

In this case, we consider the same network as in Section 5.1.1 with  $G_m = 2$  macrocells and  $G_s = 3$  small cells. All nodes in the network are equipped with  $N_{BS} = N_{AP} = N_{UE} = 3$  antennas and the transmit power levels remain the same as in Section 5.4.1. The downlink rates obtained by both approaches, and averaged over 100 independent channel realizations, are shown in Fig. 5.7. The comparison among conventional TDD and flexible duplexing is included as well for both schemes, in such a way that we can study the impact of every transmission technique on the potential benefits that UL/DL combining provides over standard TDD.

As expected, IA outperforms the M-MMSE approach with both conventional and Flexible TDD in the mid to high SNR regime. Notice that, for low SNR values, M-MMSE closes the gap with respect to IA. This is due to the strong relationship between the channel estimation impairments and the interference leakage level. More specifically, as detailed in Section 5.2.2, the channel estimation errors are modeled as a function of the SNR. Therefore, as the SNR decreases, the interference leakage remaining after applying the IA beamformers and filters is more significant, hence penalizing the performance.

Regarding the potential benefits that each transmission method can achieve by applying flexible duplexing, it can be observed in Fig. 5.7 that the improvement is similar for both techniques in absolute values. However, the impact of UL/DL optimization is higher for M-MMSE when compared to the performance of standard duplexing. It can be intuitively established that, since the residual interference after

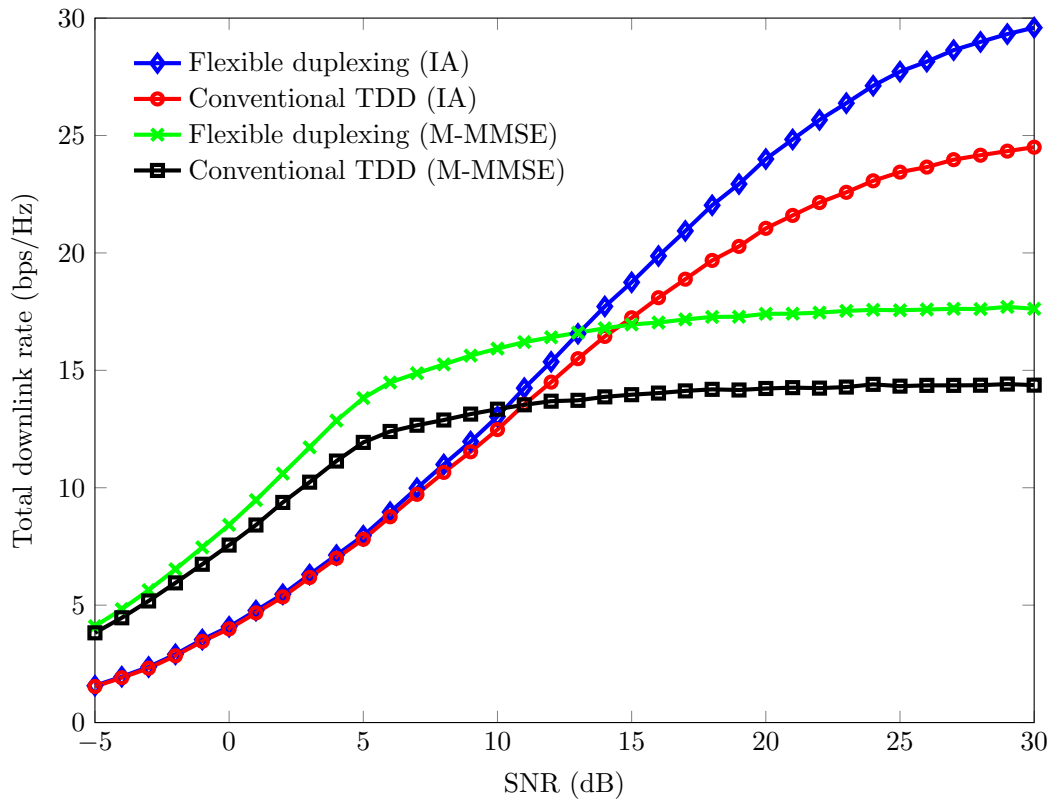


**Figure 5.7:** Average downlink rate over 100 independent channel realizations, obtained by M-MMSE and IA.

decoding is more significant in the case of M-MMSE, this strategy will be more benefited when finding the UL/DL combination that minimizes the inter-cell interference at the receivers.



# Chapter 6

## Power efficiency analysis of flexible duplexing

From the beginning of Part II to this point, we have analyzed the benefits that flexible duplexing provides. Specifically, we have investigated the maximum potential of this approach in terms of multiplexing gain throughout Chapter 4. Additionally, we have studied the margin for improvement that flexible duplexing has regarding data rate in Chapter 5. In the latter case, we observed that the computational cost of evaluating the complete set of possible UL/DL combinations in the network might be excessive. To overcome this inconvenient, statistical expressions for the average rates achieved by IA were introduced. Moreover, suboptimal approaches were developed in order to avoid the exploration of all possible UL/DL sets. To this point, however, no consideration has been made regarding power efficiency. In previous parts, the nodes in the network were assumed to have a fixed power budget, and the maximum performance subject to that constraint was derived. In this chapter we focus on minimizing the transmit power levels rather than aiming to achieve the maximum outcome of the system.

Precisely, our system is given a minimum quality of service (QoS) requirement that must be satisfied over the different cells in the network. In this scenario, our goal is to minimize the transmit power levels while still satisfying the QoS constraints, represented in this case by SINR constraints. The signal model is described in Section 6.1, where prior work on power minimization for broadcast channels is reviewed. Afterwards, the general minimization problem for flexible duplexing is formulated in Section 6.2. An algorithm to minimize transmit power for a fixed UL/DL combination is proposed in Section 6.2.1, and the same lines as in Chapter 5 are followed in Section 6.2.2 to reduce the computational expense of evaluating all possible flexible duplexing configurations. Finally, Section 6.3 includes simulations that corroborate the validity of the proposed algorithms.

### 6.1 System model

The multi-tier network in this case is modeled as in Section 5.1 for the rate analysis. Nevertheless, when studying the power efficiency advantages of flexible duplexing,

we consider single-antenna user equipments. The main reason is that, in practice, user equipments are mainly characterized by their reduced size and radio hardware simplicity when compared to the larger and more complex base stations. On top, it is worth considering that this also allows to simplify the mathematical analysis. That being said, the considered HetNet consists of 2 tiers, with  $G_m$  macrocells and  $G_s$  small cells for a total of  $G = G_m + G_s$  cells. Each cell  $g$  has an  $N_g$ -antenna base station in the macro-tier, or access point in the small tier, whereas the user equipments have a single antenna. For each cell, a single data stream per user is transmitted, and the intra-cell interference is assumed to be handled by means of resource block scheduling.

The signal at the input of the receiver in cell  $g$  is therefore given by

$$r_g = \sigma_g^2 + i_g \left[ d_{gg}^{-\alpha/2} \mathbf{h}_{gg} \mathbf{w}_g + \sum_{j=1, j \neq g}^G \left( i_j d_{gj}^{-\alpha/2} \mathbf{h}_{gj} \mathbf{w}_j + (1 - i_j) d_{gj}^{-\alpha/2} h_{gj} P_{UE_j}^{1/2} \right) \right] + (1 - i_g) \left[ \mathbf{u}_g^H d_{gg}^{-\alpha/2} \mathbf{h}_{gg} P_{UE_g}^{1/2} + \sum_{j=1, j \neq g}^G \left( i_j \mathbf{u}_g^H d_{gj}^{-\alpha/2} \mathbf{H}_{gj} \mathbf{w}_j + (1 - i_j) \mathbf{u}_g^H d_{gj}^{-\alpha/2} \mathbf{h}_{gj} P_{UE_j}^{1/2} \right) \right]$$

where  $i_g$  is a Boolean indicating whether each cell  $g$  is in downlink ( $i_g = 1$ ) or in uplink ( $i_g = 0$ ). Also,  $\alpha$  represents the path loss exponent and  $\sigma_g^2$  is the additive white Gaussian noise (AWGN) variance at the input of receiver  $g$ . The distance and the channel between the transmitter in cell  $j$  and the receiver in cell  $g$  are given by  $d_{gj}$  and  $\mathbf{H}_{gj}$ , respectively<sup>1</sup>.  $\mathbf{w}_g \in \mathbb{C}^{N_g \times 1}$  is the beamformer applied at the  $g$ -th BS/AP in downlink,  $\mathbf{u}_g \in \mathbb{C}^{N_g \times 1}$  is the unit-norm filter for the  $g$ -th BS/AP when it is in uplink mode, and the scalar values  $P_{UE_g}$  are the transmit power at the single-antenna users.

### 6.1.1 Prior work for MISO downlink channels

The power minimization algorithm that we propose in subsequent sections follows the same lines as established in [119] for MISO downlink beamforming. Recall that all cells being in downlink can be viewed as a particular case of flexible duplexing with  $i_g = 1 \forall g \in [1, \dots, G]$ . To be more specific, authors in [119] consider the problem of minimizing the total transmit power, while still fulfilling an SINR requirement at each user, i.e.,  $\text{SINR}_g \geq \gamma_g \forall g$  [120, 121]. The above formulation leads to the following optimization problem<sup>2</sup>

<sup>1</sup>The notation for channel matrices varies between lowercase, uppercase and boldface letters due to the different SISO, MISO/SIMO and MIMO channels within the considered network.

<sup>2</sup>The optimal beamforming analysis in [119] does not take into account the distance among the different nodes in the network explicitly.

$$\begin{aligned}
& \text{minimize} && \sum_{g=1}^G \|\mathbf{w}_g\|^2 \\
& \text{subject to} && \frac{\mathbf{h}_{gg}\mathbf{w}_g\mathbf{w}_g^H\mathbf{h}_{gg}^H}{\sigma_g^2 + \sum_{j \neq g} \mathbf{h}_{gj}\mathbf{w}_j\mathbf{w}_j^H\mathbf{h}_{gj}^H} \geq \gamma_g \quad \forall g,
\end{aligned} \tag{6.1}$$

or equivalently,

$$\begin{aligned}
& \text{minimize} && \sum_{g=1}^G \mathbf{w}_g^H \mathbf{w}_g \\
& \text{subject to} && \mathbf{h}_{gg}\mathbf{w}_g\mathbf{w}_g^H\mathbf{h}_{gg}^H + \gamma_g \sum_{j \neq g} \mathbf{h}_{gj}\mathbf{w}_j\mathbf{w}_j^H\mathbf{h}_{gj}^H \geq \gamma_g \sigma_g^2 \quad \forall g.
\end{aligned} \tag{6.2}$$

It is shown in [121] that all constraints must be active at the optimum, and hence the inequality in (6.2) can be replaced by an equality. The particular case of rank-one channels satisfies  $\mathbf{h}_{gj}\mathbf{w}_j\mathbf{w}_j^H\mathbf{h}_{gj}^H = |\mathbf{h}_{gj}\mathbf{w}_j|^2$ , and without loss of generality, we can incorporate the constraints  $\mathbf{h}_{gg}\mathbf{w}_g \geq 0$ , leading to the following reformulation of the problem

$$\begin{aligned}
& \text{minimize} && \sum_{g=1}^G \mathbf{w}_g^H \mathbf{w}_g \\
& \text{subject to} && |\mathbf{h}_{gg}\mathbf{w}_g|^2 \geq \gamma_g \left( \sigma_g^2 + \sum_{j \neq g} \mathbf{h}_{gj}\mathbf{w}_j\mathbf{w}_j^H\mathbf{h}_{gj}^H \right), \\
& && \mathbf{h}_{gg}\mathbf{w}_g \geq 0 \quad \forall g.
\end{aligned}$$

Nevertheless, these constraints are simply an affine transformation of the convex second-order cone  $\{\mathbf{x}, y \mid \|\mathbf{x}\|^2 \leq y^2, y \geq 0\}$ , showing that this is a convex problem and therefore can be efficiently solved by means of standard schemes for convex optimization [122]. Despite the original constraint set in (6.2) not being convex, authors in [119] show that it can be still efficiently solved using convex optimization. For this purpose, matrices  $\mathbf{W}_g = \mathbf{w}_g\mathbf{w}_g^H$  are introduced, keeping in mind that  $\mathbf{h}_{gj}\mathbf{w}_j\mathbf{w}_j^H\mathbf{h}_{gj}^H = \text{Tr}[\mathbf{h}_{gj}^H\mathbf{h}_{gj}\mathbf{w}_j\mathbf{w}_j^H] = \text{Tr}[\mathbf{R}_{gj}\mathbf{W}_j]$ . From there, the problem can be rewritten as

$$\begin{aligned}
& \text{minimize} && \sum_{g=1}^G \text{Tr}[\mathbf{W}_g] \\
& \text{subject to} && \text{Tr}[\mathbf{R}_{gg}\mathbf{W}_g] - \gamma_g \sum_{j \neq g} \text{Tr}[\mathbf{R}_{gj}\mathbf{W}_j] = \gamma_g \sigma_g^2, \\
& && \mathbf{W}_g = \mathbf{W}_g^H, \\
& && \mathbf{W}_g \succeq 0 \quad \forall g.
\end{aligned} \tag{6.3}$$

Notice that, with the additional rank-one constraints, (6.3) is equivalent to (6.2), and hence a rank-one solution for (6.3) is a solution for (6.1) as well. Relaxing the rank of matrices  $\mathbf{W}_g$  leads to a semidefinite optimization problem whose solution is a lower bound for the original problem. This approach is known as Lagrangian relaxation [123, 124], since it is the Lagrangian dual of the dual of the original problem.

The obvious limitation of the scheme in [119] is that it only operates with downlink MISO channels. On the contrary, the method cannot be directly applied when multi-antenna receivers are allowed. For this reason, in the following we develop an algorithm that allows to minimize transmit power by optimizing both beamformers and filters, as well as the transmit power level at the uplink user equipments.

## 6.2 Power minimization in flexible duplexing networks

Our goal in the described scenario is to minimize the transmit power over 2 consecutive slots while satisfying an SINR requirement. As in Chapter 5, we assume that all cells switch from DL to UL or viceversa every slot:

$$\begin{aligned} \mathcal{P}_2 : \underset{\substack{\{\mathbf{w}_g\}, \{\mathbf{u}_g\}, \\ \{P_{UE_g}\}, \mathcal{I}}}{\text{minimize}} \quad & \sum_{g=1}^G \left( a_g \|\mathbf{w}_g\|^2 + (1 - a_g) P_{UE_g} \right) \\ \text{s. t.} \quad & \text{SINR}_g \left( \{\mathbf{w}_j\}, \{P_{UE_j}\}, \mathbf{u}_g, \mathcal{I} \right) \geq \gamma_g \quad \forall g, j \\ & \text{SINR}_g \left( \{\mathbf{w}_j\}, \{P_{UE_j}\}, \mathbf{u}_g, \bar{\mathcal{I}} \right) \geq \gamma_g \quad \forall g, j, \end{aligned} \quad (6.4)$$

where  $\gamma_g$  represents the target SINR for cell  $g$ , and  $a_g \in [0, 1]$  represents the predefined priority ratio between minimizing uplink and downlink power levels. Furthermore,  $\mathcal{I} \stackrel{\text{def}}{=} \text{cat}_g(i_g)$  is the set of Boolean variables  $i_g$ . Note that the  $\text{SINR}_g$  at cell  $g$  depends on the UL/DL configuration, the filter at the  $g$ -th BS/AP in uplink, and the beamformers and power levels at all the transmitters in the network. As mentioned before, all cells switch their transmit direction every slot, thus we also consider the SINR constraints for the complementary UL/DL set  $\bar{\mathcal{I}}$ . Notice that, despite the cost function includes just the norm of the beamformers,  $\|\mathbf{w}_g\|^2$ , we take  $\mathbf{w}_g$  as optimization variables, i.e., we optimize both norm and transmit angle, as well as the angle of the unit-norm filters  $\mathbf{u}_g$  at the multi-antenna receivers.

The set  $\mathcal{I}$  of indication variables  $i_g$  turns (6.4) into a discrete optimization problem. For this reason, we decouple our power minimization scheme into a transmit power minimization for all (or a subset) of the possible UL/DL combinations, followed by a discrete search of the UL/DL setting that provides the optimal solution. In order to solve the problem for a given UL/DL configuration, we apply the MinPower-MaxSINR algorithm presented in the following.

$$\begin{aligned}
\mathcal{P}_3 : \underset{\substack{\{\mathbf{w}_g\}, \{\mathbf{u}_g\}, \\ \{P_{UE_g}\}}}{\text{minimize}} \quad & \sum_{g=1}^G \left( a_g i_g \|\mathbf{w}_g\|^2 + (1 - a_g) (1 - i_g) P_{UE_g} \right) \\
\text{subject to} \quad & i_g \mathbf{h}_{gg} \mathbf{w}_g d_{gg}^{-\alpha} \mathbf{w}_g^H \mathbf{h}_{gg}^H + (1 - i_g) \mathbf{u}_g^H \mathbf{h}_{gg} P_{UE_g} d_{gg}^{-\alpha} \mathbf{h}_{gg}^H \mathbf{u}_g \\
& \geq \gamma_g \left( \sigma_g^2 + i_g \sum_{\substack{j=1 \\ j \neq g}}^G \left( \underbrace{i_j \mathbf{h}_{gj} \mathbf{w}_j d_{gj}^{-\alpha} \mathbf{w}_j^H \mathbf{h}_{gj}^H}_{\text{BS/AP to UE interference}} + \underbrace{(1 - i_j) h_{gj} P_{UE_j} d_{gj}^{-\alpha} h_{gj}^H}_{\text{UE to UE interference}} \right) \right. \\
& \left. + (1 - i_g) \sum_{\substack{j=1 \\ j \neq g}}^G \left( \underbrace{i_j \mathbf{u}_g^H \mathbf{H}_{gj} \mathbf{w}_j d_{gj}^{-\alpha} \mathbf{w}_j^H \mathbf{H}_{gj}^H \mathbf{u}_g}_{\text{BS/AP to BS/AP interference}} + \underbrace{(1 - i_j) u_g^H \mathbf{h}_{gj} P_{UE_j} d_{gj}^{-\alpha} \mathbf{h}_{gj}^H \mathbf{u}_g}_{\text{UE to BS/AP interference}} \right) \right) \quad \forall g
\end{aligned} \tag{6.5}$$

### 6.2.1 MinPower-MaxSINR algorithm

In order to address the power minimization for a given UL/DL combination, we rewrite (6.4) for a fixed set  $\mathcal{I}$  as in (6.5). The filters  $\mathbf{u}_g$  at the BS/AP in uplink are initialized to the maximum ratio combining (MRC) of the direct channel, turning (6.5) into a power minimization problem in an equivalent MISO interference channel with SINR constraints, which has been proven to be convex in [119]. Therefore, in order to solve (6.5) for fixed  $\mathbf{u}_g$ , we can rely on standard convex optimization methods [122].

Let us assume that we have solved (6.5) for a set of fixed receiving filters  $\mathbf{u}_g$  and a given SINR constraint,  $\gamma_g$ . The main intuition behind MinPower-MaxSINR is that, by fixing the transmitters to the obtained solution of (6.5) and calculating the MaxSINR filters in (6.6), we achieve a higher or equal SINR  $\gamma_g^* \geq \gamma_g$  at the multi-antenna receivers,

$$\mathbf{u}_g^* = \text{ev}_{\max} \left( \mathbf{Q}_g^{-1/2} \mathbf{H}_{gg} P_{UE_g} d_{gg}^{-\alpha} \mathbf{H}_{gg}^H \mathbf{Q}_g^{-1/2} \right) \quad \forall g, \tag{6.6}$$

where  $\mathbf{Q}_g$  is the interference-plus-noise covariance matrix

$$\begin{aligned}
\mathbf{Q}_g = \sigma_g^2 + \sum_{j=1}^G \left( i_j \mathbf{H}_{gj} \mathbf{w}_j d_{gj}^{-\alpha} \mathbf{w}_j^H \mathbf{H}_{gj}^H \right. \\
\left. + (1 - i_j) \mathbf{h}_{gj} P_{UE_j} d_{gj}^{-\alpha} \mathbf{h}_{gj}^H \right) \quad \forall g.
\end{aligned}$$

Accordingly, if we reconsider (6.5) for the initial constraints  $\gamma_g$  with the new filters  $\mathbf{u}_g^*$ , we can obtain a solution with a lower or equal power budget. We repeat this sequence until a termination criterion,  $\text{Thres}$ , is satisfied within a predefined maximum number of iterations  $\text{MaxIter}$ . The main steps to implement the proposed MinPower-MaxSINR scheme can be found in Alg. 3.

**Algorithm 3:** MinPower–MaxSINR for a fixed UL/DL combination.

---

```

Input:  $\{\mathbf{H}_{gj}\}, \{d_{gj}\}, \{N_g\}, \mathcal{I}, \text{MaxIter}, \text{Thres}$ 
Output: Sets  $\{\mathbf{w}_g\}, \{\mathbf{u}_g\}$  and  $\{P_{UE_g}\}$  and a feasibility indicator,  $\text{FeasibilityFlag}$ 
/* Initialization */
Set  $\{\hat{\mathbf{u}}_g\}$  to the MRC filter
FeasibilityFlag = true,  $k = 1$ 
while  $k \leq \text{MaxIter}$  do
    Solve (6.5) for fixed  $\{\hat{\mathbf{u}}_g\}$ 
    if  $\{\mathbf{w}_g^*, P_{UE_g}^*\} == []$  then
        FeasibilityFlag = false
        break
    else
         $\{\mathbf{w}_g\} = \{\mathbf{w}_g^*\}, \{P_{UE_g}\} = \{P_{UE_g}^*\}$ 
        Obtain MaxSINR filters  $\{\mathbf{u}_g^*\}$  as in (6.6)
        Power  $P(k)$  = cost function in (6.5)
        /* Check termination condition */
        if  $(P(k-1) - P(k)) / P(k-1) > \text{Thres}$  then
             $\{\hat{\mathbf{u}}_g\} = \{\mathbf{u}_g^*\}, k = k + 1$ 
        else
             $\{\mathbf{u}_g\} = \{\mathbf{u}_g^*\}$ 
            return
    return

```

---

Notice that different UL/DL sets  $\mathcal{I}$  will lead to different interference levels at the input of the receivers and hence to different solutions for the minimization problem. Therefore, a discrete search considering the different UL/DL combinations is required in order to achieve a solution for (6.4).

## 6.2.2 Determining the best UL/DL configuration

Finding the optimal solution for (6.4) requires evaluating all possible sets  $\mathcal{I}$ , i.e., a total of  $2^G$  UL/DL combinations. Despite the networks under study being not dense in terms of number of cells, we aim to reduce the computational cost of the transmit direction selection. For this purpose, we propose a suboptimal approach, based on the hierarchical switching schemes in Chapter 5, that allows to reduce the number of evaluations to  $G$ . Recall that the main idea consists in starting in conventional TDD mode. Then, a cell in the macro-tier switches transmit direction with respect to the rest of cells, and the transmit power is minimized via MinPower–MaxSINR. If the required power is lower, the cell keeps the direction change, whereas if the power increases, the cell goes back to the previous state. This procedure is repeated sequentially until every macrocell has evaluated the benefit of the UL/DL switching, and then the same sequence is carried out for small cells. We have selected the HS–Macro hierarchical criterion due to the fact that power levels are usually higher

---

**Algorithm 4:** Hierarcical switching for minimum transmit power.

---

```

Input:  $\{\mathbf{H}_{gj}\}, \{d_{gj}\}, \{N_g\}, \mathcal{I}$ 
Output: Sets  $\{\mathbf{w}_g\}, \{\mathbf{u}_g\}$  and  $\{P_{UE_g}\}$  and  $\mathcal{I}$ 
/* Initialization */
 $\mathcal{I} = \text{zeros}(1, G);$  // cat( $i_g$ )
MinTotalPower = MinPower-MaxSINR( $\mathcal{I}$ )
for  $g = 1$  to  $G$  do
    /* Cell  $g$  switches */
     $\mathcal{I}(g) = \tilde{\mathcal{I}}(g)$ 
    /* Evaluate the new setting */
    TotalPower = MinPower-MaxSINR( $\mathcal{I}$ )
    if TotalPower < MinTotalPower then
        | MinTotalPower = TotalPower
    else
        |  $\mathcal{I}(g) = \tilde{\mathcal{I}}(g)$ 
/*  $\{\mathbf{w}_g\}, \{\mathbf{u}_g\}, \{P_{UE_g}\}$  associated to  $\mathcal{I}$  */
return

```

---

in macrocells, and hence they have a larger room for improvement. The steps to complete the HS sequence are formulated in Alg. 4.

### 6.2.3 Feasibility and complexity

Throughout Section 6.2.1, we have assumed that the power minimization problem is feasible for the given SINR constraints. However, for some channel realizations, spatial distributions ( $\{d_{gj}\}$ ), and/or SINR requirements  $\gamma_g$ , (6.5) could be infeasible. In such cases, we are left with two straightforward approaches, namely, discard the infeasible scenario, or more practically, reduce the SINR requirement so that the problem becomes feasible. Nevertheless, a deeper analysis on feasibility is beyond the scope of this work.

Regarding the computational complexity of the algorithm for (6.5), let us recall that the proposed scheme is an iterative combination of well-known convex optimization techniques and the closed-form MaxSINR receivers. Details on time complexity for the former can be found in [122]. On the other hand, each calculation of a MaxSINR filter implies a singular value decomposition (SVD). Therefore, it has complexity  $\mathcal{O}(\min\{mn^2, m^2n\})$ , being  $m$  and  $n$  the number of rows and columns of the input matrix, respectively.

As mentioned before, the task of finding the optimal set  $\mathcal{I}$  (i.e., the UL/DL with minimum transmit power), requires  $2^G$  evaluations of MinPower-MaxSINR. Nevertheless, we have reduced the computational cost to  $G$  evaluations with the suboptimal HS approach.

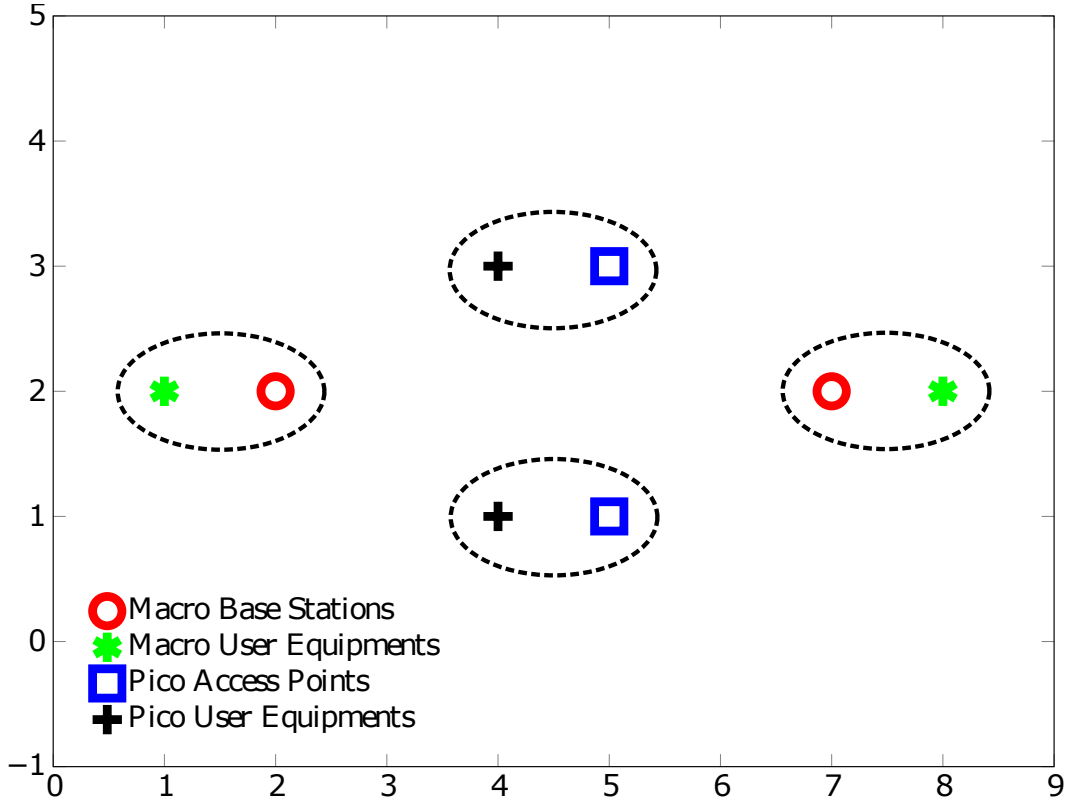


Figure 6.1: Normalized location of the nodes in the system (Network 5).

### 6.3 Simulation results

In order to verify the performance of the proposed algorithm together with flexible duplexing in terms of transmit power, we consider a 2-tier HetNet comprised of  $G_m = 2$  macrocells and  $G_s = 2$  small cells. The BS and AP are equipped with  $N_g = N = 7$  antennas  $\forall g$ , and the baseline SNR is set to 20 dB. Additionally, we take into account the inherent UL/DL asymmetry by setting the priority variables  $a_g = 0.8 \forall g$ , and we assume free space propagation ( $\alpha = 2$ ). As a termination criterion for Alg. 3, we set an improvement threshold  $\text{Thres} = 0.01$  with respect to the previous iteration, and we consider a maximum of  $\text{MaxIter} = 5$  iterations. In this context, we evaluate the proposed algorithm for a range of SINR constraints. As a benchmark for comparison, we also consider the method in [119], which has been conveniently adapted to work in the scenario under study. The results of 1000 independent channel realizations have been averaged.

Figure 6.2 shows the total transmit power benefits over 2 time slots with respect to the conventional TDD approach with fixed receiving filters [119]. From Fig. 6.2, we characterize two main sources of benefit.

- The black curve with square markers represents the benefit of applying MinPower–MaxSINR instead of the benchmark method.

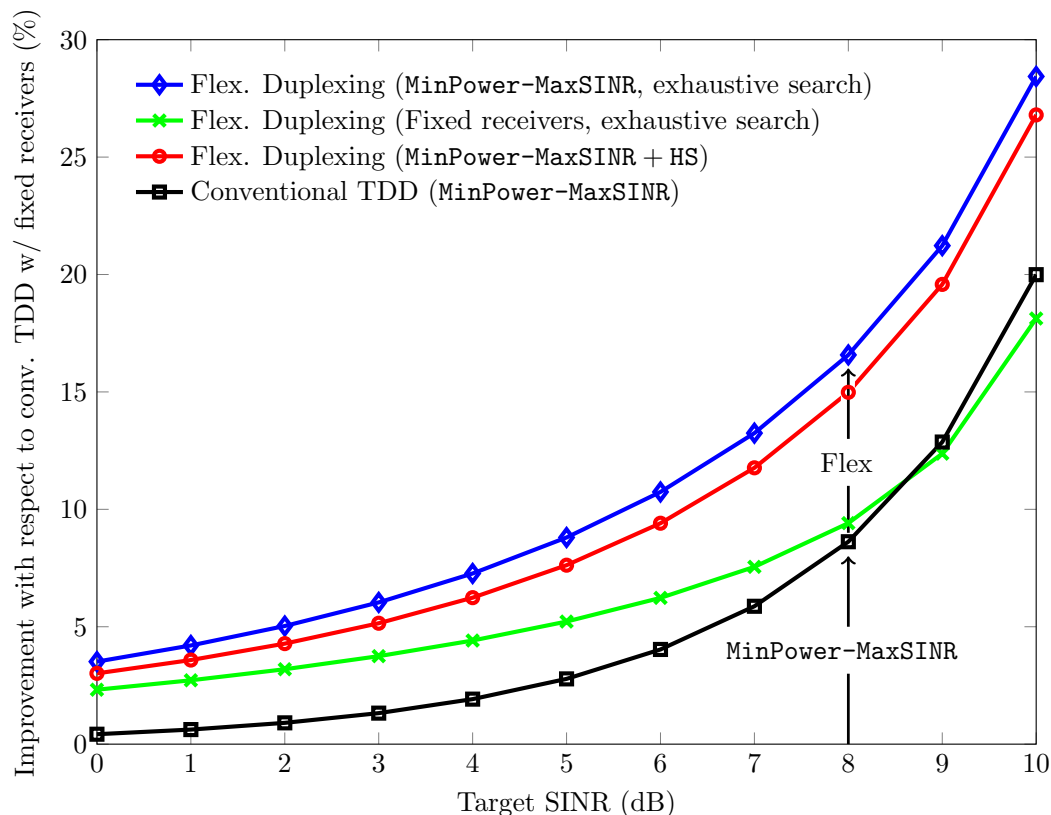


**Figure 6.2:** Total power benefits, with respect to conventional TDD w/ fixed receivers, by MinPower-MaxSINR, flexible duplexing and the suboptimal HS scheme.

- The additional improvement due to flexible duplexing is associated to the gap between the black, square marked line and the diamond marked line in blue.

Notice that, despite the benefits of flexible duplexing being significant, the power results obtained by MinPower-MaxSINR in conventional TDD mode are close to those attained by the method in [119] for the best UL/DL combination. Hence, we can state that, besides flexible duplexing, the proposed minimization technique applied for every UL/DL setting plays an important role.

Finally, the red curve with circle markers in Fig. 6.2 represents the total power benefit that can be achieved by implementing MinPower-MaxSINR and flexible duplexing with HS. Specifically, we focus on the comparison between the exhaustive search strategy and the suboptimal HS approach. Notice that the results provided by HS ( $G$  total evaluations of  $\mathcal{P}_2$ ) are significantly close to those obtained by exhaustive search ( $2^G$  total evaluations), with the advantage of having a much lower computational cost.



# Part **IV**

## **Experimental analysis of flexible duplexing**



# Chapter 7

## Flexible duplexing experiments: context, setup and results

In previous parts, we have studied the benefits of flexible duplexing in HetNets relying on different figures of merit. Specifically, we have analyzed the performance improvements in terms of degrees of freedom, throughput, and power efficiency. Nevertheless, such studies have been conducted in a theoretical context, and some assumptions have been made in order to overcome the mathematical difficulties of the analysis. On the contrary, when applying these schemes in real-world scenarios, the aforementioned theoretical assumptions turn out to be excessively optimistic, and several impairments could penalize the system performance. For this reason, we go a step further and evaluate the potential benefits of flexible duplexing together with interference alignment in an experimental environment. The chapter is organized as follows: first, we provide a discussion on the main practical difficulties related to IA implementations. Once the main challenges have been described, we present the experimental setup on which we have carried out the measurement campaign. Finally, the experimental results are shown and analyzed in detail.

### 7.1 An overview on interference alignment testbeds

All throughout the entire study in previous chapters, flexible duplexing and interference alignment have been jointly used as a combined approach to minimize the impact of multiuser interference. Therefore, in order to provide a wider perspective on the experimental part of this work, we provide a brief review of the most remarkable implementations of IA. The main practical impairments that arise in IA experiments are introduced, and some of the solutions adopted to overcome such mismatches are briefly described. Furthermore, we include statistics about the different experiments regarding hardware devices, size and cost of implementation, as well as a reflection on the main requirements for further real-world evaluations.

The recently developed interference alignment concept has revealed that the throughput of a wireless network can be significantly improved compared to that exhibited by conventional transmission schemes such as TDMA and FDMA. Unfortunately, it is extremely difficult to take into account all practical limitations in the

analytical investigation of IA, yielding theoretical results that are frequently based on assumptions which are hardly realizable in real-world scenarios. Examples of such practical aspects are the impact of imperfect channel state information, energy loss due to spatial collinearity between desired signal and interference subspaces, detection and synchronization errors, and imperfect hardware. Consequently, the experimental evaluation of IA techniques is crucial to better understand the aforementioned practical limitations on the performance of existing IA techniques, as well as to propose new research topics around the IA concept to overcome such limitations.

The original IA concept assumes perfect CSI knowledge in all terminals to design the corresponding beamformers and filters. In practice, however, users can acquire only a noisy version of the CSI, yielding a significant performance degradation in terms of the achievable degrees of freedom, as shown in [125] for a pilot-assisted channel estimation technique in a K-user interference network with single-antenna users. The CSI acquisition problem is mitigated in TDD systems by exploiting channel reciprocity, although calibrated RF equipment is required [126]. For FDD systems, IA experiments with perfect [127, 14] and realistic analog wireless [128] feedback channels have been reported in the literature. Furthermore, in most of the theoretical IA works, the block-fading channel model assumption plays a pivotal role due to its mathematical tractability [125]. In practice, guaranteeing a constant channel during a block transmission is not possible, leading to the additional problem of outdated CSI at the transmitters.

Another practical limitation in practice is the finite SNR at the receivers. However, experimental results show that, despite the imperfections in both CSI acquisition and testbed hardware, IA outperforms conventional communication schemes such as TDMA and greedy interference avoidance in the mid-to-high SNR regime [127]. In this sense, an optimal trade-off between network resources dedicated to CSI acquisition and feedback with respect to those devoted to data transmissions must be determined to maximize the throughput [125, 129, 130]. Error vector magnitude (EVM) experimental results for a pilot-assisted maximum signal-to-interference-plus-noise ratio scheme corroborate the existence of an optimal resource allocation scheme [130] and an optimal number of training symbols [127].

Time and frequency synchronization between network nodes is of utmost importance when experimentally evaluating IA techniques, and it can be implemented in a centralized [131] or distributed manner [126, 128]. Theoretical IA works usually assume that beamformers operate after frame detection and synchronization. In practical systems, however, frame detection and synchronization are applied immediately after the analog-to-digital conversion, hence being affected by interference and yielding a strong performance degradation of such tasks, thus impacting dramatically on the final system performance. For most of the spatial IA implementations in multicarrier systems, IA decoding is implemented in a conventional per-subcarrier approach in the frequency domain (post-FFT). However, if the decoders are applied at a sample level in time domain (pre-FFT), most of the multiuser interference is suppressed at the very beginning of the receiver signal processing chain. In that situation, the effective SINR is improved, whereas synchronization tasks perform similar

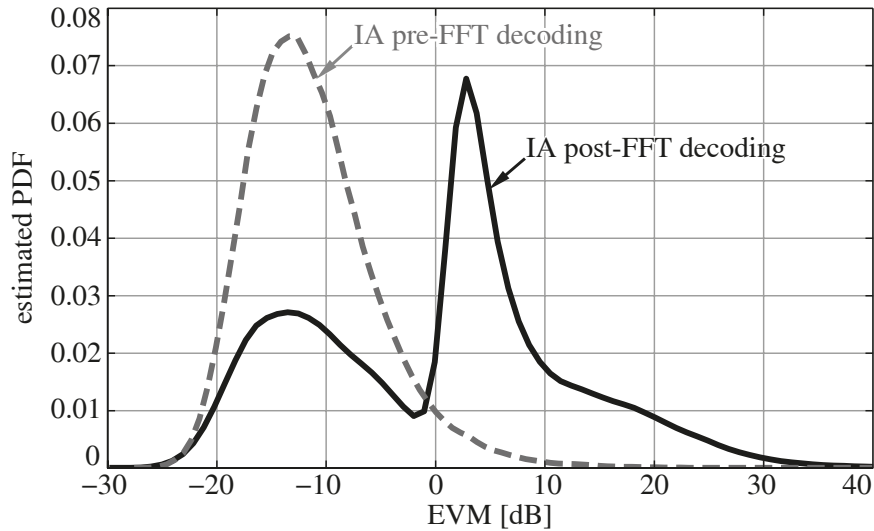


**Figure 7.1:** PDF for the EVM of pre-FFT and post-FFT IA decoding in asynchronous transmission [dB].

to the interference-free case because they operate after filtering out the interference [127, 14]. Figure 7.1 shows the estimated probability density function (PDF) for the EVM achieved by both schemes. As expected, when there is no coordination among users, post-FFT decoding is not capable of successfully detecting the desired frame.

On the contrary, pre-FFT IA decoding overcomes this issue, since synchronization tasks are carried out once multi-user interference (MUI) has been successfully suppressed at each receiver. Hence, it provides a satisfactory performance, as observed in Fig. 7.1. Note that practical impairments, such as CSI estimation errors and collinearity, affect both pre-FFT and post-FFT to the same extent, so we can assume that the differences between both results are mainly due to timing offsets and synchronization.

Hardware imperfections are ignored in many IA algorithm designs. However, nonlinear distortions, phase noise, IQ imbalance, and frequency offset degrade IA performance [127, 132]. For instance, the measurement results of IA in the 3-user  $2 \times 2$  MIMO interference channel in [132] show that hardware imperfections can reduce the maximum achievable SINR up to 10 dB compared to the theoretical predictions. To compensate the interference leakage under non-ideal conditions, power control is suggested as a complementary interference management technique [133].

### 7.1.1 Highlights of testbed implementations

In this section we provide statistical information on IA experiments and publications, as well as financial costs of these IA implementations. Various options that span from low- to high-end solutions are also summarized.

As the IA concept evolves, testbeds incorporate a mixture of dedicated hardware components and commercial off-the-shelf modules (we refer to them as dedicated platforms). When the concept matures, the amount of dedicated hardware components in the testbed platforms overrun. Commercial off-the-shelf products are still the leading choices for IA implementations within the research community.

### Analysis of the costs of equipment in IA experiments

In Table 7.1, the equipment used in each of the reported IA testbeds and its estimated costs are listed. As can be seen in the list, a very affordable IA setup is demonstrated in [131] where transmit antenna selection is applied, and two antennas out of three are selected. The next affordable setup is reported in [128]. With a similar total cost, high-performance universal software radio peripherals (USRPs) support  $2 \times 2$  MIMO configurations, as shown in Table 7.1. The first IA real-time implementation is introduced in [134], where blind interference alignment (BIA) is implemented for a 2-user  $2 \times 1$  broadcast channel. In this setup, there are two antennas at the transmitter, whereas at the receiver, one of two antennas is selected. Except for [131, 134], all configurations in Table 7.1 are outlined for the 3-user  $2 \times 2$  interference channel with a single stream per user,  $(2 \times 2, 1)^3$ , including the equipment used in the recent implementation of a massive MIMO testbed by the University of Bristol and Lund University collaboration. With a comparable total cost and testbed setup, a similar equipment list is used in the centralized PXI configuration. Finally, in the distributed PXI configuration, a separate chassis is used for each transmitter. In Fig. 7.2, the estimated costs of selected configurations from Table 7.1,

- Configuration C: high performance USRPs
- Configuration F: centralized PXI
- Configuration G: distributed PXI

are plotted vs. the network size. In the massive MIMO demonstration by the universities of Bristol and Lund, 16 users are served by a 128-antenna transmitter. Accordingly, in order to implement IA in the  $(9 \times 8, 1)^{16}$  scenario, by using the same equipment listed in Table 7.1 for configurations F and G, a total cost of nearly US\$2 million is estimated. As shown in Fig. 7.2, to scale the network DoF by a factor of 4, that is, from 3:  $(2 \times 2, 1)^3$  to 12:  $(8 \times 7, 3)^4$ , the cost is expected to increase nearly 4 times, whereas by scaling the DoF approximately by a factor of 5, that is, from 3 to 16:  $(9 \times 8, 1)^{16}$ , the cost is expected to scale by a factor of 20. Hence, for large network sizes where IA is significantly competitive, large capital investments are required.

### IA testbed platforms and experiments

The number of solutions devoted to experimental research in wireless communications is growing every year, particularly with the increased interest in wireless sensor

**Table 7.1:** Main hardware devices needed for every testbed and total estimated cost.

Configuration type		[131]	[128]	High perf. USRP	[134]	Bristol & Lund	Cent. PXI	Dist. PXI
		A	B	C	D	E	F	G
Equipment	Unit cost*	Number of devices in a configuration						
OctoClock CDA-2990 782978-01	1.1	1	-	1	-	1	1	1
NI USRP-2943R 783925-01	6.8	-	-	6	-	3	3	3
NI USRP-2953R GPS Clock 783928-01	8.1	-	-	-	-	3	3	3
NI PXIe-1082 Chassis 780321-01	3.8	-	-	-	3	-	-	3
NI PXIe-1085 Chassis 783588-01	10.0	-	-	-	-	1	1	-
NI PXIe-7976R FlexRIO FPGA 783625-01	11.0	-	-	-	-	3	3	3
NI PXIe-8840 RT Controller 783001-33	5.1	-	-	-	-	1	-	3
NI PXIe-8880 Controller 783513-33	8.0	-	-	-	-	1	-	-
USRP N210 782747-01	2.1	6	-	-	-	-	-	-
USRP B210 782981-01 / 784190-01	1.4	3	-	-	-	-	-	-
NI USRP-2921 781907-01	2.8	-	12	-	-	-	-	-
GPSDO Kit for USRP N200/N210 782779-01	0.9	-	6	-	-	-	-	-
NI PXIe-8130 Controller	5.1	-	-	-	3	-	-	-
NI PXIe-7965R FlexRIO FPGA 781207-01	10.1	-	-	-	4	-	-	-
NI 5781 Baseband Transceiver 781267-01	3.3	-	-	-	4	-	-	-
XCVR2450	0.5	-	-	-	4	-	-	-
Total cost* (thousand USD)		18	40	42	82	94	97	105

networks (WSN) and the Internet of Things (IoT) from the research community. Publicly accessible testbed facilities are great opportunities for IA researchers to experimentally evaluate their algorithms. However, among the large-scale testbed facilities that offer public access for researchers to execute automated and manageable exper-

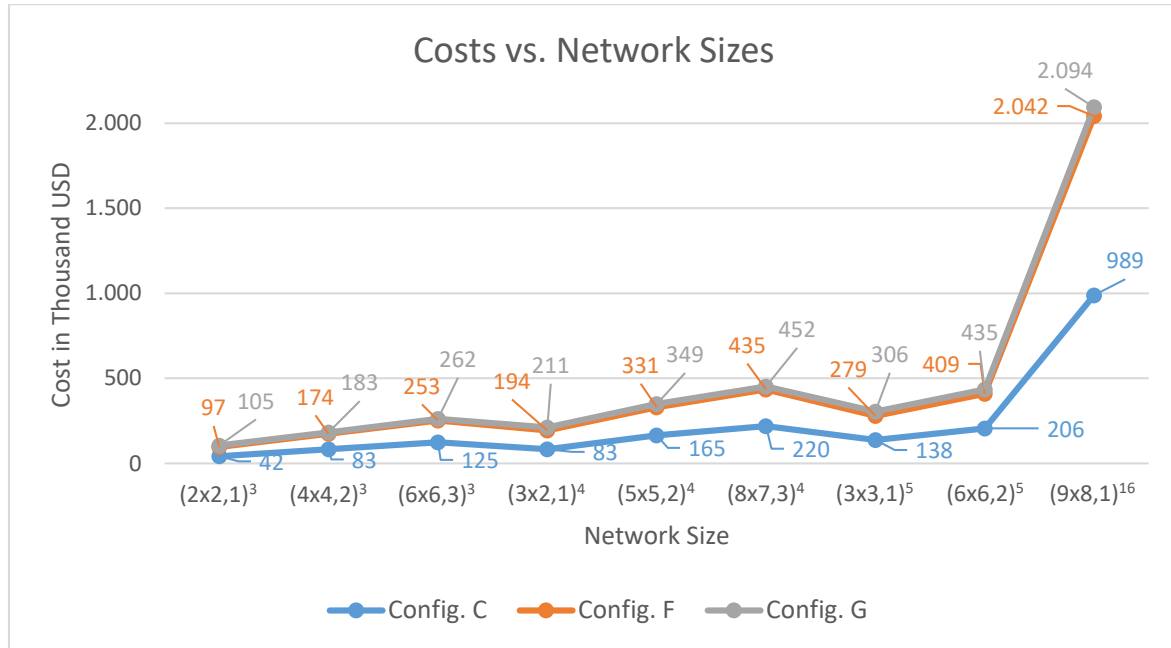


Figure 7.2: .

iments, only a few of them are suitable for physical-layer experimentation. A good example is CorteXlab at the University of Lyon, which contains a mixture of low-power, general-purpose, and real-time high-performance nodes. Other small-scale publicly available facilities are CREW and CORE+ project consortiums.

There are different platforms available for the implementation of an IA testbed. National Instruments and Ettus USRPs together with the open source universal hardware driver and GNU Radio are among the preferred choices for low-budget cases. Open source implementations of communication standards like open-LTE for the case of LTE and the enormous user community make this solution very attractive. At an increased cost, National Instruments USRPs can be preferred since they support LabView, a powerful software that is another proprietary product of National Instruments. Other examples of low-cost solutions available in the market are RTL-SDR, HackRF, and Nuand BladeRF. Unfortunately, their simple designs and limited capabilities make complex IA implementations on these platforms infeasible.

When the budget is not a severe constraint, high-end PXI-based products present much better solutions. There are several PXI hardware vendors, such as Keysight and National Instruments. The main advantage of National Instruments solutions lies on the software side, especially their integration with LabView and with other powerful software tools like MATLAB by Mathworks.

Many manufacturers offer hardware equipment besides the integrated solutions, allowing to develop a part-by-part testbed. 4DSP, Nutaq, and Innovative Integration are just some examples. Some of the manufacturers offer modules for Xilinx-based boards, and typically they do not provide full solutions or open source drivers. At a lower level, Texas Instruments, Maxim Integrated, and Analog Devices are among the manufacturers continuously offering better components for software-defined radio

(SDR) solutions. For example, Analog Devices has introduced a transceiver (AD-FMCOMMS5-EBZ) with up to  $4 \times 4$  antennas and 56 MHz bandwidth on a single board. At a much higher level, the Wireless Open Access Research Platform (WARP) is an example of a full bundle of solutions built from the ground up with the aim of prototyping advanced wireless networks. Several alternatives similar to WARP can be found within the wireless research community, for example, the SDR4All project from Supélec.

Frequently, research institutions opt for developing their testbeds based on commercial off-the-shelf hardware, sometimes combined with custom-designed parts. Examples of such testbeds are those developed by the Vodafone Chair for Mobile Communications Systems at Technische Universität Dresden, KTH Testbed, OpenAir-Interface at Eurecom, the so-called Vienna MIMO Testbed developed at the Institute of Telecommunications at Technische Universität Wien, and the one developed at the Heinrich Hertz Institute at the Fraunhofer Institute for Telecommunications.

Once the hardware required to experimentally evaluate IA techniques is ready, a challenge that arises is the generation of a representative and sufficiently large amount of channel realizations guaranteeing repetitive and reproducible results. Fortunately, many clever and inspiring approaches are found in the literature, for example, considering antenna switching instead of reconfigurable antennas [134], utilizing two different reconfigurable antenna architectures that use different patterns, or simply sliding the receive antenna.

### 7.1.2 Future directions

In this section we provide an overview on the future requirements to transform IA into an attractive solution to be considered for the next generations of wireless communication systems.

#### Scalability

As mentioned before, existing experimental setups cover simplified scenarios with a reduced number of nodes and antennas per node. However, real-world wireless networks usually include a large number of users and base stations equipped with several antennas each. Even though the implementation of sophisticated nodes is much more expensive, this aspect is of utmost importance regarding the evaluation of IA in realistic scenarios. Experimental evaluation of wireless communication systems in general requires certain measurement concepts and techniques such as the treatment of uncertainties in the results [135]. As the network size scales, the application of this discipline becomes more complex and also more vital, and hence such measurement concepts and techniques need to be adapted to the particular case of IA as well.

### Outdoors and high mobility

Few IA testbed implementations have considered outdoor and/or mobile environments, whereas the majority have addressed only static indoor scenarios. To the best of our knowledge, there is only one IA testbed implementation that is close to a mobile functional stage since the beams are physically transmitted over the air and the complete system is realized in real time [128] with CSI at the receiver end only (Blind IA). Nowadays, testbed equipment can be powered by small batteries and controlled using a laptop (e.g., B-family USRPs), thus making it possible to assess IA in high-mobility scenarios in the near future [136].

### Software requirements

Until now, the discussions are typically dominated by hardware specifications. However, a common repository to share and improve open source IA software by the developers is perhaps another immediate need. Such an approach can provide huge momentum for in-depth research and for the expansion of IA applications. In this sense, it is worth mentioning that the GTEC Group at University of A Coruña has developed the so-called GTIS Project, a control package that allows to configure and control compatible USRP devices with MATLAB, as well as accessing the nodes configuration and transmission remotely via SSH. The libraries are under continuous upgrading and provide the researchers with more friendly software tools when compared to the UHD and GNU Radio libraries. Despite not being IA-dedicated, GTIS supports the required functionalities and features to implement IA experiments, such as frequency, time, and phase synchronization, among others.

### Different network topologies

The IA testbed implementations summarized in the previous sections can be gathered under two groups: IA with channel state information at the transmitters (CSIT) in interference networks and IA with no CSIT, for example, BIA in broadcast networks.

Another promising direction is the implementation of IA in relay networks, either with or without CSIT. For the former, innovative techniques are emerging, such as aligned network coding and aligned interference neutralization. For the latter, BIA in relay networks is particularly appealing since IA drawbacks in broadcast or X networks are eliminated via the relay nodes. For conventional SISO interference channels without relays, time-varying channels with long symbol extensions are required to obtain the optimal DoF. This demands an overwhelming amount of channel feedback overhead to each transmitter. However, in the relay-aided SISO IC, only two time slots are required, and hence the feedback overhead is greatly reduced. Moreover, the relays are located in between the transmitters and the receivers, and thus have more accurate CSI feedback from the receivers compared to the CSI feedback to the transmitters, which are located farther from the receivers. Hence, the relay-aided BIA schemes are appealing from a practical perspective. Finally, as mentioned above,

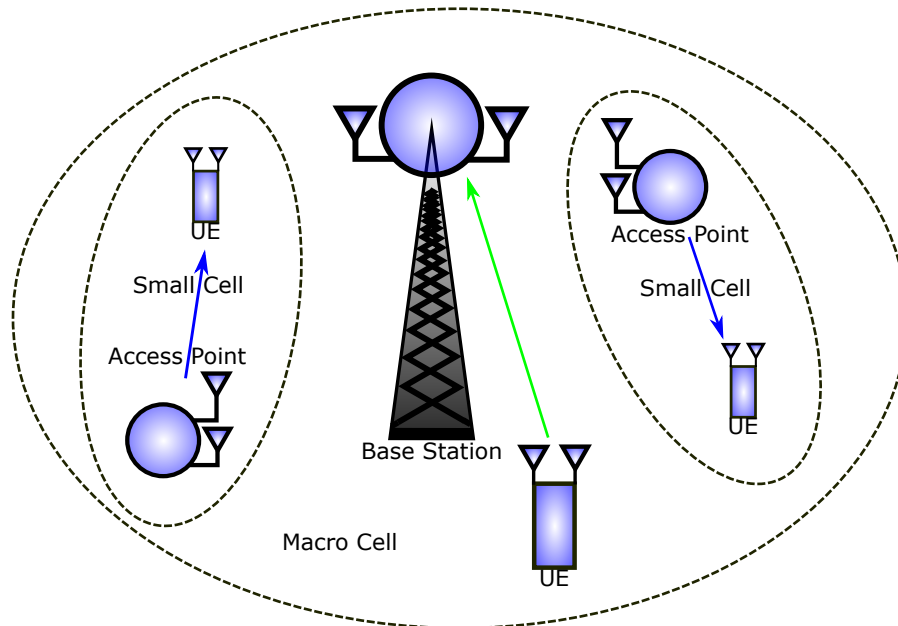


**Figure 7.3:** Network topology under evaluation.

extending the BIA schemes to interference broadcast relay channels is also important to serve more users with fewer base stations deployed in a cellular network.

Nevertheless, regarding next-generation communications, more complex and advanced network topologies, such as heterogeneous networks, should also be considered. Some of the HetNet scenarios studied in previous chapters seem to be addressable in terms of IA testbed implementation. Altogether, a successful implementation of IA techniques in this context would be a significant step forwards in terms of the feasibility of alignment-based transmissions for the next-generation wireless communications. For this reason, we have considered interference alignment as the main candidate to evaluate the performance benefits of flexible duplexing empirically. The joint implementation of flexible duplexing and interference alignment with CSIT and real-time precoding and decoding brings wireless communications a step closer to the next generation of wireless networks.

## 7.2 Experimental evaluation of flexible duplexing

After going through the main challenges that can arise when implementing interference alignment, we provide a detailed description of the experimental setup that we have built in order to study the benefits of applying flexible duplexing. The scenario under evaluation is a 3-cell network with a macrocell and 2 small cells (see Fig. 7.3). As in Chapters 5 and 6, each cell has a single active user. All the nodes in the network are equipped with 2 antennas, and there is an OFDM stream per link. Therefore, we are working with a set of multi-carrier  $(2 \times 2, 1)^3$  interference channels, each one

associated to a UL/DL combination. Notice that the different hierarchy and role of the nodes in the network are determined based on the transmit power levels and the location/distance between nodes. In the following, we describe the main hardware devices in the scenario, as well as the software tools that have allowed us to configure and control the different base stations, access points, and user equipments. Additionally, we explain the physical characteristics of the transmissions and the frame format that we have used to convey the symbol sequences. The main transmission strategies to be compared are introduced, and finally, we provide a selection of the most remarkable results.

### 7.2.1 Multiuser MIMO testbed

The MIMO HetNet that we have implemented is based on Ettus Universal Software Radio Peripheral (USRP) devices. Specifically, each node in the network is associated to a 2-antenna USRP B210, with Analog Devices AD9361 RF frontend and Xilinx Spartan 6 XC6SLX150 field-programmable gate array (FPGA). These transceivers are capable of both up and down conversion ranging from 70 MHz up to 6 GHz with a maximum instantaneous bandwidth of 30.72 MHz<sup>1</sup>. Therefore, B210 boards are conveniently suitable for experiments in the 2.4 GHz industrial, scientific and medical (ISM) radio band.

Even though several practical mismatches could impair the measurements, most of them have been studied in previous works [127], whilst for this campaign we wish to analyze the benefits of flexible duplexing isolatedly. For this reason, we rely on an Ettus OctoClock-G external reference, connected to all the nodes through measured cables, in order to guarantee time and frequency synchronization. More specifically, pulse-per-second (PPS) and 10 MHz reference signals are sent to the B210 to avoid frequency offsets and/or frame detection misalignments throughout the measurement procedures.

Additionally, the boards are connected to high-performance PC hosts, in such a way that we can configure the elements in the network, write the signals to be transmitted by the corresponding transmitters, and retrieve the signals at the receivers. For this purpose, we have relied on the GTIS Project libraries developed at University of A Coruña by the GTEC Group. This package provides an interface between MATLAB code and the UHD/GNU Radio libraries, so that the different devices in the experiment can be configured and controlled in a more convenient way. Also, the nodes connected to the PC hosts can be accessed either locally, or via secure shell (SSH), allowing to perform the measurements remotely in such a way that not even the researcher carrying out the procedure contaminates the scenario. Figure 7.4 shows the basic scheme for a  $2 \times 2$  transmitter/receiver pair, including transmitting and receiving USRP B210 boards, PC hosts, and the Octoclock device that guarantees time and frequency synchronization.

---

<sup>1</sup>Despite the maximum bandwidth being 56 MHz in single-antenna settings, in this work we focus on the MIMO case.

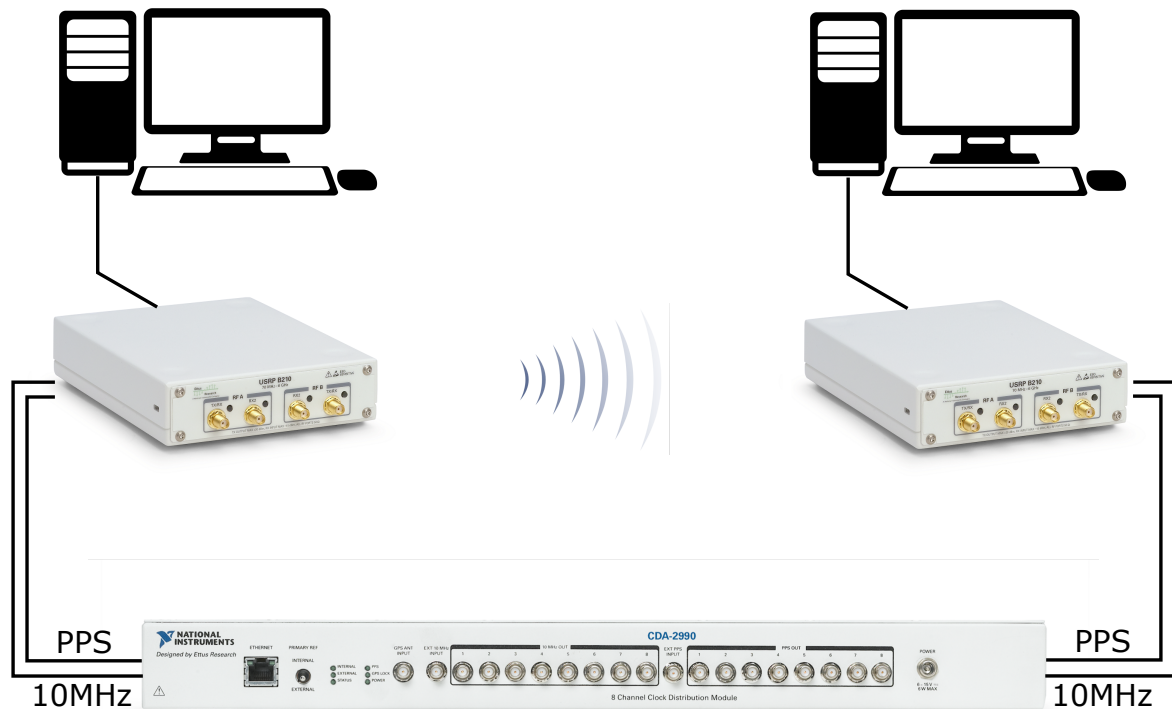
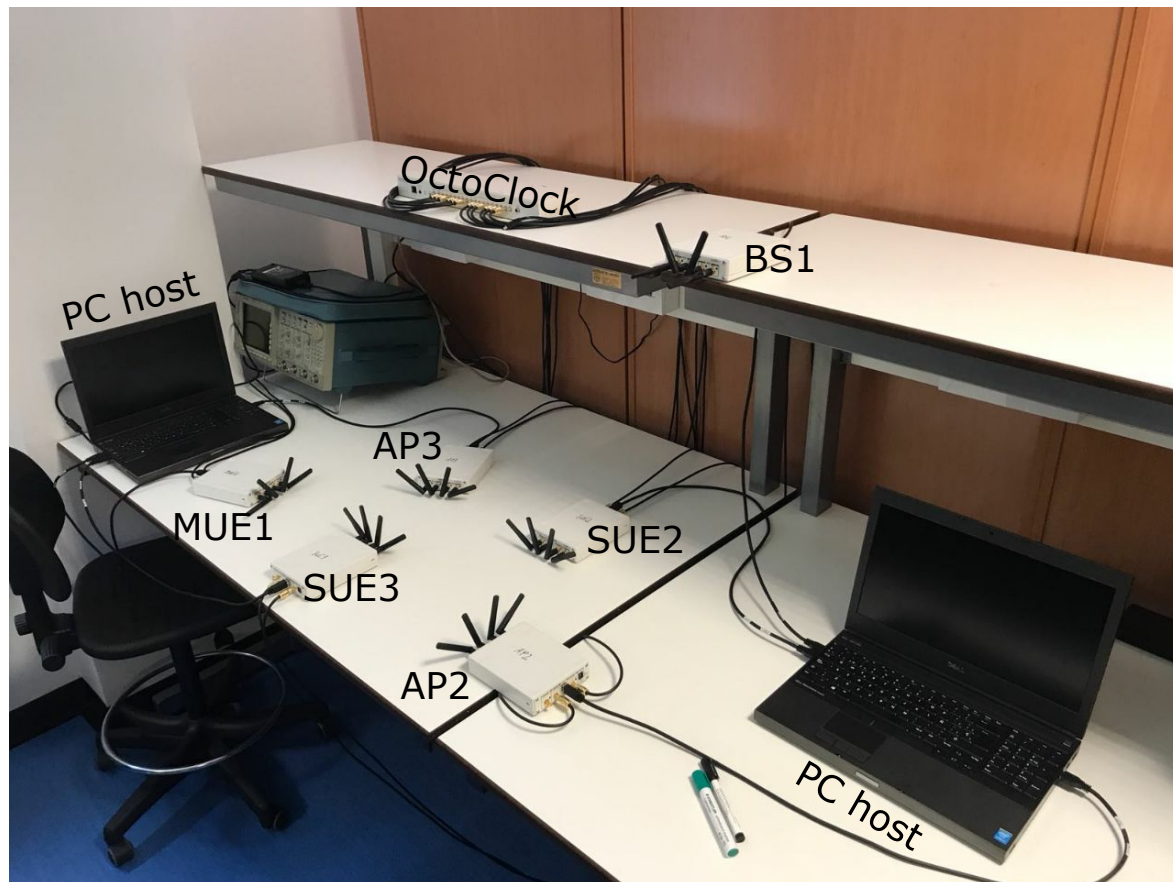


Figure 7.4: Hardware scheme for a  $2 \times 2$  point-to-point link.

### 7.2.2 Experimental setup

Figure 7.5 displays the 3-cell network in which the experiments have been conducted. As mentioned before, the setup is comprised of a macro base station (BS1) with its corresponding user equipment (MUE1), as well as two small access points (AP2 and AP3) with a user equipment each (SUE2 and SUE3). All these elements are connected to the same Octoclock-G device, which provides the required time and frequency external references. It is worth mentioning that the cables between the Octoclock and the B210 boards have been built in the same length in order to preserve the accuracy of the reference signals among different users. As presented in Fig. 7.5, the configuration is intended to emulate a network where the UEs and the small-cell APs coexist in a reduced space, being one of the UEs served by a macro BS. All the aforementioned unities are equipped with 2 antennas, with a self-inter-antenna distance of 66 millimeters given by the separation between the antenna ports in the USRP device.

Regarding the signals to be sent over the air, we have built on a variation of the IEEE 802.11a physical layer frame format. The OFDM frames have been transmitted at a center frequency of 2.487 GHz and 1 MHz bandwidth. Since the transmission strategies to be implemented should experiment similar realizations for the sake of a



**Figure 7.5:** Experimental 3-cell setup at the GTAS laboratory.

fair comparison, we have checked that the indoor channel in the laboratory remains invariant for a number of OFDM symbols (see Fig. 7.6).

As in the case of 802.11, each frame includes a total of 52 subcarriers (64-point FFT), 48 of which allocate data symbols. The frame headers comprise the conventional short-training symbols (ST) for frame detection purposes, as well as long-training symbols (LT) allowing to correct slight frequency offsets in settings with no frequency synchronization. The signal field (SF) has been included as standard, despite no rate adaptation being performed throughout the measurement campaign. Additionally, in order to estimate all the SISO channels between each antenna pair within the 3-cell network, we have modified the frame header by adding a structured sequence of long-training symbols and zero-padding. The format described above is depicted in Fig. 7.7. Finally, a total of 21 OFDM data symbols are transmitted within each frame, in order to compare three different transmission strategies, namely:

- Interference alignment.
- DET transmission + M-MMSE reception.
- M-MMSE receivers only.

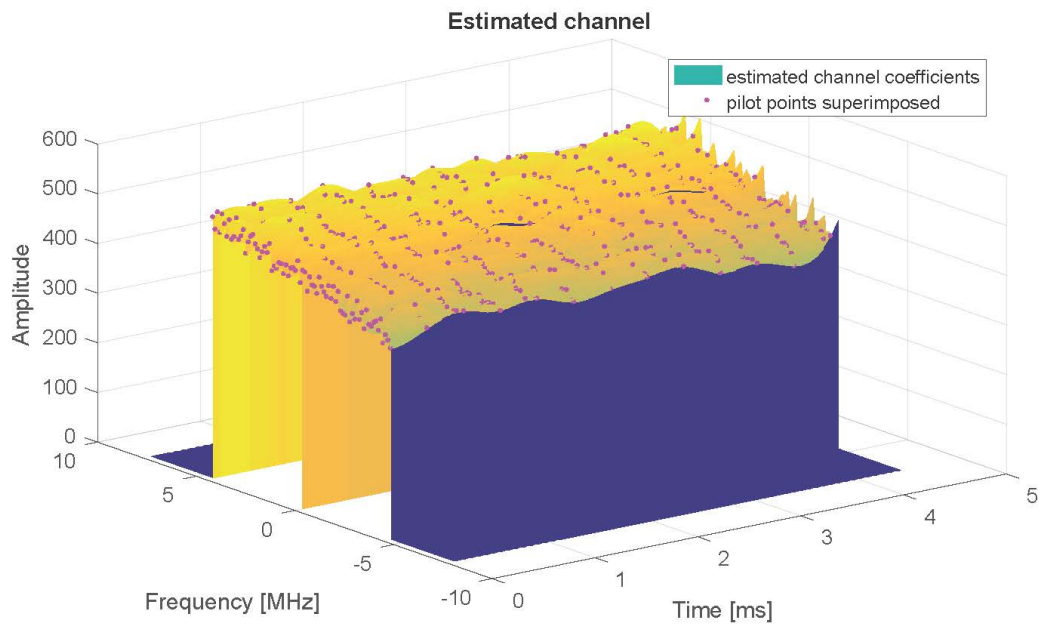


**Figure 7.6:** Indoor channel in the GTAS laboratory at a center frequency of 2.487 GHz.

Tx1	10	2	SF	$\frac{2}{\text{LT}}$	Ant 1	0	0	0	0	DATA
	ST	LT		0	0					
Tx2	10	2	SF	0	0	$\frac{2}{\text{LT}}$	Ant 1	0	0	DATA
	ST	LT		0	0	0	0			
Tx3	10	2	SF	0	0	0	0	$\frac{2}{\text{LT}}$	Ant 1	DATA
	ST	LT		0	0	0	0	0	0	

**Figure 7.7:** Frame structure for each user in the network.

For all three techniques, each data subcarrier includes QPSK symbols, making a total of 2016 bits per frame.

### 7.2.3 Measurement methodology

The relevance of the results rely on a well-designed measurement procedure. In this section, we describe the main steps that we have performed throughout the experiments. First, for a given UL/DL combination, the following steps are performed:

1. **Initial channel estimate:** For the first transmission, no channel knowledge is available. Therefore, an initialization frame with no relevant data symbols is transmitted in order to obtain the first channel estimate.
2. **Precoder/decoder design:** Once we have an estimate of the channel, we obtain the IA precoders and decoders, and the DET precoders. This calculation is performed in the frequency domain, i.e., in a per-subcarrier basis.
3. **Data transmission:** For each frame and user, 7 IA-precoded OFDM symbols are included, followed by 7 DET-precoded symbols and 7 symbols transmitted by both antennas with no additional precoding.
4. **Channel estimate and on-line symbol decoding:** Once the transmitted frames are detected at the receivers, the CSI is updated and the M-MMSE filters are calculated. The IA decoders are applied to the first 7 data symbols, and the remaining 14 are M-MMSE decoded. With the new channel estimate, IA precoders and decoders, as well as DET precoders, are calculated for the next transmission, or equivalently, the procedure continues back at step 2.

Unlike the first frame, which is sent without any previous channel knowledge, the precoders and decoders for transmission number  $n$  can be calculated with the channel estimate obtained from the previous frame  $n - 1$ . This way, there is no need for alternating training/data transmission stages for each iteration, improving the efficiency of the experimental procedure.

For each experiment, the EVM for the received symbols is calculated as

$$\text{EVM}_s = \frac{\sum_n |\hat{z}_{s,n} - z_{s,n}|^2}{\sum_n |z_{s,n}|^2} \quad (7.1)$$

where  $s$  is the subcarrier index,  $n$  is the OFDM data symbol index,  $z_{s,n}$  is the originally transmitted symbol and  $\hat{z}_{s,n}$  is the decoded symbol at the receiver. Finally, the median EVM for the symbols decoded with the three considered schemes is obtained. The reason for this is that, throughout the measurement campaign, a sparse amount of frames have been affected by external perturbations. Despite being a reduced number of cases, these outliers have a significant impact on the mean EVM. In order to discard the aforementioned outliers, and after checking that the PDF of the EVM is approximately symmetric around its mean (without considering the affected realizations), we can assume that the median is a sufficiently accurate approximation for the mean EVM.

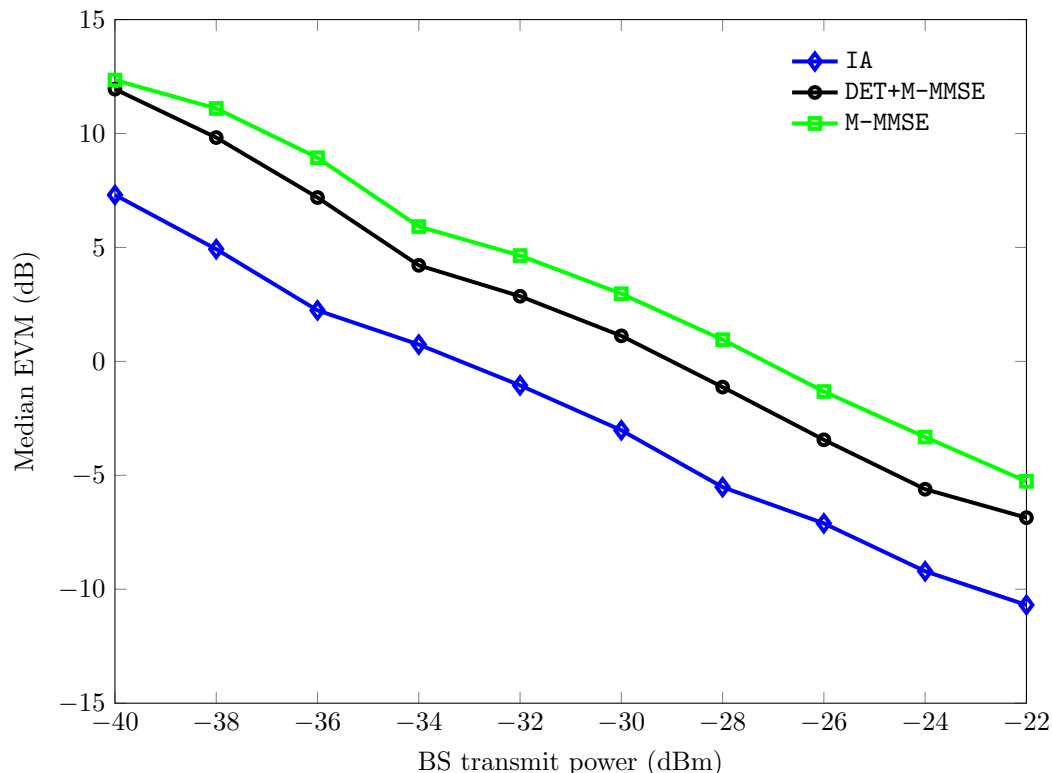


**Figure 7.8:** Median EVM at MUE 1 for the three schemes under test in [DL UL UL] mode.

## 7.2.4 Experimental results

In this campaign, we wish to study the performance of our setup for different UL/DL combinations within a range of interference regimes. For this purpose we have fixed the transmit power at the APs to  $-31$  dBm and the UEs to  $-34$  dBm in the small cells<sup>2</sup>. The steps described in Section 7.2.3 are repeated for several transmit power levels at the downlink macro BS and different UL/DL configurations in the small cells. In other words, we analyze the impact of inter-cell interference coming from the macrocell onto the different small cells, and how selecting the best UL/DL mitigates such impact. Specifically, 100 frames are transmitted by each node for each BS transmit power. Further, the EVM versus the BS transmit power is obtained in such a way that different UL/DL settings can be compared, including the conventional TDD approach.

The median EVM obtained by the three techniques under comparison is shown in Fig. 7.8 for the setting [DL UL UL]. In other words, the macrocell is in downlink whereas the small cells are in uplink. Lower transmit power levels at the BS translate into a lower desired signal quality at the receiver in the macrocell. Conse-

<sup>2</sup>Even though transmit power levels are allowed to be higher by wireless communication standards, recall that this indoor testbed is a small-scale representation of a realistic scenario.

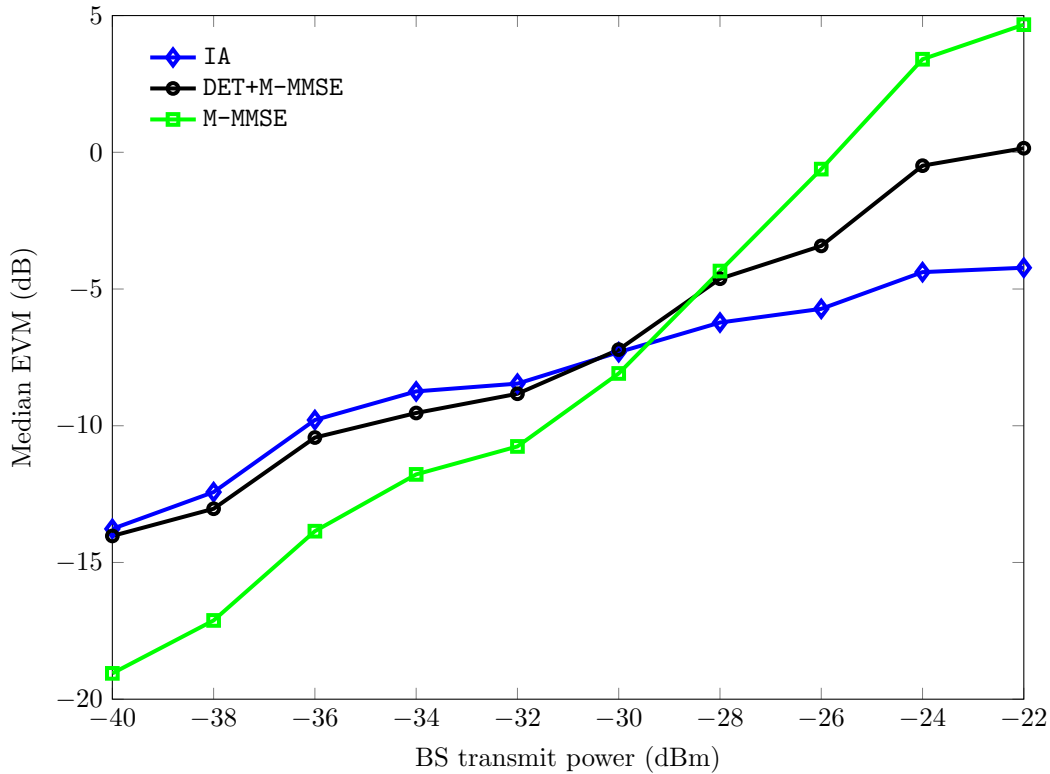


**Figure 7.9:** Median EVM at SUE 2 for the three schemes under test in [DL DL UL] mode.

quently, the lower SINR provokes higher EVM for all the communication strategies under evaluation. On the contrary, the SINR increases for higher power levels at the macrocell, hence improving the EVM results at MUE 1. As expected, IA provides the best performance out of the three techniques, whilst M-MMSE is slightly outperformed by DET+M-MMSE as well. Notice that IA precoders and decoders are specifically designed to suppress the interference at the unintended receivers. On the other hand, the M-MMSE techniques simply aim to minimize the error at the receiver, thus they take no advantage from any knowledge about the interfering signals.

Figures 7.9 and 7.10, respectively, show the results at SUE 2 and SUE 3 for different UL/DL combinations. In this case, the macrocell is in downlink mode, one of the small cells is in uplink, and the other small cell is in downlink, i.e., [DL DL UL] or [DL UL DL]. The main difference when focusing on the small cells is that, unlike the previous case, an increase in the transmitted power at the macro BS implies a higher inter-cell interference. Therefore, as the BS power increases, the SINR at the small cells decreases hence compromising the EVM. From Fig. 7.10, we can distinguish two different regimes, namely,

- **From  $-40$  to  $-35$  dBm BS transmit power** M-MMSE with no precoding is, surprisingly, the best out of the three communication schemes. The main reason for this is the quality of the channel estimates. Specifically, even though channel

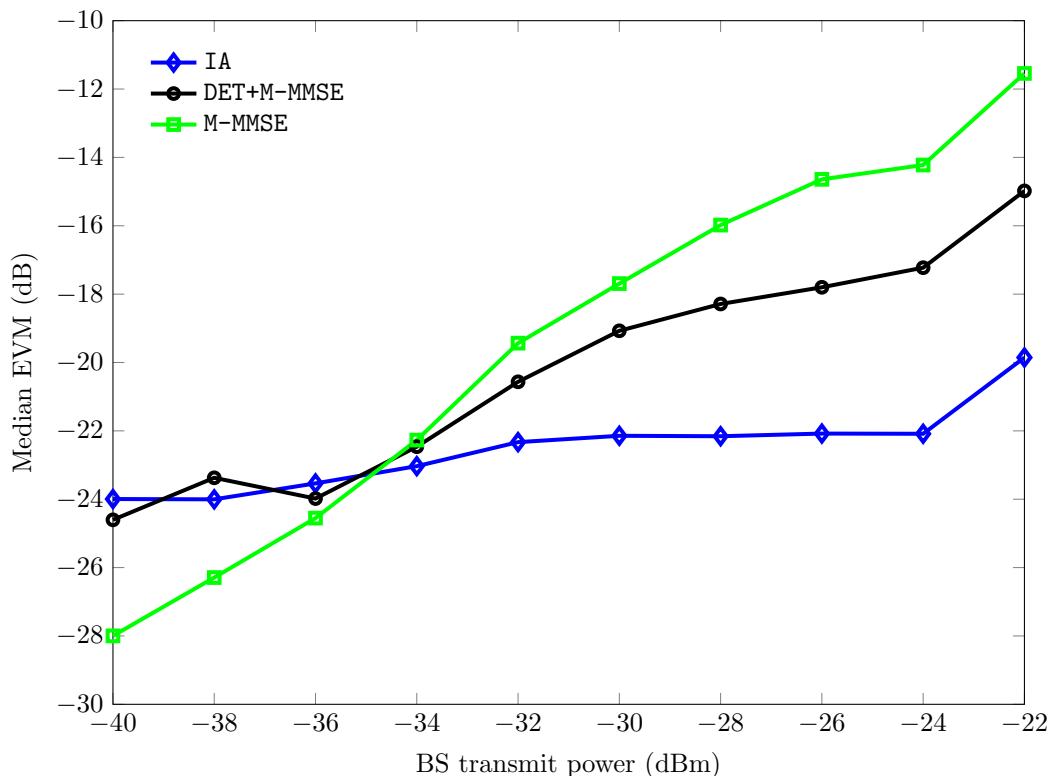


**Figure 7.10:** Median EVM at SUE 3 for the three schemes under test in [DL UL DL] mode.

estimation tasks are carried out in a TDMA fashion, thus free of interference, the SNR of training symbols is lower for low transmit power regimes at the BS. The impact of such impairment is less significant for M-MMSE, which requires CSI at the receivers only. On the contrary, each user applying DET+M-MMSE requires the channel estimates from its own transmitter to all receivers, both at the transmitter and receiver ends. Additionally, IA requires global CSI knowledge, hence being the most penalized technique.

- **From  $-35$  to  $-22$  dBm BS transmit power** the SNR for channel estimation increases, and therefore the quality of the estimates is improved. In this situation, the precoding-based techniques take full advantage of their channel knowledge and outperform M-MMSE. We can state that IA provides the best results in this regime, maintaining a remarkable performance even when the interfering signal strength is higher than the desired signal. Recall that transmit power for AP at the small cells is  $-31$  dBm, whereas the BS at the macrocell is capable of transmitting up to  $-22$  dBm.

Once we have studied the different precoding/decoding methods, we focus on the performance benefits that flexible duplexing provides when compared to conventional TDD configurations. For this purpose, Fig. 7.11 shows the EVM degradation

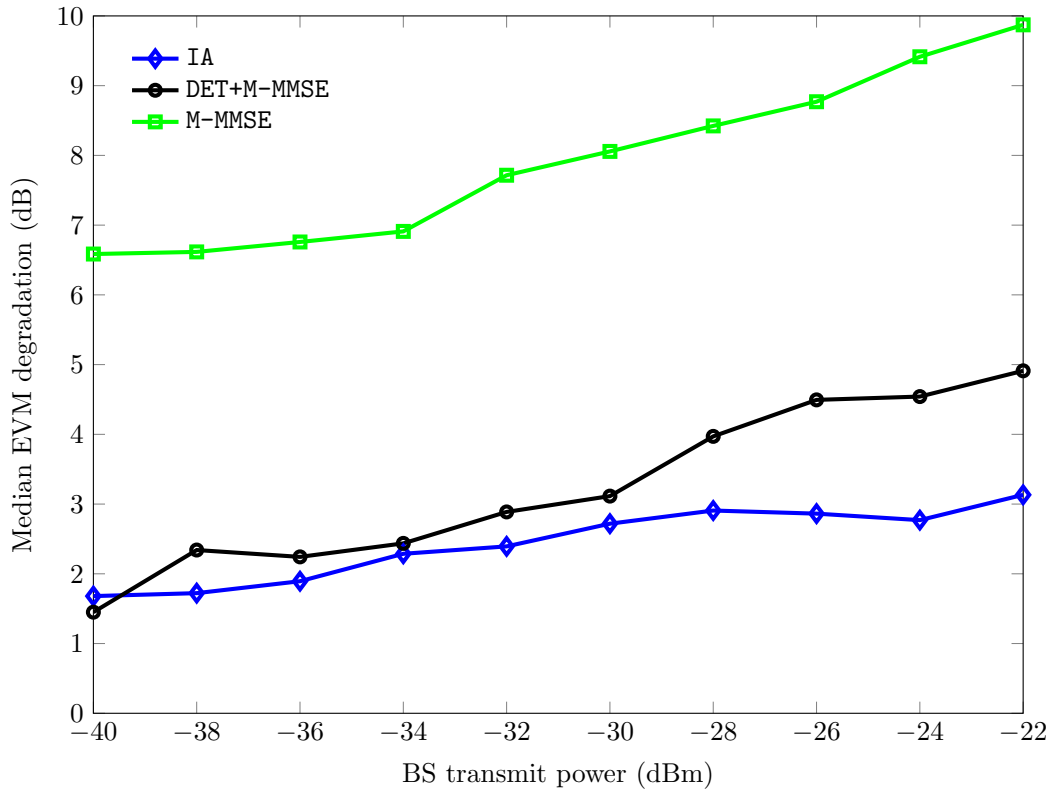


**Figure 7.11:** EVM degradation at SUE 3 for the three schemes under test in conventional TDD mode with respect to [DL UL DL] mode.

suffered at SUE 3 in conventional TDD mode with respect to the best UL/DL combination previously presented in Fig. 7.10. Flexible duplexing clearly outperforms conventional TDD regardless of the interference management technique applied at the transmitters and receivers. Nevertheless, different improvement levels can be quantified for the different strategies. Despite IA being the scheme with the best performance in the experiments, the M-MMSE-based methods are more benefited by selecting the UL/DL combination with the lowest interference level at the receivers.

The main intuition behind this result is that, IA being specifically designed to suppress the interference at the unintended receivers, a consistent performance is provided regardless of the UL/DL configuration in the network. For ideal scenarios, indeed, the flexible duplexing mode may cause no difference when implementing IA. However, the practical impairments given in real-world scenarios, such as channel estimation errors or different spatial distributions, provoke different interference leakage levels depending on the UL/DL setting. For this reason, improvements up to 3 dB have been achieved by selecting the appropriate configuration.

On the other hand, DET+M-MMSE and M-MMSE are not specifically intended to handle the interfering signals, thus residual interference is left even in ideal models. Practical misalignments emphasize such interference leakage and hence a selection of the best UL/DL mode is crucial, especially in the case of M-MMSE. Benefits up to 10 dB can

be attained for low-SINR regimes, as observed in Fig. 7.11. Recall that beamforming-based techniques, in this case IA and DET+M-MMSE, use the multiple antennas at the transmitter to concentrate the transmitted power in a specific spatial direction, thus having a reduced impact on other receivers. In some way, we could state that flexible duplexing has less room for improvement in such cases. However, M-MMSE takes full advantage of flexible duplexing since the different UL/DL combinations are the only factor making a difference in terms of interference at the receivers.



Part **V**

**Conclusion**



# Conclusions and further lines

Throughout this thesis, we have followed a long “roadtrip” which has taken us from the theoretical perspective of small cell heterogeneous networks towards the practical implementation of flexible duplexing. During this journey, we have analyzed the diverse aspects of next-generation mobile networks. The potential multiplexing gain that could be achieved has been investigated, and the throughput improvements have been characterized. Also, in a world where *green* technology is required to converge towards globally sustainable networks, we have put an exclamation point on power efficiency. In addition to the theoretical advances, we have addressed the challenge of implementing flexible duplexing with real-world devices.

## 8.1 Conclusions

In the foregoing lines, we briefly summarize the contributions and conclusions corresponding to each of the studies that have been performed in the thesis:

- In first place, we have addressed the analysis of HetNets together with flexible duplexing from a theoretical perspective. We have relied on a more general network model such as the  $X$  networks. We have developed an algorithm that allows to calculate interference alignment precoders and decoders in the context of arbitrary MIMO  $X$  networks, being the first algorithm capable of calculating IA solutions for such generic scenarios. The proposed algorithm is based on homotopy continuation, a numerical method for solving systems of nonlinear equations. After validating the performance of the homotopy continuation scheme, the algorithm has been applied to evaluate the DoF benefits of flexible duplexing in 2-cell HetNets where each cell handles multiple users. In order to extend such result, multi-cell networks have been considered, and necessary conditions have been established for the feasibility of IA. The simulation results obtained by the proposed algorithm clearly demonstrate that flexible duplexing outperforms the conventional TDD approach in terms of multiplexing gain.
- In order to advance a step closer towards the practical point of view, we have simplified our network model. Specifically, the network topology considers a

single active user per cell, likely to be found in small cell deployments. Furthermore, since multiple streams are usually distributed by means of OFDM, a single data stream is transmitted within each time/frequency resource block. In this context, we have characterized the rate benefits of flexible UL/DL scheduling, together with IA. Unlike most of the previous works in the literature, we have addressed the task of determining the best UL/DL combination maximizing the rate in the network. Since obtaining alignment solutions and evaluating the possible UL/DL settings are computationally expensive tasks, we propose two main approaches to reduce such computational cost. On the one hand, we reduce the complexity of calculating the rate achieved by IA. More explicitly, we propose a statistical characterization of the average rate attained by IA when a random solution is selected. This way, there is no need for calculating alignment solutions to determine the rate for a given UL/DL configuration. On top of this approximation, we propose a sub-optimal discrete search strategy that avoids exploring all the possible UL/DL sets. This approach, which relies on the hierarchy of the different cells in the network, is proven to reduce the number of evaluations significantly, with almost no performance loss with respect to the exhaustive search optimal solution.

- Analogously, we follow the same lines as in the case of the rate analysis, but considering power efficiency as well. We have addressed the task of minimizing the transmit power in the network while still satisfying a QoS requirement. Minimizing transmit power by optimizing beamformers, filters, and UL/DL settings at the same time is an extremely complicated challenge. In order to overcome this inconvenient, we have decoupled the problem into two tasks. On the one hand, we propose the MinPower-MaxSINR algorithm to minimize transmit power for a given UL/DL combination. Having a method for that purpose, we can rely on the same hierarchical tools as in the rate analysis to reduce the number of different UL/DL sets to be explored. The obtained results have shown that we have achieved two significant sources of benefit. Flexible duplexing outperforms conventional TDD in terms of power efficiency as well. In addition, the proposed MinPower-MaxSINR scheme is capable of remarkable improvements on top of those attained by means of flexible duplexing. Both strategies together hence yield to a promising future for flexible duplexing in the context of energy-efficient communications.
- Our last 1/4-mile in this journey has brought the study to the practical implementation. Flexible duplexing has been evaluated in a small-scale deployment with high-performance devices. These experiments have already served to test the applicability of interference alignment in realistic environments. For this reason, we have provided a brief review on the most remarkable advances regarding IA experiments. After settling the background, we have conducted our experimental study on two different levels:

- We have compared flexible duplexing and conventional TDD. The empirical results corroborate our theoretical conclusions, since noticeable improvement is achieved by means of flexible UL/DL combining.
- We have compared interference alignment to other well-known transmission techniques. Even though IA is considerably affected by practical impairments, such as channel estimation errors, it outperforms the other schemes under test.

It is especially worth mentioning that our experiment has represented the very first real-time implementation of IA with CSIT and on-line symbol decoding.

## 8.2 Further lines

Unfortunately, a thesis needs to be eventually closed. But new results always find their way through, and the impression is left that these research lines could be followed and studied *ad infinitum*. Therefore, we approach the end of the dissertation by establishing the most promising candidates to continue the research work in the future.

The first drawback that we have encountered, especially during Part IV, was that the theoretical models do not completely encompass the entire set of impairments and misalignments found in real-world scenarios. In this sense, more sophisticated topologies and models should be considered in future works to better understand such realistic environments. Following this consideration, it could be argued that some of the theoretical results might not translate into the same outcomes in practice immediately. The empirical work conducted in this thesis has not reached this detail depth, especially regarding the DoF evaluation corresponding to Part II. Some of the theoretical analysis are still to be complemented with additional support as well, both in terms of DoF and data rate.

Obviously, the whole set of schemes and techniques studied in this thesis are associated to network topologies and technology dictated by the current standards. However, the successive generations of wireless communications could bring different topologies, more advanced radio requirements, new information sources, or even a different mindset established by new user demands in the future. In this regard, context plays *the role*, and further works should be capable of adapting to the evolution of the global network.

More specifically, and taking into account the different lines presented in this thesis, we highlight the following lines to be further investigated:

- In terms of DoF, the study in Part III has established necessary conditions for the feasibility of IA in flexible duplexing multi-cell networks. However, an extension of the sufficient condition in [64] for generic HetNets is yet to be derived. Additionally, experimental evaluations specifically focused on multiplexing gain would complete the characterization in real-world scenarios.

- Regarding data rate, the study has provided a deeper perspective with respect to the network topology. Specifically, the asymmetry of the network has been found to condition the benefits of flexible duplexing significantly. As in the case of the DoF analysis, necessary conditions have been established, but a sufficient condition is still to be determined.

On other side, the network topology has been simplified, but more sophisticated network distributions could be the trend in the future, and therefore a complete extension of the results in Chapter 5 would be required. Specifically, multiple users per cell or multiple streams per user have not been considered in this work, but could be reconsidered for future communication standards.

- Power efficiency is arguably the most promising line to be taken into account for further advances. With the emphasis on sustainable technology and environmental-aware deployments, developing power minimization strategies is the key to keep improving the next generations of mobile networks. As in the case of the rate analysis, more sophisticated topologies may be considered in the works to come in order to give support to more advanced services. Additionally, experimental evaluations in terms of power efficiency are a need in this context.
- Finally, when addressing the experimental evaluation of flexible duplexing, several practical mismatches were avoided in order to analyze flexible duplexing isolatedly. For instance, time and frequency synchronization was externally guaranteed. However, real-world communications have to deal with frame detection difficulties and frequency offsets, and the system still needs to provide the required performance. A first advance to be made in the laboratory would be to conduct the same experiments, but with no external aids to synchronization.

In addition, the topology in the experiments has been relatively simplified. Notice that being too ambitious and evaluating a complicated topology in a first step would be unlikely to succeed. More complete networks beyond our 3-user evaluation need to be considered in further experiments in order to validate the theoretical results. In this sense, it is worth mentioning that cost is an important factor, so the right investments must be made to ensure that the experimental aspect follows the lead of theoretical advances.

Finally, future evaluations in practice should consider scenarios with user mobility and outdoor channels in order to provide a fair projection of real-world cellular networks and the ever-growing high-speed vehicular communications.

# **Appendices**



## Proofs of the results in Part II

### A.1 Proof of Theorem 3.1

Our argument is standard in Numerical Algebraic Geometry. We consider the *solution variety*

$$\mathcal{V} = \{(\mathbf{H}_{k\ell}, \mathbf{U}_k, \mathbf{V}_{j\ell}) : (3.20) \text{ holds}\} \subseteq \mathcal{I} \times \mathcal{O},$$

that is the set of possible pairs (*input, output*). We also consider the projection  $\pi_1 : \mathcal{V} \rightarrow \mathcal{I}$ . Note that for an input  $\mathbf{H} = (\mathbf{H}_{k\ell}) \in \mathcal{I}$ , the inverse image  $\pi_1^{-1}(\mathbf{H})$  of  $\mathbf{H}$  by  $\pi_1$  is just a copy of the set of possible solutions to (3.20). Of course, that set can be empty.

**Lemma A.1.** *Let  $(\mathbf{H}, \mathbf{U}_k, \mathbf{V}_{j\ell}) \in \mathcal{V}$ , and assume that  $(\mathbf{U}_k, \mathbf{V}_{j\ell})$  is a nonsingular solution of (3.20) (that is, the linear mapping (3.21) is invertible). Then, the derivative of  $\pi_1$  at  $(\mathbf{H}, \mathbf{U}_k, \mathbf{V}_{j\ell})$  is invertible.*

**Proof.** *First, since (3.21) is an invertible (thus, surjective) mapping, from the Regular Value Theorem, we have that  $\mathcal{V}$  is a smooth manifold in a neighborhood of  $(\mathbf{H}, \mathbf{U}_k, \mathbf{V}_{k\ell})$ , and the tangent space  $T$  to  $\mathcal{V}$  at  $(\mathbf{H}, \mathbf{U}_k, \mathbf{V}_{j\ell})$  is the set of vectors  $(\dot{\mathbf{H}}, \dot{\mathbf{U}}_k, \dot{\mathbf{V}}_{k\ell})$  such that*

$$(\mathbf{U}_k^T \dot{\mathbf{H}}_{k\ell}(t) \mathbf{V}_\ell + \dot{\mathbf{U}}_k^T \mathbf{H}_{k\ell}(t) \mathbf{V}_\ell + \mathbf{U}_k^T \mathbf{H}_{k\ell}(t) \dot{\mathbf{V}}_\ell)_{k,\ell} = 0. \quad (\text{A.1})$$

*The derivative of  $\pi_1$  sends  $(\dot{\mathbf{H}}, \dot{\mathbf{U}}_k, \dot{\mathbf{V}}_{k\ell})$  in  $T$  to  $\dot{\mathbf{H}}$ . Thus, it is surjective (i.e. invertible since the dimensions of  $\mathcal{V}$  and  $\mathcal{I}$  are equal by assumption) if and only if for any  $\dot{\mathbf{H}}$  one can find  $(\dot{\mathbf{U}}_k, \dot{\mathbf{V}}_{k\ell})$  satisfying (A.1). This is clear since the linear mapping (3.21) is surjective.*

Note that the solution variety is the zero set of the mapping

$$\mathbb{F} : \begin{array}{ccc} \mathcal{I} \times \mathcal{O} & \rightarrow & \mathbb{C}^b \\ (\mathbf{H}, (\mathbf{U}_k, \mathbf{V}_{j\ell}),) & \mapsto & (\mathbf{U}_k^T \mathbf{H}_{k\ell} \mathbf{V}_\ell - \mathbf{A}_{k\ell})_{k,\ell} \end{array}$$

We now use [98, Theorem 7.1.1], a somehow classical result in Numerical Algebraic Geometry which follows mainly from Chevalley's Theorem (see for example [137, p. 395]) applied to the projection  $\pi_1$  and from the Inverse Function Theorem. Instead of recalling [98, Theorem 7.1.1] in its full generality, we just write down its consequence for our problem.

**Theorem A.2.** *There exists a non-negative integer  $\mathcal{N} \in \mathbb{Z}$  such that for every  $\mathbf{H} \in \mathcal{I}$  out of some proper algebraic set  $\Sigma$ , the system  $\mathbb{F}(\mathbf{H}, (\mathbf{U}_k, \mathbf{V}_{j\ell})) = 0$  (with variables  $(\mathbf{U}_k, \mathbf{V}_{j\ell})$ ) has exactly  $\mathcal{N}$  nonsingular solutions. Moreover, if  $\bar{\mathbf{H}} \in \mathcal{I}$  and if*

$$\mathbf{H}(t) = (1 - t)\bar{\mathbf{H}} + t\mathbf{H} \notin \Sigma \quad \text{for } t \in (0, 1],$$

*then the homotopy  $\mathbb{F}(\mathbf{H}(t), (\mathbf{U}_k, \mathbf{V}_{j\ell}))$  has  $\mathcal{N}$  smooth, nonsingular solution paths, and the limit of these paths as  $t \rightarrow 0$  include all the nonsingular zeros of  $\mathbb{F}(\bar{\mathbf{H}}, (\mathbf{U}_k, \mathbf{V}_{j\ell}))$ .*

Note that in Theorem A.2 we may have  $\mathcal{N} = 0$ , which corresponds to the case that  $\pi_1^{-1}(\mathbf{H}) = \emptyset$  for (almost all)  $\mathbf{H} \in \mathcal{I}$ , that is the case that the alignment is unfeasible. We also recall [98, Lemma 7.1.2] (adapted to our notation):

**Lemma A.3.** *Fix  $\bar{\mathbf{H}} \in \mathcal{I}$ . Then, for almost all  $\mathbf{H} \in \mathcal{I}$ , the one-real-dimensional half-open line segment*

$$\mathbf{H}(t) = (1 - t)\bar{\mathbf{H}} + t\mathbf{H}, \quad t \in (0, 1],$$

*is contained in  $\mathcal{I} \setminus \Sigma$ .*

We are now ready to prove Theorem 3.1.

**Proof.** *In the notations of the theorem, from Lemma A.3 for almost all  $\mathbf{H} \in \mathcal{I}$  the segment  $\mathbf{H}(t)$  does not intersect  $\Sigma$  for  $t \in (0, 1]$  (although it might happen that  $\mathbf{H}(0) = \bar{\mathbf{H}} \in \Sigma$ ). From Theorem A.2 we then know that there is at least one smooth path  $(\mathbf{U}_k(t), \mathbf{V}_{k\ell}(t))$ ,  $t \in (0, 1]$ , of nonsingular solutions to  $\mathbf{H}(t)$ , such that the limit as  $t \rightarrow 0$  includes  $(\bar{\mathbf{U}}_k, \bar{\mathbf{V}}_{k\ell})$ . Now, by hypothesis this last is a nonsingular solution of (3.22), which in particular implies that it is an isolated solution and hence the limit as  $t \rightarrow 0$  of  $(\mathbf{U}_k(t), \mathbf{V}_{k\ell}(t))$  is exactly  $(\bar{\mathbf{U}}_k, \bar{\mathbf{V}}_{k\ell})$  (and does not contain more points), so it is a curve which is well-defined in the closed interval  $t \in [0, 1]$ . On the other hand, from Lemma A.1 and the Inverse Function Theorem there exists a local inverse (that we denote by  $\Theta$ ) of  $\pi_1$  close to  $\bar{\mathbf{H}}$  whose image is locally equal to  $\mathcal{V}$  in some neighborhood of  $(\bar{\mathbf{H}}, \bar{\mathbf{U}}_k, \bar{\mathbf{V}}_{k\ell})$ . In other words, for some  $\epsilon > 0$  the segment  $\mathbf{H}(t)$ ,  $t \in [0, \epsilon)$  can be lifted to  $\mathcal{V}$  in a unique way, given by  $\Theta(\mathbf{H}(t))$ , in such a way that the lift starts at  $(\bar{\mathbf{H}}, \bar{\mathbf{U}}_k, \bar{\mathbf{V}}_{k\ell})$ . Namely, no more than one of the smooth paths of nonsingular solutions to  $\mathbf{H}(t)$  can arrive at  $(\bar{\mathbf{H}}, \bar{\mathbf{U}}_k, \bar{\mathbf{V}}_{k\ell})$ .*

*We have proved that there exists a unique solution path  $(\mathbf{H}(t), \mathbf{U}_k(t), \mathbf{V}_{k\ell}(t))$  (which, at  $t = 1$ , defines a unique solution of (3.20)) that arrives at  $t = 0$  to the point  $(\bar{\mathbf{H}}, \bar{\mathbf{U}}_k, \bar{\mathbf{V}}_{k\ell})$ . One can thereby follow the homotopy backwards, and starting at the known solution at  $t = 0$  thus arrive to  $t = 1$  getting the solution to the target system  $\mathbf{H}$ .*

# Publications

## Publications derived from this dissertation

The work developed in this thesis has given place to the following publications.

### Journal articles

- [6] J. Fanjul, Ó. González, I. Santamaria and C. Beltrán, “Homotopy continuation for spatial interference alignment in arbitrary MIMO X networks,” *IEEE Transactions on Signal Processing*, vol. 65, no. 7, pp. 1752-1764, Apr. 2017.
- [12] C.M. Yetis, J. Fanjul, J.A. García-Naya, N.N. Moghadam and H. Farhadi, “Interference alignment testbeds,” *IEEE Communications Magazine (ComMag)*, vol. 55, no. 10, pp. 120-126, Oct. 2017.
- [13] J. Fanjul, R.D. Fernández, J. Ibáñez, J.A. García-Naya and I. Santamaria, “Experimental evaluation of flexible duplexing in small cell multi-tier MIMO networks,” submitted to *EURASIP Journal on Wireless Communications and Networking*.

### Conference contributions

- [7] Ó. González, J. Fanjul and I. Santamaria, “Homotopy Continuation for Vector Space Interference Alignment in MIMO X Networks,” in *Proceedings of the International Conference on Acoustics, Speech and Signal Processing (ICASSP)*, Florence, Italy, May. 2014, pp. 6232-6236.
- [8] J. Fanjul and I. Santamaria, “On the spatial degrees of freedom benefits of reverse TDD in multicell MIMO networks,” in *Proceedings of the European Signal Processing Conference (EUSIPCO)*, Budapest, Hungary, Aug. 2016, pp. 1363-1367.
- [9] I. Santamaria and J. Fanjul, “Statistical analysis of single-beam interference alignment schemes,” in *Proceedings of the International Workshop on Signal Processing Advances in Wireless Communications (SPAWC)*, Edinburgh, UK, Jul. 2016.

- [10] J. Fanjul and I. Santamaria, "Flexible duplexing for maximum downlink rate in multi-tier MIMO networks," in *Proceedings of the Telecommunications Forum (TELFOR)*, Belgrade, Serbia, Nov. 2018.
- [11] J. Fanjul and I. Santamaria, "Power minimization in multi-tier networks with flexible duplexing," in *Proceedings of the International Conference on Acoustics, Speech and Signal Processing (ICASSP)*, Brighton, UK, May. 2019.
- [14] J. Fanjul, C. Lameiro, I. Santamaria, J.A. García-Naya and L. Castedo, "An experimental evaluation of broadband spatial IA for uncoordinated MIMO-OFDM systems," in *Proceedings of the International Conference on Digital Signal Processing (DSP)*, Singapore, Jul. 2015, pp. 570-574.

## Related work by the author

The author has also produced the following publications, which are not directly related to the main contributions described in the thesis.

### Conference contributions

- [138] J. Fanjul, J. Ibáñez, I. Santamaria and C. Loucera, “Experimental evaluation of non-coherent MIMO Grassmannian signaling schemes,” in *Proceedings of the International Conference on Ad-Hoc Networks and Wireless*, Messina, Italy, Sep. 2017.
- [139] J. Fanjul, I. Santamaria and C. Loucera, “A quaternion-based approach to interference alignment with Alamouti coding,” in *Proceedings of the IEEE International Symposium on Signal Processing and Information Technology (ISSPIT)*, Bilbao, Spain, Dec. 2017.



# List of Figures

1.1	Relationship between flexible duplexing and the different concepts analyzed in this thesis. . . . .	8
2.1	Interference channel. Solid line arrows represent desired information, and dashed line arrows are associated to interference. . . . .	12
2.2	Relationship between SNR and DoF. . . . .	15
2.3	MinIL for the calculation of IA solutions. . . . .	17
2.4	2-tier heterogeneous network implementing flexible duplexing. . . . .	20
3.1	General MIMO X network model. Dash-dotted lines indicate that both desired signal and interference coexist in the corresponding link. . . . .	26
3.2	Interference channel. Solid line arrows represent desired information, and dashed line arrows are associated to interference. . . . .	29
3.3	Interference multiple-access channel. Solid line arrows represent desired information, and dashed line arrows are associated to interference. . . . .	30
3.4	Interference broadcast channel. Dashed line arrows are associated to interference, and dash-dotted lines indicate that both desired and interfering signals coexist in the same link. . . . .	31
3.5	Reverse TDD model. Solid line arrows represent desired information, and dashed line arrows are associated to interference. Dash-dotted lines indicate that both desired and interfering signals coexist in the same link. . . . .	32
3.6	Example of an homotopy continuation of the family (3.9) for $d = 5$ , $a = 32e^{j(\epsilon)}$ , and with $\epsilon = \{1, 10^{-1}, 10^{-2}, 10^{-3}\}$ . . . . .	35
3.7	Simple path tracking for the example in Fig. 3.6 with $\epsilon = 10^{-1}$ . . . . .	36
3.8	Average sum-rate achieved by MinIL and HC in the three considered scenarios. . . . .	46
3.9	CCDF of the sum-rate slope at SNR = $\{5, 10, 20, 55\}$ dB in Scenario 4. . . . .	47
3.10	CCDF of the sum-rate slope at SNR = $\{0, 5, 20, 35\}$ dB in Scenario 5. . . . .	48
4.1	Average sum-rate achieved by the HC method in three different network configurations. . . . .	58
4.2	Average sum-rate achieved by the IBC, IMAC and flexible duplexing configurations in Network 2. . . . .	59
4.3	Average sum-rate achieved by the IBC, IMAC and flexible duplexing configurations in Network 3. . . . .	60

5.1	Normalized locations of the nodes in the system (Network 4). . . . .	68
5.2	Average rate over 100 independent channel realizations, obtained by conventional TDD and the UL/DL that maximizes uplink rate. . . . .	69
5.3	Average rate over 100 independent channel realizations, obtained by conventional TDD and the UL/DL that maximizes downlink rate. . . . .	70
5.4	Comparison of the pairwise angle cdf between two different IA solutions for the $(2 \times 5, 1)^6$ MIMO IC. The system has a total of $P = 265$ IA solutions. . . . .	72
5.5	Average rate over 100 independent channel realizations, obtained by the HC-based algorithm and the proposed statistical approximation. . . . .	77
5.6	Downlink rate improvement (%) of flexible duplexing over conventional TDD. . . . .	79
5.7	Average downlink rate over 100 independent channel realizations, obtained by M-MMSE and IA. . . . .	81
6.1	Normalized location of the nodes in the system (Network 5). . . . .	90
6.2	Total power benefits, with respect to conventional TDD w/ fixed receivers, by MinPower-MaxSINR, flexible duplexing and the suboptimal HS scheme. . . . .	91
7.1	PDF for the EVM of pre-FFT and post-FFT IA decoding in asynchronous transmission [dB]. . . . .	97
7.2	. . . . .	100
7.3	Network topology under evaluation. . . . .	103
7.4	Hardware scheme for a $2 \times 2$ point-to-point link. . . . .	105
7.5	Experimental 3-cell setup at the GTAS laboratory. . . . .	106
7.6	Indoor channel in the GTAS laboratory at a center frequency of 2.487 GHz. . . . .	107
7.7	Frame structure for each user in the network. . . . .	107
7.8	Median EVM at MUE 1 for the three schemes under test in [DL UL UL] mode. . . . .	109
7.9	Median EVM at SUE 2 for the three schemes under test in [DL DL UL] mode. . . . .	110
7.10	Median EVM at SUE 3 for the three schemes under test in [DL UL DL] mode. . . . .	111
7.11	EVM degradation at SUE 3 for the three schemes under test in conventional TDD mode with respect to [DL UL DL] mode. . . . .	112

# List of Tables

3.1	Prob[DoF = $K^2d = 16$ ] or probability of achieving the requested number of degrees of freedom for $K = 4$ and $d = 1$ . . . . .	45
3.2	Average number of iterations and average time per iteration in Scenario 3. . . . .	49
7.1	Main hardware devices needed for every testbed and total estimated cost. . . . .	99



# List of Algorithms

1	Interference alignment via homotopy continuation in MIMO X networks.	42
2	Hierarcical switching for maximum downlink rate. . . . .	78
3	MinPower-MaxSINR for a fixed UL/DL combination. . . . .	88
4	Hierarcical switching for minimum transmit power. . . . .	89



# Bibliography

- [1] Ericsson, “Mobile data traffic surpasses voice,” Tech. Rep., 2010.
- [2] —, “Mobility report,” Tech. Rep., 2018.
- [3] Cisco, “Visual networking index: Forecast and trends, 2017-2022,” Tech. Rep., 2018.
- [4] S. Buzzi, C.-L. I, T. E. Klein, H. V. Poor, C. Yang, and A. Zappone, “A survey of energy-efficient techniques for 5G networks and challenges ahead,” *IEEE Journal on Selected Areas in Communications*, vol. 34, no. 4, pp. 697–709, Apr. 2016.
- [5] K. Demestichas, E. Adamopoulou, and M. Choras, “5G communications: Energy efficiency,” *Mobile Information Systems*, Apr. 2017.
- [6] J. Fanjul, O. González, I. Santamaria, and C. Beltrán, “Homotopy continuation for spatial interference alignment in arbitrary MIMO X networks,” *IEEE Transactions on Signal Processing*, vol. 65, no. 7, pp. 1752–1764, Apr. 2017.
- [7] Ó. González, J. Fanjul, and I. Santamaría, “Homotopy Continuation for Vector Space Interference Alignment in MIMO X Networks,” in *2014 IEEE International Conference on Acoustics, Speech and Signal Processing (ICASSP)*, May 2014, pp. 6232–6236.
- [8] J. Fanjul and I. Santamaria, “On the spatial degrees of freedom benefits of reverse TDD in multicell MIMO networks,” in *24th European Signal Processing Conference (EUSIPCO)*, Aug. 2016.
- [9] I. Santamaria and J. Fanjul, “Statistical analysis of single-beam interference alignment schemes,” in *2016 IEEE 17th International Workshop on Signal Processing Advances in Wireless Communications (SPAWC)*, Jul. 2016.
- [10] J. Fanjul and I. Santamaria, “Flexible duplexing for maximum downlink rate in multi-tier MIMO networks,” in *26th Telecommunications Forum (TELFOR)*, Nov. 2018.
- [11] —, “Power minimization in multi-tier networks with flexible duplexing,” in *submitted to IEEE International Conference on Acoustics, Speech and Signal Processing (ICASSP)*, May 2019.

- [12] C. M. Yetis, J. Fanjul, J. A. Garcia-Naya, N. N. Moghadam, and H. Farhadi, "Interference alignment testbeds," *IEEE Communications Magazine*, vol. 55, no. 10, pp. 120–126, Oct. 2017.
- [13] J. Fanjul, R. Fernández, J. Ibáñez, J. García-Naya, and I. Santamaria, "Experimental evaluation of flexible duplexing in small cell multi-tier MIMO networks," in *submitted to EURASIP Journal on Wireless Communications and Networking*, 2019.
- [14] J. Fanjul, C. Lameiro, I. Santamaria, J. A. García-Naya, and L. Castedo, "An experimental evaluation of broadband spatial IA for uncoordinated MIMO-OFDM systems," in *IEEE International Conference on Digital Signal Processing (DSP)*, Jul. 2015.
- [15] T. Han and K. Kobayashi, "A new achievable rate region for the interference channel," *IEEE Transactions on Information Theory*, vol. 27, no. 1, pp. 49–60, Jan. 1981.
- [16] A. Hindy and A. Nosratinia, "On the ergodic strong interference channel under lattice coding and decoding," in *IEEE Annual International Symposium on Personal, Indoor, and Mobile Radio Communications (PIMRC)*, Oct. 2017.
- [17] V. S. Annapureddy and V. V. Veeravalli, "Gaussian interference networks: Sum capacity in the low-interference regime and new outer bounds on the capacity region," *IEEE Transactions on Information Theory*, vol. 55, no. 7, pp. 3032–3050, Jul. 2009.
- [18] A. S. Motahari and A. K. Khandani, "Capacity bounds for the Gaussian interference channel," *IEEE Transactions on Information Theory*, vol. 55, no. 2, pp. 620–643, Feb. 2009.
- [19] X. Shang, G. Kramer, and B. Chen, "New outer bound and the noisy-interference sum-rate capacity for Gaussian interference channels," *IEEE Transactions on Information Theory*, vol. 55, no. 2, pp. 689–699, Feb. 2009.
- [20] C. Geng, N. Naderializadeh, A. S. Avestimehr, and S. A. Jafar, "On the optimality of treating interference as noise," *IEEE Transactions on Information Theory*, vol. 61, no. 4, pp. 1753–1767, Apr. 2015.
- [21] A. Carleial, "A case where interference does not reduce capacity (corresp.)," *IEEE Transactions on Information Theory*, vol. 21, no. 5, pp. 569–570, Sep. 1975.
- [22] H. Sato, "The capacity of the Gaussian interference channel under strong interference," *IEEE Transactions on Information Theory*, vol. 27, no. 6, pp. 786–788, Nov. 1981.

- [23] S. Sridharan, A. Jafarian, S. Vishwanath, and S. A. Jafar, "Capacity of symmetric K-user Gaussian very strong interference channels," in *IEEE Global Communications Conference (GLOBECOM)*, Dec. 2008.
- [24] R. H. Etkin, D. N. C. Tse, and H. Wang, "Gaussian interference channel capacity to within one bit," *IEEE Transactions on Information Theory*, vol. 54, no. 12, pp. 5534–5562, Dec. 2008.
- [25] Y. Léost, M. Abdi, R. Richter, and M. Jeschke, "Interference rejection combining in LTE networks," *Bell Labs Technical Journal*, vol. 17, no. 1, pp. 25–49, Jun. 2012.
- [26] X. Li, E. Björnson, E. G. Larsson, S. Zhou, and J. Wang, "A multi-cell MMSE detector for massive MIMO systems and new large system analysis," in *IEEE Global Communications Conference (GLOBECOM)*, Dec. 2015.
- [27] —, "Massive MIMO with multi-cell MMSE processing: exploiting all pilots for interference suppression," *EURASIP Journal on Wireless Communications and Networking*, pp. 1–15, Jun. 2017.
- [28] C. E. Shannon, "A mathematical theory of communication," *The Bell System Technical Journal*, vol. 27, pp. 379–423, 623–656, 1948.
- [29] —, "Communication in the presence of noise," *Proceedings of IRE*, vol. 37, pp. 10–21, 1949.
- [30] K. Gomadam, V. R. Cadambe, and S. A. Jafar, "Approaching the capacity of wireless networks through distributed interference alignment," in *Proceedings of IEEE Global Telecommunications Conference*, 2008.
- [31] D. Schmidt, W. Utschick, and M. Honig, "Large system performance of interference alignment in single-beam MIMO networks," in *IEEE Global Telecommunications Conference (GLOBECOM)*, 2010.
- [32] C. Geng, H. Sun, and S. A. Jafar, "On the optimality of treating interference as noise: General message sets," *IEEE Transactions on Information Theory*, vol. 61, no. 7, pp. 3722–3736, Jul. 2015.
- [33] H. Sun and S. A. Jafar, "On the optimality of treating interference as noise for K-user parallel Gaussian interference networks," *IEEE Transactions on Information Theory*, vol. 62, no. 4, pp. 1911–1930, Apr. 2016.
- [34] C. Geng and S. A. Jafar, "On the optimality of treating interference as noise: Compound interference networks," *IEEE Transactions on Information Theory*, vol. 62, no. 8, pp. 4630–4653, Aug. 2016.
- [35] —, "Power control by GDoF duality of treating interference as noise," *IEEE Communications Letters*, vol. 22, no. 2, pp. 244–247, Feb. 2018.

- [36] A. G. Davoodi and S. A. Jafar, "Aligned image sets under channel uncertainty: Settling conjectures on the collapse of degrees of freedom under finite precision CSIT," *IEEE Transactions on Information Theory*, vol. 62, no. 10, pp. 5603–5618, Oct. 2016.
- [37] —, "Transmitter cooperation under finite precision CSIT: A GDoF perspective," *IEEE Transactions on Information Theory*, vol. 63, no. 9, pp. 6020–6030, Sep. 2017.
- [38] —, "Generalized degrees of freedom of the symmetric K user interference channel under finite precision CSIT," *IEEE Transactions on Information Theory*, vol. 63, no. 10, pp. 6561–6572, Oct. 2017.
- [39] V. R. Cadambe and S. A. Jafar, "Interference alignment and degrees of freedom of the K-user interference channel," *IEEE Transactions on Information Theory*, vol. 54, no. 8, pp. 3425–3441, 2008.
- [40] M. Maddah-Ali, A. Motahari, and A. Khandani, "Signaling over MIMO Multi-Base Systems: Combination of Multi-Access and Broadcast Schemes," in *Proceedings of IEEE International Symposium on Information Theory*, 2006.
- [41] M. A. Maddah-ali, A. S. Motahari, and A. K. Khandani, "Communication over X Channel: Signalling and multiplexing gain," Tech. Rep., 2006.
- [42] S. A. Jafar and M. Fakhereddin, "Degrees of freedom for the MIMO interference channel," *IEEE Transactions on Information Theory*, vol. 53, no. 7, pp. 2637–2642, 2007.
- [43] S. A. Jafar, "Degrees of Freedom on the MIMO X Channel - Optimality of the MMK Scheme," Tech. Rep., 2006.
- [44] M. A. Maddah-ali, A. S. Motahari, and A. K. Khandani, "Communication over X Channel: Signalling and performance analysis," Tech. Rep., 2006.
- [45] H. Weingarten, Y. Steinberg, and S. Shamai, "The capacity region of the Gaussian multiple-input multiple-output broadcast channel," *IEEE Transactions on Information Theory*, vol. 52, no. 9, pp. 3936–3964, 2006.
- [46] S. A. Jafar and S. Shamai (Shitz), "Degrees of Freedom Region of the MIMO X Channel," *IEEE Transactions on Information Theory*, vol. 54, no. 1, pp. 151–170, Jan. 2008.
- [47] S. Peters and R. Heath, "Interference alignment via alternating minimization," in *2009 IEEE International Conference on Acoustics, Speech and Signal Processing (ICASSP)*, Taipei, Taiwan, Apr. 2009, pp. 2445–2448.
- [48] K. S. Gomadam, V. R. Cadambe, and S. A. Jafar, "A distributed numerical approach to Interference Alignment and applications to wireless interference networks," *IEEE Transactions on Information Theory*, vol. 57, no. 6, pp. 3309–3322, Jun. 2011.

- [49] D. Papailiopoulos and A. Dimakis, "Interference Alignment as a Rank Constrained Rank Minimization," *IEEE Transactions on Signal Processing*, vol. 60, no. 8, pp. 4278–4288, Aug. 2012.
- [50] D. Schmidt, C. Shi, R. Berry, M. Honig, and W. Utschick, "Comparison of distributed beamforming algorithms for MIMO interference networks," *IEEE Transactions on Signal Processing*, vol. 61, no. 13, pp. 3476–3489, Jul. 2013.
- [51] I. Santamaria, Ó. González, R. W. Heath, and S. W. Peters, "Maximum sum-rate interference alignment algorithms for MIMO channels," in *Proc. IEEE Global Telecomm. Conference (GLOBECOM 2010)*, Miami, FL, USA, Dec. 2010, pp. 1–6.
- [52] H. Yu and Y. Sung, "Least squares approach to joint beam design for interference alignment in multiuser multi-input multi-output interference channels," *IEEE Trans. Sig. Process.*, vol. 58, no. 9, pp. 4960–4966, Sep. 2010.
- [53] S. Bazzi, G. Dietl, and W. Utschick, "Interference alignment via minimizing projector distances of interfering subspaces," in *IEEE 13th Workshop on Signal Processing Advances in Wireless Communications (SPAWC 2012)*, Cesme, Turkey, Jun. 2012, pp. 274–278.
- [54] —, "Interference alignment with imperfect channel state information at the transmitter," in *2012 International Symposium on Wireless Communication Systems (ISWCS)*, Paris, France, Aug. 2012, pp. 561–565.
- [55] G. C. Alexandropoulos and C. B. Papadias, "A reconfigurable iterative algorithm for the K-user MIMO interference channel," *Signal Processing*, vol. 93, no. 12, pp. 3353–3362, Dec. 2013.
- [56] Ó. González, C. Lameiro, and I. Santamaría, "A Quadratically Convergent Method for Interference Alignment in MIMO Interference Channels," *IEEE Signal Processing Letters*, vol. 21, pp. 1423–1427, Nov. 2014.
- [57] X. Chu, D. L. Perez, Y. Yang, and F. Gunnarsson, *Heterogeneous Cellular Networks*. Cambridge, 2013.
- [58] R. Jain, S. Katiyar, and N. Agrawal, "Hierarchical cellular structures in high-capacity cellular communication systems," *International Journal of Advanced Computer Science and Applications (IJACSA)*, vol. 2, no. 9, pp. 51–57, Oct. 2011.
- [59] M. Elkashian, T. Q. Duong, and H.-H. Chen, "Millimeter-wave communications for 5G: fundamentals: Part I [Guest Editorial]," *IEEE Communications Magazine*, vol. 52, no. 9, pp. 52–54, Sep. 2014.
- [60] —, "Millimeter-wave communications for 5G: fundamentals: Part II [Guest Editorial]," *IEEE Communications Magazine*, vol. 53, no. 1, pp. 166–167, Jan. 2015.

- [61] J. Hoydis, K. Hosseini, S. t. Brink, and M. Debbah, "Making smart use of excess antennas: Massive MIMO, Small Cells, and TDD," *Bell Labs Technical Journal*, vol. 18, no. 2, pp. 5–21, 2013.
- [62] L. Sanguinetti, A. L. Moustakas, and M. Debbah, "Interference management in 5G reverse TDD HetNets with wireless backhaul: A large system analysis," *IEEE Journal on Selected Areas in Communications*, vol. 33, no. 6, pp. 1187–1200, Mar. 2015.
- [63] J. Kerttula, A. Marttinen, K. Ruttik, R. Jäntti, and M. N. Alam, "Dynamic TDD in LTE small cells," *EURASIP Journal on Wireless Communications and Networking*, vol. 2016, no. 1, Aug. 2016.
- [64] S.-W. Jeon, K. Kim, J. Yang, and D. K. Kim, "The feasibility of interference alignment for MIMO interfering broadcast-multiple-access channels," *IEEE Transactions on Wireless Communications*, vol. 16, no. 7, pp. 4614–4625, Jul. 2017.
- [65] M. Kountouris and N. Pappas, "HetNets and massive MIMO: Modeling, potential gains, and performance analysis," in *2013 IEEE-APS Topical Conference on Antennas and Propagation in Wireless Communications (APWC)*, Sep. 2013.
- [66] S. Lagen, A. Agustin, and J. Vidal, "Joint user scheduling, precoder design, and transmit direction selection in MIMO TDD small cell networks," *IEEE Transactions on Wireless Communications*, vol. 16, no. 4, pp. 2434–2449, Mar. 2017.
- [67] D. D. Yu and J. M. Cioffi, "Iterative water-filling for optimal resource allocation in OFDM multiple-access and broadcast channels," in *IEEE Global Telecommunications Conference (GLOBECOM)*, Nov. 2006.
- [68] W. W. L. Ho and Y.-C. Liang, "Efficient power minimization for MIMO broadcast channels with BD-GMD," in *IEEE International Conference on Communications*, Jun. 2007.
- [69] C. Hellings, M. Joham, and W. Utschick, "Power minimization in parallel vector broadcast channels with Zero-Forcing beamforming," in *IEEE Global Telecommunications Conference (GLOBECOM)*, Dec. 2010.
- [70] F. Héliot, M. A. Imran, and R. Tafazolli, "Energy-efficiency based resource allocation for the scalar broadcast channel," in *IEEE Wireless Communications and Networking Conference (WCNC)*, Apr. 2012.
- [71] J. P. González-Coma, M. Joham, P. M. Castro, and L. Castedo, "QoS constrained power minimization in the multiple stream MIMO broadcast channel," *Signal Processing*, vol. 143, pp. 48–55, Feb. 2018.
- [72] O. Taghizadeh and R. Mathar, "Interference mitigation via power optimization schemes for Full-Duplex networking," in *19th International ITG Workshop on Smart Antennas (WSA)*, Mar. 2015.

- [73] S. Lembo, O. Tirkkonen, M. Goldhamer, and A. Kliks, "Coexistence of FDD flexible duplexing networks," in *2017 European Conference on Networks and Communications (EuCNC)*, Jun. 2017.
- [74] I. Randrianantenaina, H. Dahrouj, H. Elsayy, and M.-S. Alouini, "Interference management in Full-Duplex cellular networks with partial spectrum overlap," *IEEE Access*, vol. 5, pp. 7567–7583, Mar. 2017.
- [75] A. Agustín and J. Vidal, "Degrees of Freedom Region of the MIMO X Channel with an arbitrary number of antennas," Oct. 2012. [Online]. Available: <http://arxiv.org/abs/1210.2582>
- [76] V. R. Cadambe and S. A. Jafar, "Interference Alignment and the Degrees of Freedom of wireless X networks," *IEEE Transactions on Information Theory*, vol. 55, no. 9, pp. 3893–3908, Sep. 2009.
- [77] H. Sun, C. Geng, T. Gou, and S. A. Jafar, "Degrees of Freedom of MIMO X Networks: spatial scale invariance, one-sided decomposability and linear feasibility," in *2012 IEEE International Symposium on Information Theory Proceedings*, Boston, MA, Jul. 2012, pp. 2082–2086.
- [78] L. Ke, A. Ramamoorthy, Z. Wang, and H. Yin, "Degrees of Freedom Region for an Interference Network with general message demands," *IEEE Transactions on Information Theory*, vol. 58, no. 6, pp. 3787–3797, Jun. 2012.
- [79] C. M. Yetis, T. Gou, S. A. Jafar, and A. H. Kayran, "On feasibility of Interference Alignment in MIMO Interference Networks," *IEEE Transactions on Signal Processing*, vol. 58, no. 9, pp. 4771–4782, Sep. 2010.
- [80] A. Agustín and J. Vidal, "Improved Interference Alignment precoding for the MIMO X Channel," in *IEEE International Conference On Communications (ICC) 2011*, Kyoto, Japan, 2011.
- [81] T. Gou and S. A. Jafar, "Degrees of freedom of the K user MxN MIMO interference channel," *IEEE Transactions on Information Theory*, vol. 56, no. 12, pp. 6040–6057, Dec. 2010.
- [82] P. Mohapatra, K. Nissar, and C. Murthy, "Interference alignment algorithms for the K user constant MIMO interference channel," *IEEE Transactions on Signal Processing*, vol. 59, no. 11, pp. 5499–5508, Aug. 2011.
- [83] C. Lameiro, Ó. González, and I. Santamaría, "An Interference Alignment Algorithm for Structured Channels," in *IEEE 14th Workshop on Signal Processing Advances in Wireless Communications (SPAWC 2013)*, Darmstadt, Germany, Jun. 2013.
- [84] H. Sun, C. Geng, T. Gou, and S. A. Jafar, "Degrees of Freedom of MIMO X Networks: Spatial Scale Invariance, One-Sided Decomposability and Linear Feasibility," 2012. [Online]. Available: <http://arxiv.org/abs/1207.6137>

- [85] O. González, C. Beltrán, and I. Santamaría, “A feasibility test for linear interference alignment in MIMO channel with constant coefficients,” *IEEE Transactions on Information Theory*, vol. 60, no. 3, pp. 1840–1856, Mar. 2014.
- [86] G. Sridharan and W. Yu, “Degrees of freedom of MIMO cellular networks: Decomposition and linear beamforming design,” *IEEE Trans. Inf. Theory*, vol. 61, no. 6, pp. 3339–3364, Jun. 2015.
- [87] C. Suh, M. Ho, and T. D. N. C., “Downlink interference alignment,” *IEEE Trans. Comm.*, vol. 59, no. 9, pp. 2616–2626, Sep. 2011.
- [88] R. Tresch and M. Guillaud, “Cellular interference alignment with imperfect channel knowledge,” in *Proc. IEEE Int. Conf. Comm. (ICC 2009)*, Dresden, Germany, Jun. 2009.
- [89] P. Aquilina and T. Ratnarajah, “Performance analysis of IA techniques in the MIMO IBC with imperfect CSI,” *IEEE Transactions on Communications*, vol. 63, no. 4, pp. 1259–1270, Apr. 2015.
- [90] T. Gou, C. Wang, and S. A. Jafar, “Aiming perfectly in the dark-blind interference alignment through staggered antenna switching,” *IEEE Transactions on Signal Processing*, vol. 59, no. 6, pp. 2734–2744, Jun. 2011.
- [91] S. A. Jafar, “Blind interference alignment,” *IEEE Journal of Selected Topics in Signal Processing*, vol. 6, no. 3, pp. 216–227, Jun. 2012.
- [92] M. Morales-Céspedes, J. Plata-Chaves, D. Toumpakaris, S. A. Jafar, and A. G. Armada, “Blind interference alignment for cellular networks,” *IEEE Transactions on Signal Processing*, vol. 63, no. 1, pp. 41–56, Jan. 2015.
- [93] G. Liu, M. Sheng, X. Wang, W. Jiao, Y. Li, and J. Li, “Interference alignment for partially connected downlink MIMO heterogeneous networks,” *IEEE Transactions on Communications*, vol. 63, no. 2, pp. 551–564, Feb. 2015.
- [94] M. Morales-Céspedes, J. Plata-Chaves, D. Toumpakaris, S. A. Jafar, and A. G. Armada, “Cognitive blind interference alignment for macro-femto networks,” *IEEE Transactions on Signal Processing*, vol. 65, no. 19, pp. 5121–5136, Oct. 2017.
- [95] M. Morales-Céspedes, L. Vandendorpe, and A. G. Armada, “Degrees of freedom of 2-tier networks without channel state information at the transmitter,” *IEEE Transactions on Signal Processing*, 2019.
- [96] C. Garcia and W. Zangwill, *Pathways to solutions, fixed points, and equilibria*. Prentice-Hall, 1981.
- [97] T. Y. Li, “Numerical solution of multivariate polynomial systems by homotopy continuation methods,” *Acta Numerica*, vol. 6, pp. 399–436, 1 1997.

- [98] A. J. Sommese and C. W. Wampler II, *The Numerical Solution of Systems of Polynomials Arising in Engineering and Science*. Singapore, Rep. of Singapore: World Scientific Publishing Co. Pte. Ltd., 2005.
- [99] E. L. Allgower and K. Georg, "Numerical path following," in *Handbook of Numerical Analysis*, P. G. Ciarlet and J. L. Lions, Eds. Amsterdam: Elsevier Inc., 1997, vol. 5, no. August, pp. 3–207.
- [100] D. Davidenko, "Ob Odnom Novom Metode Chislenno Resheniya Sistem Nelineynykh Uravenii," *Dokl. Akad. Nauk SSR*, vol. 87, no. 4, pp. 601–602, 1953.
- [101] R. E. Kalaba, E. Zagustin, W. Holbrow, and R. Huss, "A modification of Davidenko's method for nonlinear systems," *Computers & Mathematics with Applications*, vol. 3, no. 4, pp. 315–319, Mar. 1977.
- [102] Ó. González, C. Beltrán, and I. Santamaría, "On the number of interference alignment solutions for the K-user MIMO channel with constant coefficients," *IEEE Transactions on Information Theory*, vol. 61, no. 11, pp. 6028–6048, Nov. 2015.
- [103] P. Kerret and D. Gesbert, "Interference alignment with incomplete CSIT sharing," *IEEE Trans. Wireless Comm.*, vol. 13, no. 5, pp. 2563–2573, May 2014.
- [104] C. Wilson and V. Veeravalli, "A convergent version of the Max SINR algorithm for the MIMO interference channel," *IEEE Trans. Wireless Comm.*, vol. 12, no. 6, pp. 2952–2961, Jun. 2013.
- [105] S.-W. Jeon and C. Suh, "Degrees of Freedom of Uplink-Downlink Multiantenna Cellular Networks," 2014. [Online]. Available: <http://arxiv.org/abs/1404.6012>
- [106] B. Zhuang, R. Berry, and M. Honig, "Interference alignment in MIMO cellular networks," in *2011 IEEE International Conference on Acoustics, Speech and Signal Processing (ICASSP)*, Prague, Czech Republic, May 2011, pp. 3356–3359.
- [107] M. Razaviyayn, G. Lyubeznik, and Z.-Q. Luo, "On the degrees of freedom achievable through interference alignment in a MIMO interference channel," *IEEE Transactions on Signal Processing*, vol. 60, no. 2, pp. 812–821, February 2012.
- [108] L. Ruan, V. K. N. Lau, and M. Z. Win, "The feasibility conditions for interference alignment in MIMO networks," *IEEE Transactions on Signal Processing*, vol. 61, no. 8, pp. 2066–2077, Apr. 2013.
- [109] Ó. González, I. Santamaría, and C. Beltrán, "Finding the Number of Feasible Solutions for Linear Interference Alignment Problems," in *2013 IEEE International Symposium on Information Theory*, Istanbul, Turkey, July 2013, pp. 384–388.

- [110] S. Bazzi, G. Dietl, and W. Utschick, "Large system analysis of interference alignment achievable rates for the MIMO interference channel," *IEEE Transactions on Signal Processing*, vol. 63, no. 6, pp. 1490–1499, Mar. 2015.
- [111] T. Cai, J. Fan, and T. Jiang, "Distributions of angles in random packing on spheres," *Journal of Machine Learning Research*, vol. 14, no. 1, pp. 1837–1864, Jan. 2013.
- [112] K. Mardia, J. Kent, and J. Bibby, *Multivariate Analysis*. Academic Press, 1979.
- [113] Y. Chikuse, *Statistics on Special Manifolds*. Lecture Notes on Statistics, Springer-Verlag, 2003.
- [114] M. Eaton, "On the projection of isotropic distributions," *The Annals of Statistics*, vol. 9, no. 2, pp. 391–400, 1981.
- [115] S. D. Howard, S. Sirianunpiboon, and D. Cochran, "Invariance of the distributions of normalized Gram matrices," in *IEEE Workshop on Statistical Signal Processing (SSP)*, Jun. 2014.
- [116] L. Sun and M. R. McKay, "Tomlinson-harashima precoding for multiuser MIMO systems with quantized CSI feedback and user scheduling," *IEEE Transactions on Signal Processing*, vol. 62, no. 16, pp. 4077–4090, Aug. 2014.
- [117] A. Gupta and S. Nadarajah, *Handbook of Beta Distribution and Applications*. Marcel Dekker, 2004.
- [118] S. Shrestha, G. Fang, E. Dutkiewicz, and X. Huang, "Effect of CSI quantization on the average rate in MU-MIMO WLANs," in *2016 13th IEEE Annual Consumer Communications and Networking Conference (CCNC)*, Jan. 2016.
- [119] M. Bengtsson and B. Ottersten, "Optimal Downlink Beamforming Using Semidefinite Optimization," in *37th Annual Allerton Conference on Communication, Control, and Computing*, Sep. 1999.
- [120] F. Rashid-Farrokhi, K. R. Liu, and L. Tassiulas, "Transmit beamforming and power control for cellular wireless systems," *IEEE Journal on Selected Areas in Communications*, vol. 16, no. 8, pp. 1437–1450, Oct. 1998.
- [121] E. Visotsky and U. Madhow, "Optimum beamforming using transmit antenna arrays," in *IEEE 49th Vehicular Technology Conference*, May 1999.
- [122] M. Sousa, L. Vandenberghe, S. Boyd, and H. Lebrecht, "Applications of second-order cone programming," *Linear Algebra and its Applications*, vol. 284, no. 1, pp. 193–228, Nov. 1998.
- [123] K. Anstreicher and H. Wolkowicz, "On lagrangian relaxation of quadratic matrix constraints," *SIAM Journal on Matrix Analysis and Applications*, vol. 22, no. 1, pp. 41–55, 2000.

- [124] L. Vandenberghe and S. Boyd, "Semidefinite programming," *SIAM Review*, vol. 38, no. 1, pp. 49–95, Mar. 1996.
- [125] H. Farhadi, M. N. Khormuji, and M. Skoglund, "Pilot-assisted ergodic interference alignment for wireless networks," in *IEEE International Conference on Acoustics, Speech and Signal Processing (ICASSP)*, May 2014.
- [126] S. Gollakota, S. D. Perli, and D. Katabi, "Interference alignment and cancellation," in *ACM SIGCOMM Computer Communication Review*, Aug. 2009.
- [127] C. Lameiro, Óscar González, J. A. García-Naya, I. Santamaria, and L. Castedo, "Experimental evaluation of interference alignment for broadband WLAN systems," *EURASIP Journal on Wireless Communications and Networking*, vol. 2015, no. 180, Dec. 2015.
- [128] S. Lee, A. Gerstlauer, and R. W. Heath, "Distributed real-time implementation of interference alignment with analog feedback," *IEEE Transactions on Vehicular Technology*, vol. 64, no. 8, pp. 3513–3525, Aug. 2015.
- [129] O. El Ayach, A. Lozano, and R. W. Heath, "On the overhead of interference alignment: Training, feedback, and cooperation," *IEEE Transactions on Wireless Communications*, vol. 11, no. 11, pp. 4192–4203, Nov. 2012.
- [130] N. N. Moghadam, H. Farhadi, and P. Zetterberg, "Optimal power allocation for pilot-assisted interference alignment in MIMO interference networks: Test-bed results," in *IEEE International Conference on Digital Signal Processing (DSP)*, Jul. 2015.
- [131] M. El-Absi, S. Galih, M. Hoffmann, M. El-Hadidy, and T. Kaiser, "Antenna selection for reliable MIMO-OFDM interference alignment systems: Measurement-based evaluation," *IEEE Transactions on Vehicular Technology*, vol. 65, no. 5, pp. 2965–2977, May 2016.
- [132] P. Zetterberg and N. Moghadam, "An experimental investigation of SIMO, MIMO, interference alignment (IA) and coordinated multi-point (CoMP)," in *International Conference on Systems, Signals and Image Processing (IWSSIP)*, Apr. 2012.
- [133] H. Farhadi, C. Wang, and M. Skoglund, "Distributed transceiver design and power control for wireless MIMO interference networks," *IEEE Transactions on Wireless Communications*, vol. 14, no. 3, pp. 1199–1212, Mar. 2015.
- [134] K. Miller, A. Sanne, K. Srinivasan, and S. Vishwanath, "Enabling real-time interference alignment: Promises and challenges," in *International Symposium on Mobile Ad Hoc Networking and Computing (MobiHoc)*, Jun. 2012.
- [135] S. Caban, J. A. García-Naya, and M. Rupp, "Measuring the physical layer performance of wireless communication systems: Part 33 in a series of tutorials

- on instrumentation and measurement,” *IEEE Instrumentation and Measurement Magazine*, vol. 14, no. 5, pp. 8–17, Oct. 2011.
- [136] J. Rodríguez-Piñeiro, M. Lerch, J. A. García-Naya, S. Caban, M. Rupp, and L. Castedo, “Emulating extreme velocities of mobile LTE receivers in the downlink,” *EURASIP Journal on Wireless Communications and Networking*, vol. 2015, no. 106, Apr. 2015.
- [137] S. Lojasiewick, *Introduction to Complex Analytic Geometry*. Birkhäuser Verlag, 1991.
- [138] J. Fanjul, Jesús Ibáñez, I. Santamaria, and C. Loucera, “Experimental evaluation of non-coherent MIMO Grassmannian signaling schemes,” in *International Conference on Ad-Hoc Networks and Wireless*, Sep. 2017.
- [139] J. Fanjul, I. Santamaria, and C. Loucera, “A quaternion-based approach to interference alignment with Alamouti coding,” in *IEEE International Symposium on Signal Processing and Information Technology (ISSPIT)*, Dec. 2017.